FUNCTION THROUGH FORM IN SOFT MATTER: THE INFLUENCE OF BOUNDED GEOMETRIES IN HEATED GELS AND FLUCTUATING PROTEINS

A Dissertation
Presented to
The Academic Faculty

By

Michael S. Dimitriyev

In Partial Fulfillment
of the Requirements for the Degree
Doctor of Philosophy in the
School of School of Physics

Georgia Institute of Technology

August 2017

FUNCTION THROUGH FORM IN SOFT MATTER:
THE INFLUENCE OF BOUNDED GEOMETRIES IN HEATED GELS AND FLUCTUATING PROTEINS

Approved by:

Dr. Paul M. Goldbart, Advisor
School of Physics
Georgia Institute of Technology

Dr. Alberto Fernández-Nieves
School of Physics
Georgia Institute of Technology

Dr. Alexander Alexeev
School of Mechanical Engineering
Georgia Institute of Technology

Dr. Peter Yunker
School of Physics
Georgia Institute of Technology

Dr. Shina Tan
School of Physics
Georgia Institute of Technology

Date Approved: July 27, 2017

"It is known that there are an infinite number of worlds, simply because there is an infinite amount of space for them to be in. However, not every one of them is inhabited. Therefore, there must be a finite number of inhabited worlds. Any finite number divided by infinity is as near to nothing as makes no odds, so the average population of all the planets in the Universe can be said to be zero. From this it follows that the population of the whole Universe is also zero, and that any people you may meet from time to time are merely the products of a deranged imagination."

Douglas Adams, The Restaurant at the End of the Universe

To Andrea and my parents.

ACKNOWLEDGEMENTS

First, I would like to express my deep gratitude to Prof. Paul M. Goldbart. Having someone with such profound knowledge and endless enthusiasm about science as my advisor has been a great privilege. I've come to really appreciate his dedication and patience as a mentor, despite his role first as Chair and later as Dean. I am greatly indebted to him for all that I have learned under his careful guidance.

I would also like to thank Prof. Alberto Fernández-Nieves and his group for accepting me into their fold and introducing me to, and ultimately grounding my work in, the world of experimental soft matter. In particular, I would like to thank Prof. Ya-Wen "Winnie" Chang for being a wonderful collaborator who has patiently answered my barrages of questions regarding her experiments. Furthermore, I want to single out Perry Ellis and Alexandros Fragkopoulos for being wonderful officemates and good friends throughout our time in graduate school.

Naturally, I would also like to fellow group members Rafael Hipolito, Anton Souslov, Benjamín Loewe, and Shengnan Huang for all of our valuable conversations, their support, and for my occasional re-indoctrination to theory-land.

Finally, I want to express my thanks and love for my fiancée Andrea Welsh. She has made my life absolutely wonderful.

TABLE OF CONTENTS

LIST OF FIGURES

SUMMARY

The ability to control the behavior of a material through the prescription of spatial inhomogeneity is of increasing interest in condensed matter physics. Examples of materials such as auxetic metamaterials, which widen when stretched, and hydrogels that change shape when swollen involve patterned inhomogeneity to achieve these responses. However, as the boundary of a material breaks translational symmetry, it may also be considered a spatial inhomogeneity. We consider materials in which the boundary is the operative inhomogeneity and plays a key role in determining response to changes in environmental conditions.

We first consider a swollen hydrogel rod whose equilibration to a deswollen phase is frustrated due to an impermeable skin that forms at its boundary, trapping solvent within the gel. This constrained gel undergoes internal phase separation, which results in the formation of a solvent-poor shell, enclosing a solvent-rich core. The coaxial arrangement of these regions is unstable to symmetry breaking, which leads to polarization of the solvent distribution across the rod's cross-section, and an internal elastic stress distribution that causes the rod to bend. If the rod is curved when originally fabricated, the stress generated as a result of phase separation leads this polarization to align with the rod's curvature. In the case of a ring formed from a uniformly curved rod, this stress leads to a "Pringling" instability that buckles the ring out of its plane. If, instead, the rod is originally fabricated straight, its symmetry is spontaneously broken by the gel's polarization, which causes it to bend in the spontaneously selected direction. The Goldstone modes associated with this broken continuous symmetry twist the rod and leads to a reduction of correlations between bending directions along the rod.

We also consider allosteric regulation of proteins where the ability of a protein to bind a ligand molecule is modified by the presence of a bound ligand elsewhere on

the protein. In particular, we examine a model in which a bound ligand modifies the thermal fluctuations of elastic deformations about a static mean conformation. We model the protein as an elastic continuum and determine the change in fluctuation correlations due to the presence of a bound ligand. By treating the bound ligand as a small adjustment of the protein's boundary, we develop a perturbative approach to calculating the change in fluctuation correlations. We show that, to leading order, the increase in vibrational entropy due to binding is further increased by the presence of an already-bound ligand, which provides for a cooperative effect whose magnitude is governed by the protein shape and binding site locations.

CHAPTER 1
A TOUR OF POLYMER GEL PHYSICS

1.1 Introduction: linking thermodynamics and extreme mechanics

Within the realm of amorphous rigid materials without crystalline symmetries, polymer gels possess an interesting duality, having a rubber-like elasticity whilst being able to undergo large volume changes due to mixing with a solvent, e.g., water. There are three essential ingredients: polymers, cross-linkers, and solvent.

Polymers are typically idealized as a linear molecule that, due to thermal fluctuations in the angle between adjacent monomer units, explores random walk conformations, as shown in Fig. 1.1. The characteristic size of a polymers is specified by a radius of gyration R_g, which scales with the number of monomers $\mathcal{N}$ as $\mathcal{N}^\nu$, where $\nu = 1/2$ for an "ideal" chain, for which the self-exclusion interaction amongst chain segments is neglected. More realistically, a polymer does not intersect with itself, resulting in statistics of a self-avoiding (as opposed to ideal) random walk, for which $\nu \approx 3/5$, increasing the size of the chain. However, this is the situation in a "good" solvent where the polymer is miscible in the solvent, as opposed to the case immiscibility (a "poor" solvent) where the polymer radius is decreased due to the high energetic penalty of interaction. An intermediate case is the ϑ-solvent, where a mildly poor solvent cancels out the self-avoidance interaction of the polymer, resulting in $\nu = 1/2$ (see e.g., [1]). These solvent-polymer interactions lead to swelling behavior of gels and can be tuned by a number of variables, including changes in temperature, pH, and ion concentration.

A solution composed of many polymers can be brought to a polymer concentration where individual typically coils overlap in equilibrium. This is where the introduction

Figure 1.1: A computer-generated random walk in three dimensions representing an "ideal" polymer with $\mathcal{N} = 10^3$.

of permanent chemical cross-linker molecules can result in the formation gel due to bonding monomers. Either the linked monomers belong to two distinct polymers or the same one. If there is sufficient linking of different polymers then a system-spanning continuous network of linked polymers can form, resulting in a chemical gel. This gelation transition is related to the general class of percolation transitions [1]. Furthermore, constraints introduced by cross-linking localize polymers that previously underwent system-spanning Brownian motion, given sufficient time, and the ensuing *ergodicity breaking* of the polymer network is results in rigidity [2]. Gels are therefore similar to rubbers and have a similar entropic elasticity.

However, unlike typical rubbers, the polymers that form these gels may be miscible in a solvent, leading to swelling. As the both the entropic elastic stresses of the polymer network and the osmotic pressure of the solvent within the network have magnitudes set by the thermal energy scale $k_B T$, both are important in determining the gel's *macroscopic* equilibrium shape, particularly in gels with lower cross-linking densities, resulting in the signature ability of gels to undergo large macroscopic shape changes in response to varying solvent conditions. While there are a variety of polymer gels whose equilibrium states can be modified in various ways, we will focus on the specific case of electrically neutral hydrogels that undergo large volume changes, swelling or deswelling in response to changes in temperature by imbibing or expelling

water. Suitably prepared hydrogels have a remarkably large volume response, capable of swelling to an equilibrium volume on the order of 10^3 times their dry volume by absorbing water [3]. The volume transition can be smooth or abrupt, even discontinuous under various conditions. For example, poly(N-isopropylacrylamide) hydrogels (pNIPAM) gradually deswell under *heating* until 32°C, beyond which, owing to a change in solvent nature from good to poor, such gels abruptly expel most of the solvent and enters a deswollen phase [3].

Additionally, hydrogels can undergo shape changes beyond swelling. Mechanical constraints, such as attachment to a stiff substrate, can frustrate deswelling of the gel in a *homogeneous* manner, resulting in inhomogeneous deswelling such as surface ripples [4, 5]. Gels that are subject to inhomogeneous swelling are of particular interest, as the resulting deformations typically cannot be realized in flat space [6], leading to a variety of buckled shapes [7, 8], some of which mirror designs found in nature [9–11]. This has led to origami-inspired searches for ways to program certain shapes that are actuated upon swelling; one such method is "4D printing" [12].

In the present chapter, we will review hydrogel thermodynamics and mechanics. We will start by introducing the state functions that are used to describe the macroscopic states of hydrogels (§ 1.2) and show that models of hydrogel mechanics can be phenomenologically constructed using nonlinear elasticity (§ 1.3). We also outline the Flory-Rehner theory, which is an approximate treatment of the statistical mechanics of polymer gels and ultimately provides equations of state that are largely successful in describing such gels (§ 1.4). Finally, we discuss the volume phase transition (§ 1.5) as well as the complication of specifying a critical point due to shear rigidity (§ 1.6).

In the next chapter (Ch. 2), we will consider a hydrogel, initially swollen, that is *rapidly heated* past the volume phase transition. As we shall discuss, a thin, deswollen skin develops, constraining the gel's volume to be constant. Under this global constraint on the volume, the gel can attain a *constrained, phase-separated equilibrium*

where a solvent-rich region coexists with a solvent-poor region. Focusing our attention on hydrogel rods with a coexistent solvent-poor shell enclosing a solvent-rich core, we find that such coaxial configurations are unstable to symmetry breaking that leads to inhomogeneous stress, bending the rod. In the following chapter (Ch. 3), we will develop a reduced model to predict the equilibria of these rods in which the fields describing rod shape are coupled to a field that describes the broken-symmetry arrangement of solvent-rich and solvent-poor regions. Using our results, we speculate that hydrogel rods can be fabricated in a way that directs phase separation, leading to a novel way of actuating shape changes.

1.2 Thermodynamic description

Consider a sample of gel that is allowed to exchange solvent with its surroundings but contains a constant mass of polymer. Assuming that the gel is composed of n_s solvent molecules and n_m monomers, each molecule and monomer occupying a small volume v_s and v_m, respectively, the total volume V of the gel is given by

$$V = n_s v_s + n_m v_m \ , \tag{1.1}$$

where we assume the incompressibility of the solvent and polymers, viz., the fixing of v_s and v_m. Therefore, in addition to the temperature T, we can choose the volume V and the number of solvent molecules n_s as state functions of the system. The gel's *shear rigidity* requires that changes in hydrogel shape distort the polymer network, doing work. The work needed to change the 3 side-lengths L_i of a box-shaped sample of the gel shown in Fig. 1.2 to lengths $L_i' \equiv \Lambda_i L_i$ depends on the changes in lengths of the sides. The deformation of the gel is therefore set by the dimensionless ratios of length Λ_i such that $\Lambda_1\Lambda_2\Lambda_3 = 1$. Note that specifying the box shape is artificial: the distance between any two points $\mathbf{R}$ and $\mathbf{R} + \mathrm{d}\mathbf{R}$, e.g., two cross-links, is altered

upon deformation of the gel, which takes $\mathrm{d}\mathbf{R}$ to $\mathrm{d}\mathbf{R}'$. Assuming *affine* deformation of the gel, for which the changes in lengths are independent of position, all lengths are transformed by a deformation matrix Λ, such that

$$\mathrm{d}R'_i = \Lambda_{ij}\,\mathrm{d}R_j \ . \tag{1.2}$$

Deformed volume elements d^3R' are related to the undeformed ones via

$$\begin{aligned} \mathrm{d}^3R' \equiv \mathrm{d}R'_1 \wedge \mathrm{d}R'_2 \wedge \mathrm{d}R'_3 &= \Lambda_{1i}\Lambda_{2j}\Lambda_{3k}\,\mathrm{d}R_i \wedge \mathrm{d}R_j \wedge \mathrm{d}R_k \\ &= (\varepsilon_{ijk}\Lambda_{1i}\Lambda_{2j}\Lambda_{3k})\,\mathrm{d}^3R = (\det\,\Lambda)\,\mathrm{d}^3R \ , \end{aligned} \tag{1.3}$$

so $\det\,\Lambda$ describes the gel's volume. We factorize Λ so that

$$\hat{\Lambda} \equiv \frac{\Lambda}{(\det\,\Lambda)^{1/3}} \tag{1.4}$$

describes volume-preserving deformations, so that

$$\det\,\hat{\Lambda} \equiv 1 \ . \tag{1.5}$$

The deformation matrix $\hat{\Lambda}$ is the state function describing volume-preserving stretching of the gel, encoding information complementary to the volume: as shown in Fig. 1.2c, affine deformations stretch lengths homogeneously so that subdivisions of the gel undergo common deformations.

Our selection of state functions $(T, V, \hat{\Lambda}, n_s)$ suggests the use of the Helmholtz free-energy F as the potential for determining the equilibrium properties of the gel. As F is a homogeneous, first-order function in its extensive parameters V and n_s [13], we have

$$F(T, V, \hat{\Lambda}, n_s) = V\ F\left(T, 1, \hat{\Lambda}, \frac{n_s}{V}\right) \equiv V\ \tilde{F}\left(T, \hat{\Lambda}, \rho_s\right), \tag{1.6}$$

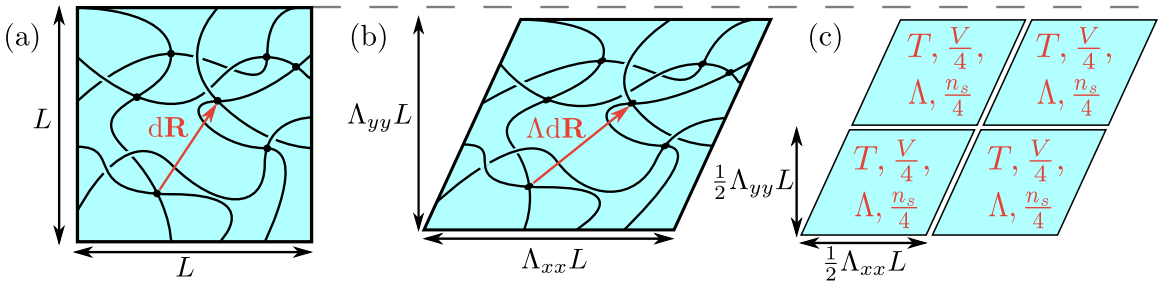

Figure 1.2: Representative sample of a cross-linked polymer network with linear dimension L and distance between two arbitrary cross-linkers given by $\mathrm{d}\mathbf{R}$ (a) prior to deformation and (b) after affine deformation, prescribed by deformation matrix Λ which is shown (c) as an intensive state function.

where $\tilde{F}$ is a free-energy density and ρ_s ($\equiv n_s/V$) is the number-density of solvent molecules. Recalling Eq. (1.1), the volume is *prescribed* by the total amount of solvent and polymer, obfuscating the interpretation of ρ_s. We can equivalently use the *polymer volume-fraction* ϕ, defined via

$$\phi \equiv \frac{n_m\, v_m}{n_s\, v_s + n_m\, v_m} = 1 - v_s\, \rho_s\,, \tag{1.7}$$

i.e., the fraction of the gel that is occupied by polymer; $\phi = 1$ corresponds to a gel that is completely devoid of solvent whereas $\phi = 0$ is the limit of an infinitely dilute gel. Therefore, F may be expressed as

$$F = \frac{v_m\, n_m}{\phi}\tilde{F}(T, \hat{\Lambda}, \phi)\,, \tag{1.8}$$

where we have changed variables from ρ_s to ϕ.

1.3 Nonlinear elasticity

Before examining a microscopic theory of polymer gels, let us inquire about the form of the free-energy cost ΔF_{def} of deforming the gel. We start by ignoring swelling effects and assume that the gel is held at the volume fraction ϕ_0 at which it was

cross-linked. We call this state of the gel its *reference state* $\mathcal{R}$ and its state after deformation a *target state* $\mathcal{T}$. The free-energy of deformation should be invariant with respect to rotations $U_{\mathcal{R}}$ of the reference state and rotations $U_{\mathcal{T}}$ of its target state, so that

$$\Delta F_{\rm def}(\Lambda) = \Delta F_{\rm def}(\Lambda U_{\mathcal{R}}) = \Delta F_{\rm def}(U_{\mathcal{T}}\Lambda)\ . \tag{1.9}$$

It is convenient to introduce the right Cauchy-Green tensor G, defined via

$$G \equiv \Lambda^T \Lambda\,, \tag{1.10}$$

which is preserved under rotations of the target state:

$$G_{\rm rot} = (U_{\mathcal{T}}\,\Lambda)^T (U_{\mathcal{T}}\,\Lambda) = \Lambda^T\, U_{\mathcal{T}}^T\, U_{\mathcal{T}}\,\Lambda = \Lambda^T\,\mathbb{1}\,\Lambda = \Lambda^T\,\Lambda = G\ . \tag{1.11}$$

Note that with $\Lambda_{ij} \equiv \partial R_i'/\partial R_j$, the tensor G_{ij} is a metric tensor describing lengths on $\mathcal{T}$ in terms of lengths on $\mathcal{R}$. To ensure that it is invariant under isometries of $\mathcal{R}$, $\Delta F_{\rm def}$ depends on the thee invariants (under rotation) of G [14], viz.,

$$\begin{aligned} I_1 &= \text{tr}\ G \\ I_2 &= \frac{1}{2}\left[(\text{tr}\ G)^2 - \text{tr}\ G^T G\right] \\ I_3 &= \det G \end{aligned} \tag{1.12}$$

where tr indicates a trace, and we note that the third invariant I_3 is unity. If $\Delta F_{\rm def}$ is an analytic function of Λ then it can be written as a power series in $\{I_1, I_2\}$. For our purposes, it is sufficient to approximate $\Delta F_{\rm def}$ by

$$\Delta F_{\rm def} \approx \frac{C}{2}\ \text{tr}\ G = \frac{C}{2}\ \text{tr}\ \Lambda^T\Lambda \tag{1.13}$$

which corresponds to the deformation of network of *phantom, Gaussian chains*, a

starting point for the theory of rubber elasticity [14, 15] and is recovered in the Flory-Rehner theory (see § 1.4). Another commonly used form that attempts to account for deviations due to large deformations is the Mooney-Rivlin theory [14], in which $\Delta F_{\mathrm{def}} = c_1 I_1 + c_2 I_2$.

Whilst polymer gels have a rubber-like elasticity and are therefore essentially incompressible at fixed polymer-volume fraction, they can compress and expand if allowed to exchange solvent with their surroundings. Recall that $\hat{\Lambda}$ is a state variable that is independent of ϕ. We define $\Lambda = \mathbb{1}$ to correspond to the state with relaxed polymer network with volume fraction ϕ_0. As Λ describes an affine deformation, the ratio $\det \Lambda$ of volume elements between the relaxed reference state and the deformed target state is also given by the ratio of the volume of the target state $n_m v_m/\phi$ to the volume of the reference state $n_m v_m/\phi_0$; thus, we have

$$\det \Lambda = \frac{\phi_0}{\phi} \,. \tag{1.14}$$

Therefore, $\det \Lambda$ can be used as a state function instead of ϕ, leading to a free-energy

$$F = F(T, V, \Lambda) \tag{1.15}$$

that is expressible terms of all three invariants given in Eq. (1.12).

1.4 Microscopic description: the Flory-Rehner mean-field theory

To arrive at concrete equations of state that describe elasticity *and* swelling, we need to incorporate the statistical mechanics of the polymer gel. We begin with an approximation of the polymer network as a collection of n_{ch} chains, where each cross-linking point is an intersection of the ends of four chains; there are thus $n_{\mathrm{ch}}/2$ cross-linkages. Other structures, such as loops and free ends, are ignored within this model.

The microscopic interaction energy U is the sum of three terms, viz.,

$$U = U_{\text{monomer}-\text{monomer}} + U_{\text{monomer}-\text{solvent}} + U_{\text{solvent}-\text{solvent}} \tag{1.16}$$

(see [1]), with each of these terms depending on particle positions. For example, $U_{\text{monomer}-\text{monomer}}$ contains an excluded volume interaction $\sum_{i\neq j}(v_m/2)\,\delta(\mathbf{R}_i - \mathbf{R}_j)$, summed over monomer positions. The Flory approach treats interactions in a mean-field approximation:

$$U \approx \frac{v}{2} V k_B T \left[\chi_{m-m}\,\rho_m^2 + 2\chi_{m-s}\,\rho_m\,\rho_s + \chi_{s-s}\,\rho_s^2\right] \tag{1.17}$$

where $\rho_m = n_m/V$ and $\rho_s = n_s/V$ are number-densities and the monomer units are taken to have the same volume as solvent molecules so that $v_m = v_s \equiv v$. Re-writing in terms of ϕ, the densities become $(\rho_m, \rho_s) = (\phi, 1-\phi)/v$, so that

$$U \approx \frac{1}{2} N k_B T \left[\chi_{m-m}\,\phi^2 + 2\chi_{m-s}\,\phi(1-\phi) + \chi_{s-s}\,(1-\phi)^2\right] \tag{1.18}$$

where $N = n_m + n_s$ is the total number of particles considered and $(\chi_{m-m}, \chi_{m-s}, \chi_{s-s})$ are the various dimensionless interaction strengths, which incorporate interactions such as van der Waals and excluded volume [1].

By treating interactions at the mean-field level, the elasticity of the polymer network can be approximated using a phantom chain model where polymer conformations are allowed to overlap one-another, leading to random-walk 'ideal' polymers. Although some degree of realism is lost, the problem gains tractability whilst retaining the essential physics – the free-energy cost of elastic deformations is simple to derive and has a form that reduces to the classical rubber elasticity model, Eq. (1.13), in the unswollen limit. The Flory-Rehner theory therefore breaks the calculation of

the free-energy into two pieces:

$$F = F_{\text{elastic}} + F_{\text{mix}} \,, \tag{1.19}$$

i.e., an elastic free-energy F_{elastic} [16] that is calculated with the phantom chain assumption, and a free-energy of mixing F_{mix} [17] that is arrived at though a mean-field approximation.

1.4.1 Elasticity of a cross-linked network of ideal chains

The elastic free-energy of the gel is approximated as proportional to the *net* conformational entropy change due to deforming n_{ch} *independent* polymer chains. Thus, we require knowledge of (i) how deformations affect the conformational entropy of a single polymer and (ii) how to determine the effect on an *ensemble* of many such polymers.

To begin, consider a singe polymer of length L with one terminal end at position $\mathbf{r}$ and the other at the origin, as shown in Fig. 1.3a. Any polymer of the same length may adopt a variety of different conformations, starting at the origin, with the other terminal point sampled from a normalized distribution $P_1(\mathbf{r})$. If the polymer is an ideal chain then its conformations adopt forms resembling the trajectory of a particle undergoing a random walk, shown in Fig. 1.3, and

$$P_1(\mathbf{r}) = \frac{1}{(2\pi\ell^2)^{3/2}} \exp\left\{-\frac{|\mathbf{r}|^2}{2\ell^2}\right\} \,, \tag{1.20}$$

as shown in Fig. 1.3b, where ℓ is a length-scale that is proportional to the radius of gyration. For a collection of n_{ch} phantom chains, the joint probability $P_{n_{\text{ch}}}$ of finding chain 1 with end-to-end vector $\mathbf{R}_1$, chain 2 with $\mathbf{R}_2$, etc. is simply the product of

individual single polymer probabilities, so that

$$\begin{aligned} P_{n_{\rm ch}}(\mathbf{R}_1, \mathbf{R}_2, ..., \mathbf{R}_{n_{\rm ch}}) &= P_1(\mathbf{R}_1) P_1(\mathbf{R}_2) \cdots P_1(\mathbf{R}_{n_{\rm ch}}) \\ &= \frac{1}{(2\pi\ell^2)^{3n_{\rm ch}/2}} \exp\left\{ -\sum_{i=1}^{n_{\rm ch}} |\mathbf{R}_i|^2 / 2\ell^2 \right\} . \end{aligned} \tag{1.21}$$

Note that $P_{n_{\rm ch}}$ is proportional to the number Ω of ways for the collection of polymers to have end-to-end vectors $(\mathbf{R}_1, ..., \mathbf{R}_{n_{\rm ch}})$. The entropy $S_{\rm chains}$ corresponding to this "macrostate" [1] is therefore

$$S_{\rm chains}(\mathbf{R}_1, ..., \mathbf{R}_{n_{\rm ch}}) = k_B \ln \Omega(\mathbf{R}_1, ..., \mathbf{R}_{n_{\rm ch}}) = -k_B \sum_{i=1}^{n_{\rm ch}} \frac{|\mathbf{R}_i|^2}{2\ell^2} + \text{const.} . \tag{1.22}$$

However, the collection of end-to-end vectors is not set but is itself distributed according to $P_{n_{\rm ch}}$. The entropy is thus the expected value of the fixed end-to-end entropy:

$$\Sigma_{\rm chains} = \langle S_{\rm chains}(\mathbf{R}_1, ..., \mathbf{R}_{n_{\rm ch}}) \rangle = -k_B \sum_{i=1}^{n_{\rm ch}} \frac{\langle |\mathbf{R}_i|^2 \rangle}{2\ell^2} + \text{const.} = -\frac{3}{2} n_{\rm ch}\, k_B + \text{const.} \tag{1.23}$$

where we observe that the free-energy $F = -TS$ resembles the energy of an ideal gas of monatomic particles in 3 dimensions, each translational degree of freedom contributing a mean energy of $(3/2)k_BT$ per particle.

Now that we know how to calculate the net entropy $\Sigma_{\rm chains}$, let us determine how deformations change this entropy, again starting from the effect on a single polymer and then extending the calculation to the collection of chains. Affine deformation of a single polymer $\mathbf{r} \to \Lambda\mathbf{r} \equiv \mathbf{r}'$ changes the probability distribution to

$$P_1'(\mathbf{r}) = \frac{\det \Lambda}{(2\pi\ell^2)^{3/2}} \exp\left\{ -\frac{|\Lambda\mathbf{r}|^2}{2\ell^2} \right\} , \tag{1.24}$$

as shown in Fig. 1.3c. If chains in a network undergo affine deformation, taking the

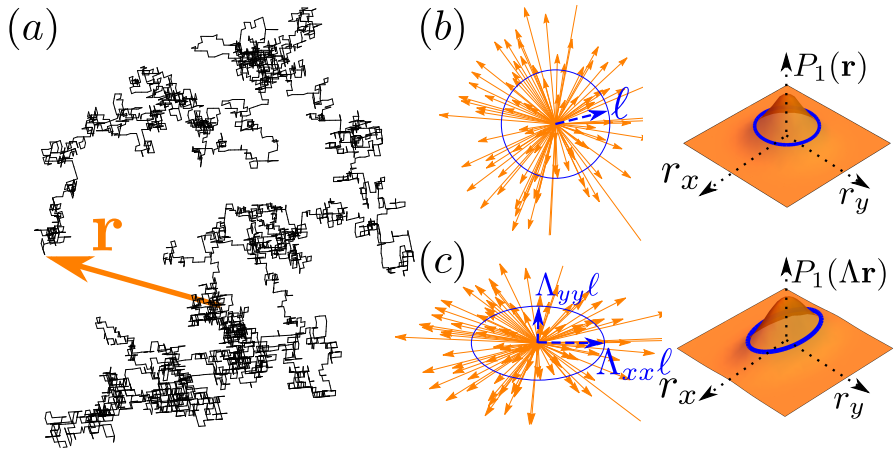

Figure 1.3: (a) Example of random walk with end-to-end vector $\mathbf{r}$. (b) shows an ensemble of end-to-end vectors sampled from an isotropic distribution with standard deviation ℓ. (c) the distribution after affine deformation Λ.

initial set of end-to-end vectors $(\mathbf{R}_1, ..., \mathbf{R}_{n_{\rm ch}})$ deformed vectors $(\Lambda\mathbf{R}_1, ..., \Lambda\mathbf{R}_{n_{\rm ch}})$, then the total entropy $\Sigma'_{\rm chains}$ after deformation is

$$\begin{aligned}\Sigma'_{\rm chains} &= \langle S'_{\rm chains}(\Lambda\mathbf{R}_1, ..., \Lambda\mathbf{R}_{n_{\rm ch}})\rangle \\ &= -\frac{1}{2} n_{\rm ch}\, k_B \,{\rm tr}\, \Lambda^T\Lambda + n_{\rm ch}\, k_B \ln\det\Lambda + {\rm const.}\,.\end{aligned} \tag{1.25}$$

Thus, the increase in chain free-energy upon deformation is given by

$$F'_{\rm chains} - F_{\rm chains} = \frac{1}{2} n_{\rm ch}\, k_B\, T \left[{\rm tr}\, \Lambda^T\Lambda - 3 - 2\ln\det\Lambda\right] \tag{1.26}$$

up to deformation-independent constants.

However, there is a reduction in the entropy that comes from the elimination of chain translational degrees of freedom due to the chemical cross-linking of *independent* chains into pairs that share center-of-mass motion [17, 18]. To show this reduction, note that the translational freedom of each chain contributes a total entropy of $k_B\, n_{\rm ch} \ln V + {\rm const.}$ where V is the system volume. After deformation, $V \to (\det\Lambda)V$ so the change in entropy is given by $k_B\, n_{\rm ch} \ln\det\Lambda$, which is provided by the last term in Eq. (1.26). However, each cross-linking event between two chains constrains

the translational motion of the chains. Thus, there is a *reduction* of the total entropy by $(k_B\, n_{\rm ch}/2) \ln \det \Lambda$ resulting in the Flory-Rehner result for the elastic free-energy:

$$F_{\rm elastic} = \frac{1}{2} n_{\rm ch}\, k_B\, T \left[\text{tr}\ \Lambda^T \Lambda - 3 - \ln \det \Lambda \right] \ . \tag{1.27}$$

It should be noted, however, that this argument is contentious [19] because the cross-linked chains are *localized*, exploring only a small sub-volume that is not appreciably stretched after affine deformation of the whole volume. Still, Eq. (1.27) is a widely adopted model for hydrogel elasticity, and changes to the contentious term do not qualitatively change our results.

1.4.2 Mixing free-energy from a mean-field approximation

To estimate the mixing free-energy, we approximate space by a lattice (as shown in Fig. 1.4) of N sites, each occupied by either a solvent molecule or a monomer; because the system is densely filled, there are n_s solvent molecules and $n_m = N - n_s$ monomers. Furthermore, let the solvent molecules and monomer units occupy common volumes, v; as the persistence length of the polymer does not figure into this theory, we are free to choose the size of monomer units for the polymers. The mixing free-energy $F_{\rm mix}$ can be decomposed into an mixing energy $U_{\rm mix}$ and mixing entropy $S_{\rm mix}$:

$$F_{\rm mix} = U_{\rm mix} - T S_{\rm mix} \ . \tag{1.28}$$

The mixing energy $U_{\rm mix}$ is the difference of the interaction energy $U(\phi)$ of gel with solvent and monomer and the energy of unmixed pure monomer $U(\phi = 1)$ and pure solvent $U(\phi = 0)$. The dilute limit has a free-energy per site of $u_{\phi=0} = k_B T \chi_{s-s}/2$ whereas the monomer-packed limit has a free-energy per site of $u_{\phi=1} = k_B T \chi_{m-m}/2$.

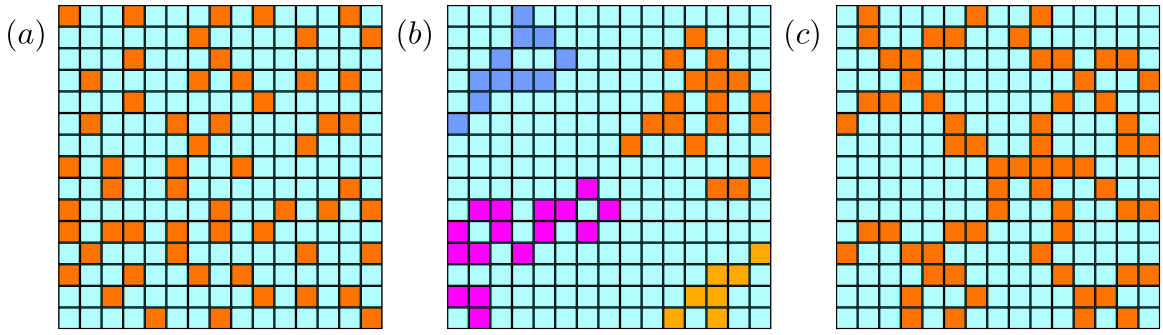

Figure 1.4: Lattice calculation of the mixing entropy. Each cell occupies a volume v. Solvent is represented by blue cells. (a) Bragg-Williams case in which the monomer units (orange) are uncorrelated. (b) Flory-Huggins case where monomers are identified with mobile polymers of degree $\mathcal{N}$. (c) Flory-Rehner case where monomer translational freedom is frozen.

Thus, the total unmixed energy is $n_m\,u(1) + n_s\,u(0)$, so the $U_{\rm mix}$ is given by

$$\begin{aligned} U_{\rm mix} &= N u(\phi) - n_m\,u_{\phi=1} - n_s\,u_{\phi=0} \\ &= N\left[u(\phi) - \phi\,u_{\phi=1} - (1-\phi)\,u_{\phi=0}\right] \\ &= N\,k_B\,T\,\chi\,\phi\,(1-\phi)\,, \end{aligned} \tag{1.29}$$

where $\chi \equiv \chi_{m-s} - \chi_{m-m}/2 - \chi_{s-s}/2$ is the so-called Flory parameter [1]. If $\chi < 0$ then $U < 0$, favoring maximally mixed polymer and solvent ($\phi = 1/2$): this occurs when the cost of monomer-solvent interactions is less the average cost of monomer-monomer and solvent-solvent interactions.

By fixing the total number of polymers and solvent molecules, we fix the energy of the system, allowing us to work in the *microcanonical ensemble*, so the entropy is given by

$$S = k_B \ln \Omega\,, \tag{1.30}$$

where Ω is the number of microstates. To proceed with determining the entropy S, we must count the number of ways that the lattice can be filled with solvent and monomers, where the monomers (i) are arranged into polymers which (ii) belong to a cross-linked network that spans space. However, as we shall demonstrate, S is

dominated by the solvent's *translational entropy*, i.e., a measure of the number of arrangements of solvent particles amongst a unique configuration of monomers. To show this, we will start with the simple case of "free" monomers that are unassociated with a larger polymer molecule, all able to explore space independently (see Fig. 1.4a) and recover the entropy of Bragg-Williams theory. After, we will progressively introduce the necessary constraints by associating the monomers into polymers and then introducing the cross-linking constraints.

Consider a binary system, consisting of n_A and n_B particles of species 'A' and 'B', respectively. E.g., 'A' represents solvent and 'B' represents free monomers as shown in Fig. 1.4a. The total number of microstates within the mean-field approximation (or, equivalently, Bragg-Williams theory [20]) is given by

$$\Omega = \frac{N!}{n_A! n_B!}\,, \tag{1.31}$$

so the entropy, using Stirling's approximation $\ln x! \approx x \ln x - x$, is

$$S \approx k_B \left[N \ln N - n_A \ln n_A - n_B \ln n_B\right] . \tag{1.32}$$

Recalling the volume fraction $\phi = n_B/N$, the entropy is

$$S \approx -N \left[(1-\phi)\ln(1-\phi) + \phi \ln \phi\right] , \tag{1.33}$$

from which we find that the state of maximum entropy is $\phi = 1/2$, corresponding to a mixed state composed equally of both species of particles.

We now associate monomers into polymer units that are free to explore the entire space, whilst localizing individual monomers to much smaller volumes around the polymers' centers of mass (see Fig. 1.4b). Let each polymer consist of $\mathcal{N}$ monomers so $n_p = n_m/\mathcal{N}$ is the total number of polymers. Whilst the individual monomers

have the adjacency condition, polymers are allowed full translational freedom on the lattice. Thus, the entropy of the localized monomers is negligible compared with the translational entropy of the polymers. The entropy S is therefore *dominated* by the translational entropy of the solvent and the polymers such that

$$S \approx -N \left[(1-\phi)\ln(1-\phi) + \frac{\phi}{\mathcal{N}} \ln \frac{\phi}{\mathcal{N}} \right] . \tag{1.34}$$

Note that while the entropy S in the dilute limit ($\phi \to 0$) disappears, S in the polymer-packed limit ($\phi \to 1$) is non-zero, contrary to the definition of a *mixing* entropy. To obtain the mixing entropy ΔS_{mix}, note first that we can define an average entropy per site via $s = S/N$. In the purely solvent case, the entropy is given by $n_s \, s_{\phi=0}$; for the purely species polymer case, the entropy per site is given by $n_m \, s_{\phi=1}$. The mixing entropy is the total entropy, less the entropy of the pure solvent and polymer, so that

$$\begin{aligned} S_{\text{mix}} &= N \, s(\phi) - n_s \, s_{\phi=0} - n_m \, s_{\phi=1} \\ &= N \left[s(\phi) - (1-\phi) \, s_{\phi=0} - \phi \, s_{\phi=1} \right] \\ &\approx -N \left[(1-\phi)\ln(1-\phi) + \frac{\phi}{\mathcal{N}} \ln \phi \right] , \end{aligned} \tag{1.35}$$

and thus is the Flory-Huggins result [1, 21] for polymer solutions.

Finally, we consider the case in which permanent cross-links are introduced, localizing polymers to small regions about the cross-link sites (see Fig. 1.4c). In this case, the polymers have constraints that reach all the way to the sample boundary, resulting in rigidity. Therefore, the translational entropy of polymers is negligible compared with the entropy of the solvent. The result may be found by considering the limit of the Flory-Huggins theory where the system consists of an infinitely long polymer, i.e., taking $\mathcal{N} \to \infty$. The mixing entropy is therefore simply given by

$$S_{\text{mix}} \approx -N(1-\phi)\ln(1-\phi) \tag{1.36}$$

which is independent of network details [1, 17, 18]. The mixing free-energy is thus

$$F_{\text{mix}} = N\,k_B\,T\,\left[(1-\phi)\ln(1-\phi) + \chi\,\phi\,(1-\phi)\right]\,, \tag{1.37}$$

which we can rewrite using the state function $V = vN$.

1.4.3 The Flory-Rehner free-energy for polymer gels

Combining the elastic (Eq. (1.27)) and mixing (Eq. (1.37)) terms yields the Flory-Rehner free-energy [16, 17], which is given by

$$\begin{aligned}\frac{F(T,V,\Lambda,\phi)}{k_BT} = \frac{n_{\text{ch}}}{2}\left[\text{tr}\,\Lambda^T\Lambda - 3 - \ln(\det\Lambda)\right] \\ + \frac{V}{v}\left[(1-\phi)\ln(1-\phi) + \chi(T)\,\phi\,(1-\phi)\right]\end{aligned} \tag{1.38}$$

where, we note, the only nonlinear scaling of the free-energy with respect to temperature occurs via the Flory parameter $\chi(T)$, and we use the full deformation matrix Λ as a state function instead of $\hat{\Lambda}$ by requiring the constraint of Eq. (1.14), i.e., $\det\Lambda = \frac{\phi_0}{\phi}$. The number n_{ch} of effective chains, viz., those contributing to the network elasticity by being cross-linked to other chains, is set at the moment of cross-linking, when the gel is at volume fraction ϕ_0, and is given by $n_{\text{ch}} = \nu_0 V(\phi/\phi_0)$ where ν_0 is the density of chains at cross-linking and is considered a material parameter of the hydrogel. The corresponding free-energy density $\tilde{F}$ is therefore

$$\begin{aligned}\frac{\tilde{F}(T,\Lambda,\phi)}{k_BT} = \frac{\nu_0}{2}\frac{\phi}{\phi_0}\left[\text{tr}\,\Lambda^T\Lambda - 3 - \ln(\det\Lambda)\right] \\ + \frac{1}{v}\left[(1-\phi)\ln(1-\phi) + \chi(T)\,\phi\,(1-\phi)\right].\end{aligned} \tag{1.39}$$

1.5 Hydrogel swelling equilibrium and volume phase transition

With the Flory-Rehner free-energy Eq. (1.39) in hand, let us determine the equilibrium volume fraction $\phi(T)$ in the case of an isotropic gel (where $\hat{\Lambda} = \mathbb{1}$). We first show that $\phi(T)$ for a gel placed in a pure solvent is determined by a constant *osmotic pressure* condition. We then develop a virial expansion of the osmotic pressure equation of state to demonstrate that the Flory parameter χ characterizes the second virial coefficient. Finally, to describe the *discontinuous volume transition* of many electrically neutral hydrogels that is not predicted within the Flory-Rehner theory, we introduce the Erman-Flory [22] corrections in the virial expansion.

Consider a hydrogel that is placed in a *good* solvent, held at fixed temperature T. In equilibrium, the gel's constituent polymer attain open, un-coiled conformations, where the solvent permeates the scaffolding of the polymer network. Solvent molecules are allowed to enter and leave the scaffolding so that the equilibrium volume fraction ϕ is determined by the chemical equilibrium condition

$$\mu(T, \phi) = \left(\frac{\partial F}{\partial n_s} \right)_T = \mu_0(T) \tag{1.40}$$

where $\mu_0(T)$ is the chemical potential of the solvent outside of the gel. Note that the solvent within the gel is identical to the solvent outside of the gel; its chemical potential μ can therefore be decomposed into $\mu = \mu_0 + \Delta\mu$ where $\Delta\mu$ is attributed to mixing with the polymer network. The correction $\Delta\mu$ is due to an *osmotic pressure* Π acting on the gel, due to the thermal motion of the polymers in the gel, and is given by

$$\Pi(T, \phi) = -\frac{\Delta\mu}{v_s} = \phi^2 \left(\frac{\partial}{\partial \phi} \frac{\tilde{F}}{\phi} \right)_T , \tag{1.41}$$

where we have taken $F = v_m \, n_m \, \tilde{F}/\phi$ and $n_s = (1 - \phi) n_m v_m / \phi v_s$. Thus, chemical equilibrium of a hydrogel in contact with pure solvent requires that $\Pi = 0$. This

equilibrium condition can be modified through the addition of hydrostatic pressure so that $\Pi(T,\phi) = \text{const.}$, which may be inverted, leading to $\phi(T)$ "isobars."

Using the free-energy density from the Flory-Rehner theory, Eq. (1.39), we find that

$$\Pi(\phi,T) = \frac{k_B\,T}{v}\left[\frac{\nu_0\,v}{2}\left(\frac{\phi}{\phi_0} - 2\left(\frac{\phi}{\phi_0}\right)^{1/3}\right) - \phi - \ln(1-\phi) - \chi(T)\,\phi^2\right], \qquad (1.42)$$

which has a scale for Π set by the energy density k_BT/v. The dimensionless parameter $\nu_0\,v$ is an effective cross-linker fraction and sets the relative contribution of the polymer network's elasticity. Expanding Eq. (1.42) in powers of ϕ yields

$$\Pi(\phi,T) = \frac{k_B\,T}{v}\left[\frac{\nu_0\,v}{2}\left(\frac{\phi}{\phi_0} - 2\left(\frac{\phi}{\phi_0}\right)^{1/3}\right) + \frac{1}{2}\big(1-2\chi(T)\big)\,\phi^2 + \sum_{m=3}^{\infty}\frac{\phi^m}{m}\right], \quad (1.43)$$

which we recognize, ignoring the non-analytic cube root, as a virial expansion of Π (see e.g., [23]). The term linear in ϕ is proportional to the chain density and results, at low ϕ, in an "ideal gas" of cross-linked chains. The second virial coefficient is $(1-2\chi(T))/2$, consistent with the characterization of the interaction energy in terms of the Flory parameter χ. Note that this term disappears for $\chi = 1/2$, resulting in a ϑ-solvent; see § 1.1. As seen in Fig. 1.5a, $\Pi = 0$ has a solution $\phi(\chi)$ that varies continuously from swollen (smaller ϕ, larger volume) to deswollen (larger ϕ, smaller volume) as the solvent quality is brought from good (i.e., $\chi < 1/2$) to poor (i.e., $\chi > 1/2$).

However, there are polymer gels, including pNIPAM [3], that possess a *discontinuous* transition for $\Pi = 0$ that cannot be realized within the model presented so far. A resolution lies in the Erman-Flory theory [22], which adds parameters in a virial expansion of the osmotic pressure, i.e.,

$$\Pi(\phi,T) = \frac{k_B\,T}{v}\left[\cdots + \frac{1}{2}\big(1-2\chi_1\big)\,\phi^2 + \frac{1}{3}\big(1-3\chi_2\big)\,\phi^3 + \cdots\right], \qquad (1.44)$$

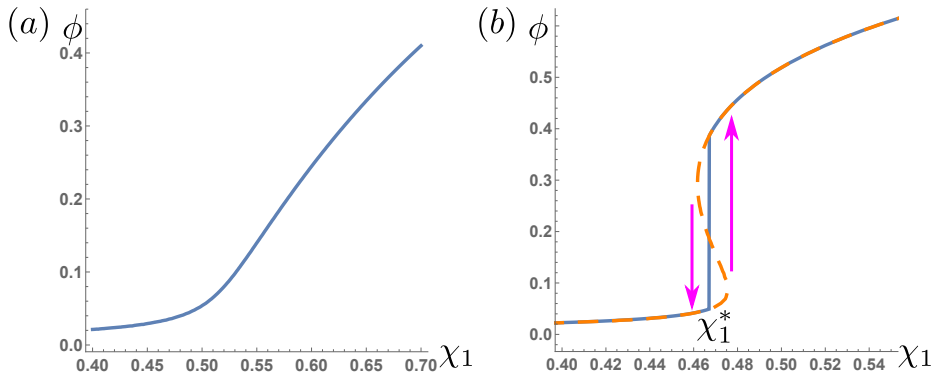

Figure 1.5: Equilibrium volume fraction $\phi(\chi_1)$ for a gel with (a) continuous transition where $\chi_2 \equiv 0$ and (b) discontinuous transition where $\chi_2 \equiv 0.56$ [24], both with $\phi_0 \equiv 0.1$ and $\nu_0 v \equiv 10^{-4}$.

where the Flory parameter χ is expanded in powers of the volume fraction, i.e.,

$$\chi(T, \phi) = \chi_1 + \chi_2 \phi + \cdots \tag{1.45}$$

and $\chi_1, \chi_2, \ldots$ are empirically determined parameters. Gels that exhibit a discontinuous volume transition can be well modeled by keeping χ_2 constant and using $\chi_1(T)$ as the solvent quality parameter [24, 25], as shown in Fig. 1.5b. The discontinuity in $\phi(\chi_1)$ is due to the emergence of a *second* free-energy minimum, which constitutes a *metastable equilibrium state*, as well as an unstable equilibrium, as shown in Fig. 1.6. Due to thermal fluctuations, an unconstrained sample of gel should always reach its global free-energy minimum, with a cross-over in equilibrium volume fraction occurring when the two free-energy minima are equal, which occurs at $\chi_1 = \chi_1^*$. Realistically, the gel remains in a metastable state near the cross-over, leading to a hysteresis effect, where the deswelling transition for a swollen gel occurs at a value of χ_1 that exceeds χ_1^* and the swelling transition for a deswollen gel occurs at one that lies below χ_1^*.

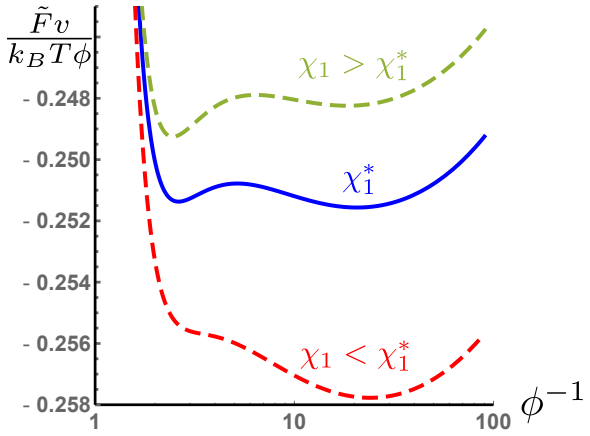

Figure 1.6: The total free-energy with multiple equilibria for the three cases in the vicinity of the transition value of χ_1^* the Flory parameter χ_1.

1.6 At the critical point: complication of shear rigidity

We compete this chapter by examining the gel's thermodynamic stability to *inhomogeneous perturbations*, highlighting one way in which the polymer network's shear rigidity alters the intuition gained from studying the thermodynamic description of fluids. The stability is determined by second variations of the gel's total free-energy F with respect to the gel's configuration. For an inhomogeneous gel, the free-energy density $\tilde{F}$ varies from point to point. As $\tilde{F}$ is a density with respect to the target space $\mathcal{T}$, we can approximate F as a sum of $\tilde{F}(\mathbf{R})$ over small volumes d^3R, so that

$$F = \int_{\mathbf{T}} \mathrm{d}^3R\, \tilde{F}(\mathbf{R})\,. \tag{1.46}$$

Note that there are generally additional terms that depend on the gradient of the state functions, which are not seen in the homogeneous theory; we consider the limit in which variations of these state functions are small enough to be ignored (see § 2.4.1 for a more detailed discussion). Variations in the hydrogel's configuration result in changes in $\mathcal{T}$ so we find it convenient to define an equivalent free-energy density on

the reference space $\mathcal{R}$ via

$$F = \int_{\mathcal{R}} \mathrm{d}^3 r \, \mathcal{F}(\mathbf{r}) \,, \tag{1.47}$$

where $\mathbf{r} \in \mathcal{R}$ so that $\mathcal{F}(\mathbf{r})/\phi_h \equiv \tilde{F}(\mathbf{R}(\mathbf{r}))/\phi(\mathbf{R}(\mathbf{r}))$.

Consider a gel that is in equilibrium with pure solvent, and has a homogeneous equilibrium volume fraction ϕ_h. We will determine the stability of the gel by calculating the second variation of the free-energy $\delta^2 F$ in two different ways. In first calculation, we consider variations in the volume fraction ϕ whilst fixing the gel to be isotropic, so $\tilde{\Lambda} = \mathbb{1}$. In our second calculation, we relax the isotropy constraint and consider inhomogeneous variations of the gel's shape. We conclude the difference in the two calculations is a hallmark of the gel's shear rigidity.

First, we consider variations of the volume fraction ϕ of the form

$$\phi(\mathbf{r}) = \phi_h + \delta\phi(\mathbf{r}) \,, \tag{1.48}$$

whilst constraining the gel to remain isotropic everywhere, so $\hat{\Lambda} = \mathbb{1}$. Then the deformation matrix, expanding to second order in inhomogeneous variations $\delta\phi(\mathbf{r})$, is given by

$$\Lambda = \left(\frac{\phi_0}{\phi}\right)^{1/3} \mathbb{1} \approx \left(\frac{\phi_0}{\phi_h}\right)^{1/3} \left(1 - \frac{1}{3}\frac{\delta\phi}{\phi_h} + \frac{2}{9}\left(\frac{\delta\phi}{\phi_h}\right)^2\right) \mathbb{1} \,, \tag{1.49}$$

which allows us to compute the second variations of the free-energy F as

$$\delta^2 F|_{\phi_h} = \frac{1}{2} \int_{V_h} \mathrm{d}^3 r \, \left.\frac{\partial^2 \mathcal{F}}{\partial \phi^2}\right|_{\phi=\phi_h} \delta\phi^2 \,. \tag{1.50}$$

Thus, the thermodynamic stability of the gel requires that

$$\begin{aligned} \left.\frac{\partial^2 \mathcal{F}}{\partial \phi^2}\right|_{\phi_h} &= \left.\frac{\partial^2}{\partial \phi^2}\frac{\phi_h \tilde{F}}{\phi}\right|_{\phi_h} = \left.\frac{\phi_h}{\phi^3}\left[\phi\frac{\partial \Pi}{\partial \phi} - 2\Pi\right]\right|_{\phi_h} \\ &= \left.\frac{\phi_h}{\phi^3}\left[K - 2\Pi\right]\right|_{\phi_h} = \frac{1}{\phi_h^2} K > 0 \end{aligned} \tag{1.51}$$

where K is the *osmotic bulk modulus* and we have noted that in equilibrium, $\Pi = 0$. Thus stability breaks down for vanishing K, i.e., diverging compressibility. As a diverging response function is the signature of critical phenomena, it follows that $K = 0$ marks a critical point for a homogeneous equilibrium gel.

The foregoing argument relies on a spatial modulation of the gel's volume fraction that *does not shear the gel* so that the deformation matrix is given by Eq. (1.49). However, it is not clear that the gel can achieve a deformed shape described by the points $\mathbf{R}(\mathbf{r})$ such that $\Lambda_{ij}(\mathbf{r}) = (\phi_0/\phi_h)^{1/3}\partial R_i/\partial r_j = (\phi_0/\phi(\mathbf{r}))^{1/3}\delta_{ij}$. As was shown by Onuki [26] and later by Golubović and Lubensky [27], the critical point for elastic materials that undergo a volume transition is not $K = 0$ but rather $K + (4/3)\mu = 0$, where μ is the shear modulus of the gel. To see this, consider fluctuations in shape characterized by a displacement field $\mathbf{R} - \mathbf{r} \equiv \mathbf{u}(\mathbf{r})$, which results in a deformation matrix

$$\Lambda_{ij} = \left(\frac{\phi_0}{\phi_h}\right)^{1/3}\left[\delta_{ij} + \frac{\partial u_i}{\partial x_j}\right] . \tag{1.52}$$

By expanding the free-energy to quadratic order in the strain $u_{ij} = (u_i/\partial r_j + u_j/\partial r_i)/2$, we find that the second variation of the free energy has a linear elastic form given by

$$\delta^2 F = \frac{1}{2}\int_{V_h} \mathrm{d}^3 r \left[2\mu u_{ij}u_{ij} + \left(K - \frac{2}{3}\mu\right)u_{ii}^2\right] \tag{1.53}$$

where $\mu \equiv \nu_0(\phi_h/\phi_0)^{1/3}$. Integrating by parts and taking the boundary of the gel to be at infinity (or, equivalently, assuming that we are considering small strain fluctuations deep within the bulk of the gel) we find that

$$\delta^2 F = -\frac{1}{2}\int_{V_h} \mathrm{d}^3 r\ \mathbf{u}\cdot\left[-\mu\boldsymbol{\nabla}\times\boldsymbol{\nabla}\times\mathbf{u} + \left(K + \frac{4}{3}\mu\right)\boldsymbol{\nabla}\boldsymbol{\nabla}\cdot\mathbf{u}\right] . \tag{1.54}$$

Decomposing the displacement field into $\mathbf{u} = \mathbf{u_t} + \mathbf{u}_{||}$, i.e., the (divergence-free, $\boldsymbol{\nabla}\cdot\mathbf{u_t} = 0$) transverse part and the (curl-free, $\boldsymbol{\nabla}\times\mathbf{u}_{||} = 0$) longitudinal part,

the fluctuations in the gel's shape are decomposed into transverse excitations, with modulus $\mu > 0$, and longitudinal excitations, with modulus $K + (4/3)\mu$. As the transverse excitations are divergence free, the longitudinal excitations reflect inhomogeneous variations in the gel's volume fraction. Thus, in order for this true critical point to be reached, the bulk modulus must become negative with a magnitude large enough to compensate for the added shear modulus. Note, however, that we have neglected the effect of the boundary, which generally complicates the decomposition into transverse and longitudinal parts. Interestingly, we can therefore expect that the gel's shape can have an impact on defining its critical point; this too is a consequence of the shear rigidity.

In the following, we explore another case in which the shear rigidity leads to important consequences for its thermodynamics. We will consider how constrained, phase-coexistent equilibria couple to the shape of the gel.

CHAPTER 2
BENDING INSTABILITY OF RAPIDLY HEATED POLYMER GEL RODS

2.1 Introduction: polymer gels with a volume constraint

In the previous chapter, we discussed how polymer gels swell in the presence of a solvent in order to attain an osmotic equilibrium. This relies on the gel's porous boundary which allows passage of solvent molecules between its interior and a surrounding bath. Furthermore, any *quasistatic* change in the solvent quality, e.g. through small changes in temperature, alters the osmotic equilibrium and thus changes the gel's volume due to losing or gaining solvent molecules. We also introduced gels that undergo a discontinuous volume phase transition between a large-volume swollen phase and a small-volume deswollen phase, exemplified by the hydrogel pNIPAM, which enters its deswollen phase when heated past its transition temperature of $\sim 32^{\circ}$C. When the gel undergoes homogeneous changes in volume fraction, it simply changes its volume by *affine* rescaling, without otherwise distorting its shape. However, when the gel undergoes inhomogeneous changes in volume fraction, there are shape distortions beyond a simple rescaling due to the shear rigidity, which we demonstrated by showing that the critical point for the volume phase transition, indicated by a diverging compressibility, is modified by a finite shear modulus. Now we will address what happens to a swollen gel when the change in solvent quality is no longer performed in a quasistatic manner but as a sudden impulse, resulting in a period of arrested deswelling and constrained volume.

As many physical processes happen far from the quasistatic limit, understanding the behavior of systems brought across a phase transition is of fundamental and

practical importance. For example, for systems that undergo a "rapid quench" from a disordered phase to an ordered phase spawn a variety topological defects, e.g. vortices in superfluids, due to spontaneous symmetry breaking at different points in space that, for short times after the quench, are not causally related [28]. The distribution of similarly generated is thought to play a key role in providing structure to the universe after rapidly cooling from big bang conditions [29, 30] and has been studied in soft matter in the context of a quench from isotropic to nematic order in liquid crystals [31, 32]. For swollen of polymer gels, rapid changes in solvent quality reveal complicated equilibration dynamics due to increased polymer-solvent friction that restricts solvent flow at higher volume fraction. For example, swollen hydrogel spheres of pNIPAM that are rapidly heated past the transition temperature have a prolonged period during which the volume is preserved [3]. This is due to the formation of a thin deswollen skin on the gel's outer surface which halts the flow of solvent and *arrests* deswelling. The resulting anisotropic stress of the stretched polymer network leads to a mechanical equilibrium that is unstable and results in buckling of the gel's surface, forming alternating patterns of thin and thick deswollen skin that deforms the gel, ballooning the surface outwards at the thinner parts and creasing it at the thicker.

2.1.1 Internal phase separation from rapid quench

During the prolonged period of arrested deswelling due to the formation of the deswollen skin, the remainder of the hydrogel equilibrates *under a global volume constraint*. Macroscopically, as the total solvent inside the gel is conserved, equilibration no longer requires chemical or osmotic equilibrium with the solvent bath. Instead, equilibration must happen at fixed volume, as shown schematically in Fig. 2.1. However, as the gel is now in a poor solvent, the polymer *locally* favors a packed state with high ϕ that it cannot achieve homogeneously; the only recourse is to undergo inhomogeneous changes in volume fraction, leading to *internal phase separation* and

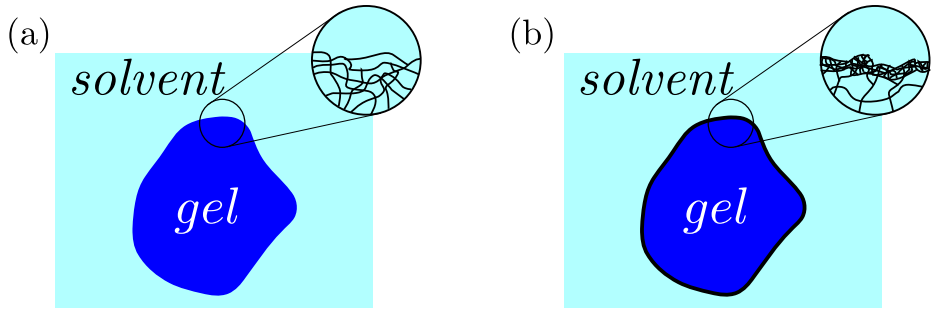

Figure 2.1: Polymer gel in two situations: (a) allowed to exchange solvent with surroundings, where equilibrium condition is imposed by constant chemical potential or osmotic pressure; (b) solvent exchange blocked by thin de-swollen skin after rapid heating, leading to constrained equilibration at constant volume.

the formation of solvent-rich and solvent-poor domains.

To describe the inhomogeneous gel, we choose the reference state $\mathcal{R}$ to correspond to the homogeneous gel at volume fraction ϕ_h. We can define the deformation matrix Λ as

$$\Lambda_{ij} = \frac{\partial R_i}{\partial r_j} \tag{2.1}$$

rather than the definition used in the previous chapter which was in reference to the relaxed state of the polymer matrix at ϕ_0. The total free-energy is

$$F = \int_{\mathcal{R}} \mathrm{d}^3 r \left[\frac{1}{2} \mu \ \mathrm{tr}\ \Lambda^T \Lambda + \mathcal{F}_{\mathrm{rem}}(\phi) \right] \tag{2.2}$$

where the shear modulus is $\mu = \nu_0 (\phi_h / \phi_0)^{1/3}$ in the Flory-Rehner theory and $\mathcal{F}_{\mathrm{rem}}(\phi)$ is the remaining free-energy density that depends on the volume fraction ϕ alone. Note that this free-energy and our ensuing analysis are in fact independent of the Flory-Rehner Eq. (1.39) or any microscopic theory and completely general for materials with shear rigidity and a volume phase transition: instead of the volume fraction ϕ, the invariant $I_3 = \det \Lambda$ may be used, generalizing Eq. (2.2) to a nonlinear elastic description of a material.

The target state $\mathcal{T}$ refers to the constrained equilibrium state, after the impulsive

change in solvent quality, e.g. by heating the gel rapidly. Assuming that the amount of solvent that has left the gel during formation of the thin skin is insubstantial, arrested deswelling results in a conservation of the total solvent

$$\int_{\mathcal{T}} \mathrm{d}^3 R \, (1 - \phi) = \int_{\mathcal{R}} \mathrm{d}^3 r \, (1 - \phi_h) \, . \tag{2.3}$$

As the total amount of polymer is unchanged, the solvent constraint above is equivalent to a volume constraint

$$V - V_h = \int_{\mathcal{T}} \mathrm{d}^3 R - \int_{\mathcal{R}} \mathrm{d}^3 r = \int_{\mathcal{R}} \mathrm{d}^3 r \, (\det \Lambda - 1) = \int_{\mathcal{R}} \mathrm{d}^3 r \left(\frac{\phi_h}{\phi} - 1 \right) = 0 \, . \tag{2.4}$$

Due to the volume constraint, in order for part of the gel to deswell and locally lower its free-energy, another part of the gel has to swell further, locally increasing its free-energy. If we ignore the shear rigidity of the contiguous polymer network, the result is the formation of a homogeneous solvent-poor region with volume fraction $\phi_p > \phi_h$ and a homogeneous solvent rich region with volume fraction $\phi_r < \phi_h$. In fact, this is analogous to the constrained phase separation of water into liquid and vapor phases with the equilibrium values of ϕ_p and ϕ_r determined by (i) a common tangent construction, detailing mechanical and chemical equilibrium, and (ii) a lever rule, specifying the portion of the total volume occupied by each phase; for more details, refer to Appendix A. Thus, we can partition the reference space $\mathcal{R}$ into two domains: the solvent-poor region $\mathcal{R}_p$, occupying a fraction f of the total volume, and the solvent-rich region $\mathcal{R}_r$ occupying the remaining $1 - f$ of the total volume. The volume constraint Eq. (2.4) reduces to

$$f \left(\frac{\phi_h}{\phi_p} - 1 \right) + (1 - f) \left(\frac{\phi_h}{\phi_r} - 1 \right) = 0 \tag{2.5}$$

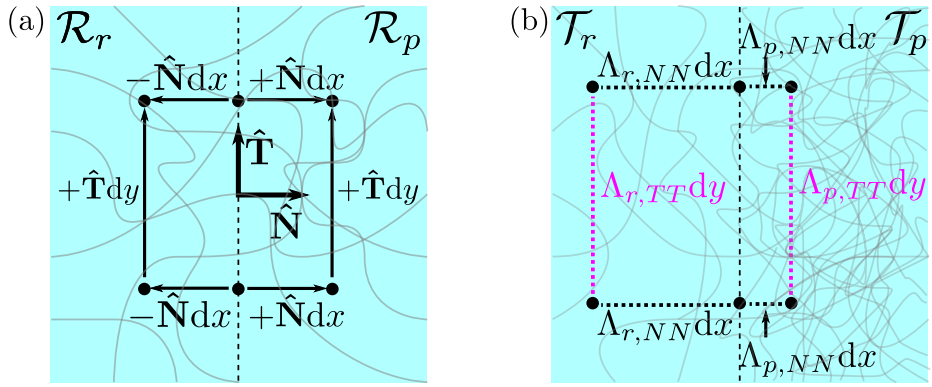

Figure 2.2: (a) Points in the reference space, the homogeneous gel, a distance dx normal $\hat{\mathbf{N}}$ to the interface and a distance dy from each other tangential $\hat{\mathbf{T}}$ to the interface. (b) Same points in the target space, the deformed gel, are mapped to different distances from the interface in each phase but are stretched the same distance tangential to the interface, requiring $\Lambda_{r,TT} = \Lambda_{p,TT}$.

yielding a lever rule

$$f = \frac{\phi_r^{-1} - \phi_h^{-1}}{\phi_r^{-1} - \phi_p^{-1}} \tag{2.6}$$

that corresponds exactly to the lever rule in fluid systems. Whilst the lever rule is a consequence of mass and volume conservation and therefore independent of the gel's shear rigidity, the mechanical and chemical equilibrium equations no longer satisfy a simple common tangent construction.

For a hydrogel to remain contiguous across a phase interface, the two phases stretch the same amount along the interface. Therefore, in addition to a balance of stress and chemical potential, the deformation matrix Λ satisfies a lamination condition where its tangential components must be continuous at the interface; see Fig. 2.2. As a consequence of the gel's shear rigidity, the deformation caused by the interface leads to long-range distortion of the polymer matrix. Phase coexistence of gels is thus profoundly affected by sample shape and the common tangent construction holds true only in the limiting case of a one-dimensional gel [33].

2.1.2 Geometry and phase coexistence

For a fluid system with phase coexistence between liquid and vapor phases, thermodynamics predicts the densities and fraction of the two phases but not their shape or spatial arrangement; additional physics must be considered. From experience, we know that the liquid phase accumulating "downward" at the "bottom" of the container. This is due to gravity breaking the isotropy of space so that the denser phase is pulled in one direction, displacing the less dense phase. In the case of polymer gels, the two phases are not distinguished by mass but rather by packing of polymers as the gel is mainly composed of water and polymer with assumed negligible free volume. Due to the gel's shear rigidity, inhomogeneous deformations to the polymer matrix require stress balance which depends on gel shape. Thus, we expect that gel shape can influence the organization of solvent-rich and solvent-poor domains. The boundary of the gel breaks *translational* symmetry and consequently provides a location for the deswollen phase to form. As the surface skin is deswollen, we expect that the solvent-poor phase will "grow" from the boundary inward, resembling heterogeneous nucleation as the free-energy cost of creating interface between two phases is less when grown from an inhomogeneity or a surface.

Rapid heating of spheres [3] and cylinders [34] each exhibit the formation of a surface layer that buckles after some time. However, both of these geometries are have uniform boundaries and the arrangement of solvent-rich and solvent-poor regions conforms to the boundary shape until buckling breaks symmetry. Note that we are ignoring the effect of cylinder end-caps which break translational symmetry and are known to deswell before the middle section of the cylinder in the case of *unconstrained*, "triphasic equilibrium" [22, 24] of swollen and deswollen phases with pure solvent. Toroids, on the other hand, may be thought of as bent cylinders that curve about an axis of revolution. By having a *ring curvature*, the symmetry of its cylindrical cross-section is broken so that we may describe directions as "towards the axis" or "away

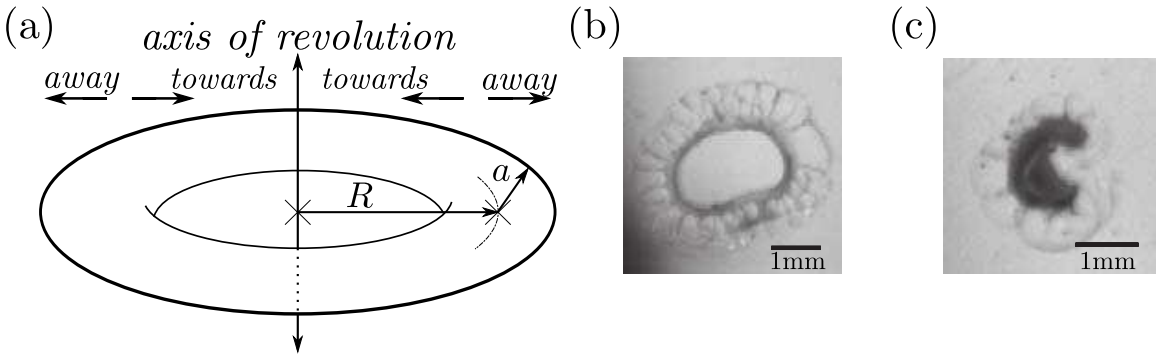

Figure 2.3: (a) Toroid schematic with ring radius R and tube radius a as well as designation of directions "towards" and "away" from axis of revolution. (b) Image showing the solvent rich phase shrinking towards the axis. (c) Image showing "Pringling" of the toroid. Experimental images from [35].

from the axis;" see Fig. 2.3a. Rapid heating experiments performed on pNIPAM hydrogel toroids show that the distribution of solvent-rich and solvent-poor domains is indeed related to the broken symmetry direction of the toroid [35]. As shown in Fig. 2.3b, the solvent-poor phase forms towards the axis of revolution, displacing the solvent-rich phase away from the axis. We can understand this simply by observing that a toroid that is allowed to fully deswell will do so by undergoing affine rescaling, decreasing its volume without shearing its polymer network, and thus decreases its ring radius, shrinking towards the axis; a toroid that is allowed to swell will grow away from the axis. A phase-coexistent toroid, complicated by coherency strains between the two phases, should nonetheless have a solvent-poor region that shrinks towards the axis in order to minimize the shear deformation of its polymer network and a solvent-rich region that swells away for the same reason.

This internal phase separation further has the consequence of buckling the toroid in a manner that results in large deflections, for example resulting in the "Pringle" shape of Fig. 2.3c. Variation in the swelling stress across the cross-section of the toroid result in a *swelling torque* acting on the center-of-mass of the cross-section, which buckles the toroid above a threshold set by the shear rigidity. We therefore have a situation where (i) the spatial arrangement of coexistent phases is influenced

by geometry which (ii) leads to deformation of the gel, changing its geometry.

To better understand and formalize this picture, we consider a generalization of the toroid geometry to one of a rod, with circular cross-section, that is allowed to curve in space. The geometry of the rod is set by a centerline, a space curve as in Fig. 2.6b, which is simply a planar ring in the case of a toroid.

2.1.3 Outline of the theory for curved polymer gel rods

To determine the effect of curvature and torsion on gel rods, we greatly simplify the problem by considering the limit of slender rods, where the tube radius a is much smaller than the rod length L as well as any variation of the rod along its length, e.g. the radius of curvature and torsion, κ^{-1} and τ^{-1}, where κ and τ are the centerline curvature and torsion as defined in Appendix B. This allows us to treat curvature and torsion of the rod as contributing small corrections κa, τa to the free-energy. Corrections to the deformation matrix that depend on the curvature and torsion are taken to be small, resulting in a small strain field that is superimposed on a background of an un-curved rod that has undergone internal phase separation. Furthermore, we expect that the phase interface breaks the cross-section's symmetry in response to the rod's curvature.

We will proceed by first determining the phase coexistent equilibrium of a straight cylindrical rod of circular cross-section, yielding volume fractions ϕ_p and ϕ_r for the two phases as well as deformation matrices Λ_p and Λ_r. Next, we will introduce small variations in the geometry of the rod, both for the reference state $\mathcal{R}$ and the target state $\mathcal{T}$, allowing the rod to be curved in the homogeneous state prior to the rapid heating and for the rod to change its shape in equilibrium; we will also vary the interface shape. Expanding the free-energy to quadratic order in the inhomogeneous strain about a background of the symmetric straight rod leads to a linear elasticity calculation for the equilibrium strain field in terms of rod and interface

geometry. Integrating out the cross-section strain variation, we arrive at an effective one-dimensional elastic model coupling rod shape to interface shape. Crucially, we find that the interface shape is coupled to rod curvature in a manner that "polarizes" the coaxial arrangement of solvent-rich and solvent-poor regions, resulting in a larger distribution of solvent-poor region towards the axis. Furthermore, we find that this polarization unstable to spontaneous symmetry breaking.

This motivates us to develop a Landau theory in the next chapter to predict the equilibrium shape of the rod in terms of a vector order parameter characterizing the polarization of the solvent distribution. We find that the spontaneous symmetry breaking leads to an ordered "ferromagnetic" phase of constant rod curvature which supports spin wave-like Goldstone modes that describe modulations in the curvature direction of the rod. As a result, we find that the spin wave rigidity is related to the rod's torsional rigidity. We end by speculating that the presence of these "twist modes" may be seen experimentally and that our model may lead to a new approach for programming shape change in hydrogel rods.

2.2 Phase coexistence in the case of a straight cylinder

We seek the constrained, phase-coexistent equilibrium specific to a swollen cylinder of circular cross section that has undergone rapid heating. In particular, we will determine the equilibrium state that maintains the translational and axial symmetry of the cylinder, addressing the *stability* this symmetric equilibrium later. Using the initial swollen state as the cylinder's reference configuration, we take advantage of the cylinder's symmetry and use cylindrical coordinates $\{\rho, \theta, z\}$ so that the equilibrium configuration is a mapping to cylindrical coordinates in the target space $\{P, \Theta, Z\}$, as shown in Fig. 2.4. Cylindrical symmetry of the reference and deformed configuration requires that

$$P = P(\rho), \quad \Theta = \theta, \quad Z = \Lambda_\ell z \tag{2.7}$$

where Λ_ℓ is the ratio of the deformed length to the initial length. The deformation matrix is, in cylindrical coordinates,

$$\Lambda = \begin{bmatrix} \frac{\mathrm{d}P}{\mathrm{d}\rho} & 0 & 0 \\ 0 & \frac{P}{\rho} & 0 \\ 0 & 0 & \Lambda_\ell \end{bmatrix} \tag{2.8}$$

or, $\Lambda = (\mathrm{d}P/\mathrm{d}\rho)\hat{\mathbf{P}} \otimes \hat{\boldsymbol{\rho}} + (P/\rho)\hat{\boldsymbol{\Theta}} \otimes \hat{\boldsymbol{\theta}} + \Lambda_\ell \, \hat{\mathbf{Z}} \otimes \hat{\mathbf{z}}$.

The phase coexistent regions are coaxial, forming an interface at $P = P_b$ in the target space, which we map to $\rho = b$ in the reference space. As deswelling initially occurs at the gel's outside surface, we can assume that the solvent-poor region corresponds $b < \rho \leq a$, resulting in a layer of thickness $h = a - b$, with $\rho \leq a$ the solvent-rich region. To simplify the problem, we take the thin solvent-poor layer limit $h/a \ll 1$, so $f \approx 2h/a \ll 1$. By the lever rule Eq. (2.6), this corresponds with an initially highly swollen gel with $\phi_h \ll 1$ and a solvent-rich region that is almost unchanged from its initial volume fraction, $\phi_r \approx \phi_h$. By treating the solvent-poor region as very thin, we can neglect any variation of the deformation matrix along its thickness. Taylor expanding $P(\rho)$ in the solvent poor region,

$$P(\rho) \approx P(b) + (\rho - b)\Lambda_n + \mathcal{O}(h^2) \tag{2.9}$$

where $\rho - b \sim \mathcal{O}(h)$ and Λ_n is the first derivative of P at b. The resulting deformation matrix is, to leading order,

$$\Lambda_p = \begin{bmatrix} \Lambda_n & 0 & 0 \\ 0 & \Lambda_t & 0 \\ 0 & 0 & \Lambda_\ell \end{bmatrix} \tag{2.10}$$

where Λ_n is identified as the ratio of the deformed layer thickness to the original h

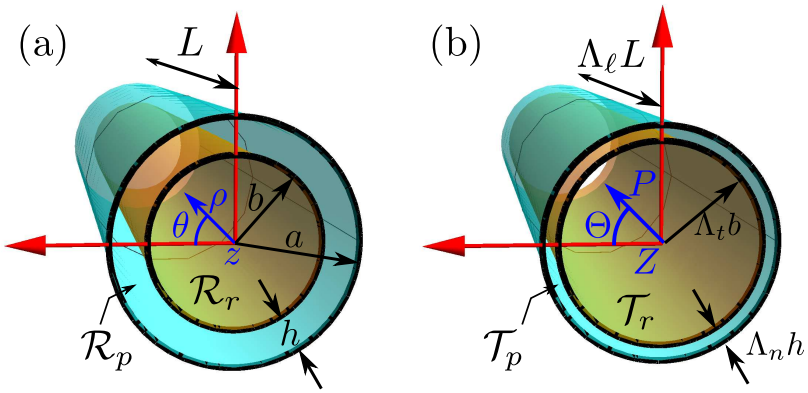

Figure 2.4: Schematic of phase-separated cyinder (a) before and (b) after deformation along with cylindrical coordinates.

and $\Lambda_t \equiv P(b)/b$ is the stretch of the interface, transverse to the cylindrical axis.

For the solvent rich region, we can likewise assume a power series expansion of $P(\rho)$. By the lamination condition, the transverse stretch of the interface has to be continuous so $P(b)/b = \Lambda_t$. If we truncate the series expansion at linear order, $P(\rho) \approx \Lambda_t\, \rho + \ldots$, then

$$\Lambda_r = \begin{bmatrix} \Lambda_t & 0 & 0 \\ 0 & \Lambda_t & 0 \\ 0 & 0 & \Lambda_\ell \end{bmatrix} \tag{2.11}$$

so that the deformation matrix is constant throughout the solvent rich region. We will make this approximation as it is consistent with the lamination condition and allows for the designation of two volume fractions

$$\phi_p \approx \frac{\phi_h}{\Lambda_n\, \Lambda_t\, \Lambda_\ell}, \quad \phi_r \approx \frac{\phi_h}{\Lambda_t^2\, \Lambda_\ell} \tag{2.12}$$

while describing free-energy cost due to an anisotropic coherency strain via the deformations Λ_t and Λ_ℓ, and thus captures the essential physics of the problem.

After changing variables from $(\Lambda_n, \Lambda_t, \Lambda_\ell)$ to $(\phi_r, \phi_p, \Lambda_\ell)$, the total free-energy is

for the cylinder is

$$\begin{aligned}\frac{F_{\rm cyl}}{\pi\, a^2} =&(1-f)\left[\frac{1}{2}\mu\left(\Lambda_\ell^2+2\frac{\phi_h}{\phi_r\,\Lambda_\ell}\right)+\mathcal{F}_{\rm rem}(\phi_r)\right]\\ &+f\left[\frac{1}{2}\mu\left(\Lambda_\ell^2+\phi_h\frac{\phi_p^{-2}+\phi_r^{-2}}{\phi_r^{-1}\,\Lambda_\ell}\right)+\mathcal{F}_{\rm rem}(\phi_p)\right]\\ &+p\left[(1-f)\frac{\phi_h}{\phi_r}+f\,\frac{\phi_h}{\phi_p}-1\right]\end{aligned} \tag{2.13}$$

where p is a Lagrange multiplier that enforces the volume constraint and represents a constraining pressure exerted by the thin skin. Equilibrium is determined by the stationary condition $\delta F_{\rm cyl}=0$, yielding, to leading order in f, stress equilibrium equations

$$\Lambda_\ell^3-(1-f)\frac{\phi_h}{\phi_r}-f\,\phi_h\,\frac{\phi_p^{-2}+\phi_r^{-2}}{2\phi_r^{-1}}=0 \tag{2.14}$$

$$\frac{\phi_r^2}{\phi_h}\,\frac{\partial\mathcal{F}_{\rm rem}}{\partial\phi_r}-\mu\,\frac{1}{\Lambda_\ell}+f\,\mu\,\frac{1+\phi_r^2/\phi_p^2}{2\,\Lambda_\ell}=p \tag{2.15}$$

$$\frac{\phi_p^2}{\phi_h}\,\frac{\partial\mathcal{F}_{\rm rem}}{\partial\phi_p}-\mu\,\frac{\phi_r}{\phi_p\,\Lambda_\ell}=p \tag{2.16}$$

as well as a chemical equilibrium equation

$$\mathcal{F}_{\rm rem}(\phi_r)-\mathcal{F}_{\rm rem}(\phi_p)+\frac{1}{2}\mu\,\left(\frac{\phi_h}{\phi_r}-\frac{\phi_h\,\phi_r}{\phi_p^2}\right)=-p\left(\frac{\phi_h}{\phi_r}-\frac{\phi_h}{\phi_p}\right) \tag{2.17}$$

and the lever rule Eq. (2.6).

Using Flory-Rehner to provide a definite form for the gel free-energy, we find that there are indeed solutions to the above system of equations for physically relevant parameters. Using $\mu=10^{-4}k_BT/v$ and $\chi_2=0.56$ our results are shown in Fig. 2.5 for $\phi_h\in\{0.010,0.015,0.020\}$, i.e. cases of gels that are very swollen prior to rapid heating. As expected, at the onset of phase coexistence, the change in solvent-rich volume fraction is very small whereas the change in solvent-poor volume fraction is quite dramatic. While the values for f shown can become substantial for larger χ_1,

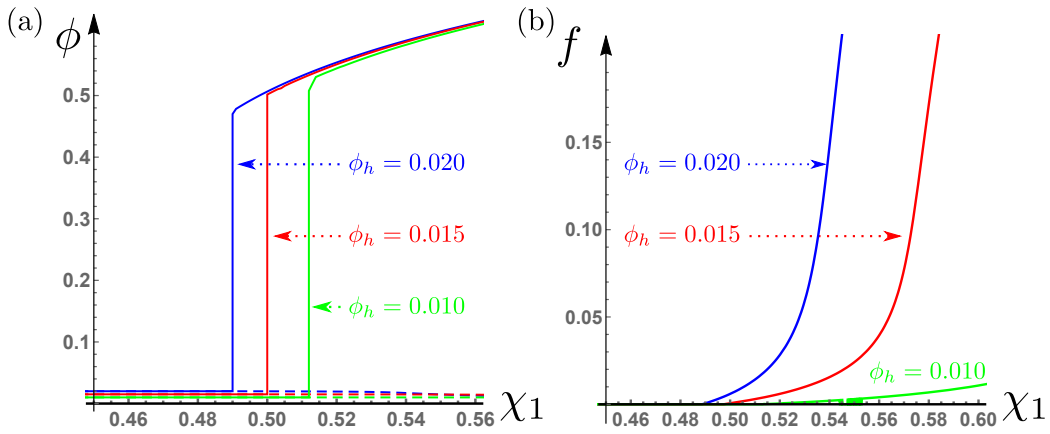

Figure 2.5: (a) Values of ϕ_p (solid) and ϕ_r (dashed) after constrained phase separation as a function of χ_1. (b) Fraction of solvent-poor phase in the reference state f.

the equilibrium equations hold only for small f.

2.3 Phase coexistence in a broken-symmetry rod

Now that we know how to solve for the equilibrium of a straight, symmetric cylinder that maintains its symmetry throughout phase separation, we address the problem of breaking axial symmetry through (i) interface shape $b \mapsto b(\theta) \equiv b_0(1 + \Gamma(\theta))$ and (ii) curving the centerline; Fig. 2.6 is representative of such a symmetry-broken configuration. Whereas the symmetric cylinder is described by a deformation matrix of purely radial dependence, $\Lambda_0(\rho)$, which we have approximated as piecewise, $\Lambda_0 = \Lambda_r + (\Lambda_p - \Lambda_r)\Theta(\rho - b)$, the broken-symmetry deformation matrix depends on θ. If the rod curves gently, we expect that the θ-dependence is contained in a small correction to Λ_0; the same can be assumed for small interface anisotropy Γ. Therefore, we will use the symmetric equilibrium obtained in the previous section as a "vacuum" configuration on which we will superimpose a small, inhomogeneous deformation field due to symmetry breaking.

We decompose the deformation matrix as

$$\Lambda = \Lambda_{\text{int}}\, \Lambda_{\text{ext}}\, \Lambda_0 \tag{2.18}$$

where Λ_{ext} is the deformation due to specifying a curved rod shape for the hydrogel, which is held fixed as an *external* constraint. In response, the hydrogel undergoes *internal* deformations, Λ_{int}, in order to achieve equilibrium. As Λ_{ext} and Λ_{int} represent small deformations composed with the large deformation Λ_0 due to phase separation, we can expand $\Lambda_{\text{ext}} = \mathbb{1} + u_{\text{ext}}$ and $\Lambda_{\text{ext}} = \mathbb{1} + u_{\text{int}}$, where u_{ext} and u_{int} are small, *inhomogeneous* strain fields.

To determine the strain, consider a sequence of configurations

$$\begin{array}{ccccc} \mathcal{R} & \xrightarrow{\Lambda_1} & \mathcal{R}' & \xrightarrow{\Lambda_2} & \mathcal{T} \\ \mathbf{r} & \mapsto & \mathbf{r}' & \mapsto & \mathbf{R} \end{array}$$

where points $\mathbf{R}$ in the target space ($\mathcal{T}$) are related to points $\mathbf{r}'$ in an intermediate deformed reference space ($\mathcal{R}'$) via an equilibrating displacement field $\mathbf{u}$

$$\mathbf{R}(\mathbf{r}') = \mathbf{r}' + \mathbf{u}(\mathbf{r}') \tag{2.19}$$

where $\mathbf{u}(\mathbf{r}')$ is a vector field defined on $\mathcal{R}'$. This sort of decomposition is used when a material undergoes a large plastic deformation Λ_1, followed by a small elastic deformation Λ_2. Therefore deformation matrix $\Lambda_{2,\mu\nu} = \nabla'_\nu R_\mu = \delta_{\mu\nu} + \nabla'_\nu u_\mu = \Lambda_{\text{int}}$ is the internal deformation matrix so $u_{\text{int}} = \boldsymbol{\nabla'}\mathbf{u}$ is the internal strain field. In turn, $\mathbf{r}'$ and $\mathbf{r}$ can be represented in tube coordinates $\{x'_1, x'_2, s'\}$ and $\{x_1, x_2, s\}$ (see Appendix B) as

$$\begin{aligned} \mathbf{r}' &= \boldsymbol{\ell}'(s') + x'_a\, \hat{\mathbf{d}}'_{\mathbf{a}}(s') \\ \mathbf{r} &= \boldsymbol{\ell}(s) + x_a\, \hat{\mathbf{d}}_{\mathbf{a}}(s)\ . \end{aligned} \tag{2.20}$$

We take the reference state $\mathcal{R}$ to be a rod of homogeneous volume fraction ϕ_h whose centerline is given by $\boldsymbol{\ell}$.

Each slice through the cross section in $\mathcal{R}$ is locally a cylinder resembling Fig. 2.6c

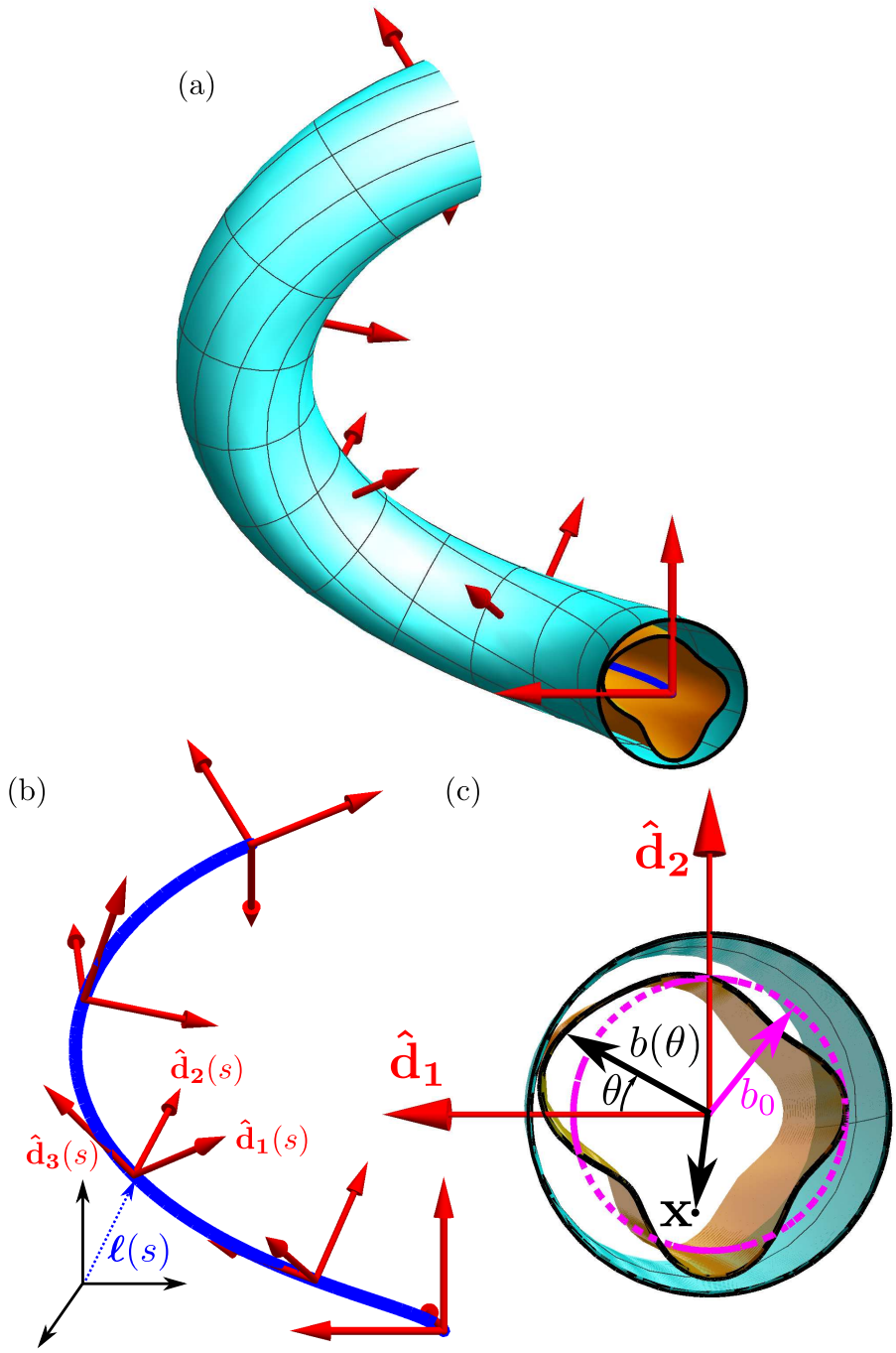

Figure 2.6: Geometry of the broken-symmetry gel rod. (a) shows the overall shape of a bent and twisted rod with the deformed phase interface shown in orange. (b) a focus on the centerline $\boldsymbol{\ell}$ showing the rotating curve frame $\{\hat{\mathbf{d}}_1, \hat{\mathbf{d}}_2, \hat{\mathbf{d}}_3\}$. (c) cross-section with symmetric and asymmetric phase interfaces described by radii b_0 and $b(\theta)$ and representative transverse point $\mathbf{x}$.

where the transverse coordinates have a polar representation

$$x_2(\rho,\theta) = \rho\cos\theta, \quad x_3(\rho,\theta) = \rho\sin\theta \tag{2.21}$$

and the phase interface is at $\rho = b(\theta)$. We choose the intermediate state $\mathcal{R}'$ as one in which the deformed rod has undergone phase separation with isotropic deformation Λ_t in the solvent-rich region and a stretch Λ_t tangential to the interface and Λ_n normal to the interface in the solvent-poor region

$$\rho'(\rho,\theta) = \begin{cases} \Lambda_t\,\rho & \text{for } \rho < b(\theta) \\ \Lambda_t\,b(\theta) + \hat{\boldsymbol{\rho}}' \cdot \hat{\mathbf{N}}'(\theta)\,\Lambda_n\,\rho & \text{for } b(\theta) \le \rho < a \end{cases} \tag{2.22}$$

where $\hat{\mathbf{N}}'(\theta)$ is the interface normal and is calculated below. Similarly, we assume that the longitudinal coordinate $s' = \Lambda_\ell\, s$ is the result of a simple stretch of s. Note that s' is generally *not* an arclength parameter, whereas we may take s to be one. There is a parametric dependence of the mapping $\rho'(\rho,\theta)$ on undeformed arclength s due to varying interface shape along the centerline; we will take $\partial b/\partial s$ to be on the same order as $\mathrm{d}\kappa/\mathrm{d}s$ and $\mathrm{d}\tau/\mathrm{d}s$ and thus higher order. There is additional deformation due to bending and twisting the centerline, appearing through covariant differentiation $\Lambda_{1,\mu\nu} = \nabla_\nu r'_\mu$. We find Λ_1 for the solvent-rich region:

$$\begin{aligned} \Lambda_1 \approx{}& \Lambda_t\,\hat{\mathbf{d}}'_{\mathbf{m}} \otimes \hat{\mathbf{d}}_{\mathbf{m}} + \varepsilon_{mn3}\left[\tau'\,\Lambda_\ell\,x'_m - \tau\,\Lambda_t\,x_m\right]\hat{\mathbf{d}}'_{\mathbf{m}} \otimes \hat{\mathbf{d}}_{\mathbf{3}} \\ &+ \Lambda_\ell\left[1 + \varepsilon_{mn3}(\kappa'_m\,x'_n - \kappa_m\,x_n)\right]\hat{\mathbf{d}}'_{\mathbf{3}} \otimes \hat{\mathbf{d}}_{\mathbf{3}} \end{aligned} \tag{2.23}$$

where we keep the leading order corrections in rod shape, namely the initial and deformed curvature, κ and κ', and torsion τ and τ' (see Appendix B for more details).

Identifying $\Lambda_2 = \Lambda_{\text{int}}$ as the deformation due to the equilibrating displacement field $\mathbf{u}$, we therefore have $\Lambda_1 = \Lambda_{\text{ext}}\,\Lambda_0 = (\mathbb{1} + u_{\text{ext}})\,\Lambda_0$. Factoring out Λ_0, the external

strain in the solvent-rich region is

$$u_{\text{ext}} \approx \varepsilon_{mn3} \left[\left(\Delta\kappa_m + \frac{\Lambda_t - 1}{\Lambda_t} \kappa_m \right) x'_n \, \hat{\mathbf{d}}'_3 \otimes \hat{\mathbf{d}}'_3 + \left(\Delta\tau + \frac{\Lambda_\ell - 1}{\Lambda_\ell} \tau \right) x'_m \, \hat{\mathbf{d}}'_n \otimes \hat{\mathbf{d}}'_3 \right] \tag{2.24}$$

where $\Delta\kappa_m \equiv \kappa'_m - \kappa_m$ and $\Delta\tau \equiv \tau' - \tau$. Notice that u_{ext} contains the usual dependence on changes in curvature and torsion for elastic rods [36] but also depends on the curvature and torsion *prior to deformation*, accounting for the additional inhomogeneous strain of swelling a curved gel; this correction disappears if the gel does not undergo phase separation and is typically small when $\phi_r \approx \phi_h$. The internal and external strain fields can be combined into a total strain field u:

$$\Lambda = (\mathbb{1} + u)\,\Lambda_0 = (\mathbb{1} + u_{\text{int}})\,(\mathbb{1} + u_{\text{ext}})\,\Lambda_0 = (\mathbb{1} + u_{\text{int}} + u_{\text{ext}} + u_{\text{int}}\,u_{\text{ext}})\,\Lambda_0 \,. \tag{2.25}$$

As we are considering *small* symmetry breaking strain, we can approximate u as the superposition, $u \approx u_{\text{int}} + u_{\text{ext}}$.

2.3.1 Deformation of the solvent-poor region

In order to determine the deformation matrix for the thin, solvent-poor region, we again take the approximation that variations of the deformation matrix through the layer are negligible. Due to the lamination condition, the components of Λ tangential to the interface are continuous across the interface and are thus determined by the deformation matrix in the solvent rich region. Assuming that the variation of the interface shape is gradual along the rod's length compared with variation in the cross-section, the interface tangent space is spanned by orthonormal basis $\{\hat{\mathbf{T}}, \hat{\mathbf{d}}_{\mathbf{3}}\}$ in $\mathcal{R}$ where $\hat{\mathbf{T}}$ is the interface tangent vector that is transverse to the rod:

$$\hat{\mathbf{T}} = \frac{\partial_\theta b(\theta)}{|\partial_\theta b|} \approx \hat{\boldsymbol{\theta}} + \hat{\boldsymbol{\rho}}\,\partial_\theta \Gamma \tag{2.26}$$

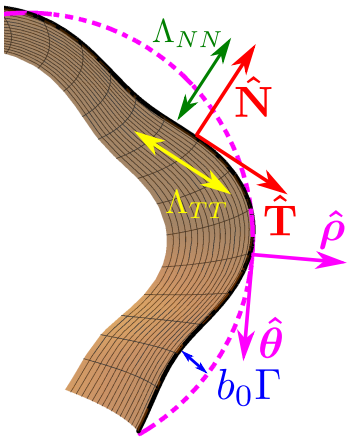

Figure 2.7: Cut-away of a representative interface shape with interface tangent $\hat{\mathbf{T}}$ and normal $\hat{\mathbf{N}}$.

which is perpendicular to the rod normal

$$\hat{\mathbf{N}} \approx \hat{\boldsymbol{\rho}} - \hat{\boldsymbol{\theta}}\partial_\theta\Gamma \tag{2.27}$$

where $\partial_\theta\Gamma = \partial_\theta b/b_0$; see Fig. 2.7. Therefore, the tangential components of Λ are, to lowest order in interface deformation Γ,

$$\begin{aligned}
\Lambda_{33} &\approx (1 + u_{33})\,\Lambda_l \\
\Lambda_{TT} &\approx \Lambda_t + (u_{\theta\theta} + (u_{\rho\theta} + u_{\theta\rho})\partial_\theta\Gamma)\,\Lambda_t \\
\Lambda_{T3} &\approx (u_{\theta 3} + u_{\rho 3}\partial_\theta\Gamma)\,\Lambda_l \\
\Lambda_{3T} &\approx (u_{3\theta} + u_{3\rho}\partial_\theta\Gamma)\,\Lambda_t\ .
\end{aligned} \tag{2.28}$$

As mixed normal-tangential components of the deformation matrix are of $\mathcal{O}(h)$, we can ignore them. Therefore, the only other component to consider is the pure normal component, $\Lambda_{NN} = \hat{\mathbf{N}} \cdot \Lambda\hat{\mathbf{N}}$. Per our assumption that the thickness is deformed by Λ_n, we have $\Lambda_{NN} = (1 + u_{NN}(\theta))\Lambda_n$ where $u_{NN} \approx u_{\rho\rho} - (u_{\rho\theta} + u_{\theta\rho})\partial_\theta\Gamma$. However, as we shall show, u_{NN} is determined by the other strain components when we assume incompressibility of the polymer network.

2.3.2 The total free-energy

We now expand the free-energy about the symmetric equilibrium Λ_0 in terms of the strain u. Decomposing the reference space $\mathcal{R}$ into a solvent-rich region $\mathcal{R}_r$ and a solvent-poor region $\mathcal{R}_p$ breaks the volume integral into

$$\begin{aligned}\int_{\mathcal{R}} \mathrm{d}^3 r &= \int_{\mathcal{R}_r} \mathrm{d}^3 r + \int_{\mathcal{R}_p} \mathrm{d}^3 r \\ &= \int_0^L \mathrm{d}s \Big\{ \int_{\mathcal{R}_r^{xs}} \mathrm{d}^2 x\, \gamma + \int_{\mathcal{R}_p^{xs}} \mathrm{d}^2 x\, \gamma \Big\}\end{aligned} \tag{2.29}$$

where transforming to tube coordinates $\{x_1, x_2, s\}$ decomposes the volume integration into integration over cross sections regions $\mathcal{R}_r^{xs}$ and $\mathcal{R}_p^{xs}$ and integration over the rod length, along with Jacobian determinant $\gamma = 1 + \varepsilon_{mn3}\, \kappa_m\, x_n$ (see Appendix B). Transforming transverse coordinates to polar form, $\mathrm{d}^2 x = \mathrm{d}\rho\, \mathrm{d}\theta\, \rho$, where $\mathcal{R}_r^{xs} = \{(\rho, \theta) \,|\, \rho < b(\theta); 0 \le \theta < 2\pi\}$ and $\mathcal{R}_p^{xs} = \{(\rho, \theta) \,|\, b(\theta) < \rho < a; 0 \le \theta < 2\pi\}$. Taking the thin shell approximation for the solvent-poor region, the integrand is evaluated at $\rho = b(\theta)$ and

$$\int_{\mathcal{R}_p^{xs}} \mathrm{d}^2 x\, \gamma \approx \int_0^{2\pi} \mathrm{d}\theta \int_{b(\theta)}^{a} \mathrm{d}\rho\, b(\theta)\, \gamma_b(\theta) \approx \int_0^{2\pi} \mathrm{d}\theta\, h(\theta)\, b(\theta)\, \gamma_b(\theta) \tag{2.30}$$

where $h(\theta) \equiv a - b(\theta)$ is the non-uniform thickness of the solvent-poor region and $\gamma_b(\theta) \equiv \gamma(\rho = b(\theta))$.

The total free-energy is therefore decomposed as $F = F_r + F_p$ where the solvent-rich part is

$$\begin{aligned}F_r = \int_0^L \mathrm{d}s \Big\{ \int_{\mathcal{R}_r^{xs}} \mathrm{d}^2 x\, \gamma \Big[\frac{1}{2}\mu \Big(\mathrm{tr}\big(\Lambda_r^T \Lambda_r\big) + \mathrm{tr}\big(\Lambda_r^T (u + u^T) \Lambda_r\big) + \mathrm{tr}\big(\Lambda_r^T u^T u \Lambda_r\big) \Big) \\ + \mathcal{F}_{\mathrm{rem}} \left(\frac{\phi_r}{\det\, u} \right) + p \left(\frac{\phi_h}{\phi_r} \det\, u - 1 \right) \Big]\end{aligned} \tag{2.31}$$

and the solvent-poor part is

$$F_r = \int_0^L \mathrm{d}s \Bigg\{ \int_0^{2\pi} \mathrm{d}\theta\, h\, b\, \gamma_b \Bigg[\frac{1}{2}\mu \Bigg(\mathrm{tr}\big(\Lambda_p^T \Lambda_p\big) + 2\Lambda_n^2 u_{NN} + 2\Lambda_t^2 u_{TT} + 2\Lambda_\ell^2 u_{33} + \Lambda_n^2 u_{NN}^2 + \Lambda_t^2 (u_{TT}^2 + u_{3T}^2) + \Lambda_\ell^2 (u_{33}^2 + u_{T3}^2) \Bigg) + \mathcal{F}_{\mathrm{rem}} \left(\frac{\phi_p}{\det\, u} \right) + p \left(\frac{\phi_h}{\phi_p} \det\, u - 1 \right) \Bigg] \Bigg\} \tag{2.32}$$

where ϕ_r and ϕ_p correspond with the symmetric equilibrium values obtained in the previous section.

2.3.3 Symmetric strain

Note that the strain u is an asymmetric tensor, $u^T \neq u$, and can be decomposed as

$$u = \frac{u + u^T}{2} + \frac{u - u^T}{2} = \epsilon + \omega \tag{2.33}$$

where $\epsilon = (u + u^T)/2$ is the symmetric part and $\omega = (u - u^T)/2$ is the antisymmetric part. However, as ω is antisymmetric, it describes local rotations of the gel. This can be seen by imaging a rotation U centered at $\mathbf{r}$ that takes points $\mathrm{d}\mathbf{r}$ to $\mathrm{d}\mathbf{R}$, centered at $\mathbf{R}$ via

$$\mathrm{d}R_i = U_{ij}\, \mathrm{d}r_j \tag{2.34}$$

so the rotation matrix U plays the role of the deformation matrix Λ. But pure rotations are isometries of space, so

$$\mathrm{d}r^2 = \mathrm{d}R^2 = \mathrm{d}R_i\, \mathrm{d}R_i = U_{ij}\, U_{ik}\, \mathrm{d}r_j\, \mathrm{d}r_k \tag{2.35}$$

requiring that $U^T U = \mathbb{1}$. Thus, we can express U in exponential form as $U = \exp(\theta_i\, T_i)$ where θ_i is a set of angles and $U^{-1} = \exp(-\theta_i\, T_i) = U^T$ implies that $T_i = -T_i$. As $\Lambda = \mathbb{1} + u$, we can approximate u by expanding the rotation matrix

U to linear order in small rotations: $U \approx \mathbb{1} + \theta_i T_i$. Thus, the antisymmetric strain $\omega \approx \theta_i T_i$ originates from a small rotation of the gel. However, as rotations do not change gel lengths, the free-energy must be independent of rotations. Therefore, we will expand the free-energy in terms of the symmetric strain ϵ, simply achieved by taking $u \mapsto \epsilon$.

2.3.4 Rubber-like incompressibility

With the deformation matrix Λ expressed in terms of small symmetric strain ϵ, we can now expand the free-energy density in powers of ϵ about the symmetric "vacuum" of Λ_0, borrowing the terminology of quantum field theory. Much like a saddle-point expansion in QFT, we can determine the stability of the symmetric rod to symmetry breaking by the expansion truncating to quadratic order. However, the small inhomogeneous strain will yield only small variations in the polymer volume fractions away from their vacuum values ϕ_r and ϕ_p: the values of ϵ we are considering are not large enough to cause parts of the gel to transition between solvent-rich and solvent-poor phases. Thus, we may regard the phase-separated gel as a composite medium where the two phases have a fixed degree of swelling and are therefore rubber-like. The free-energy cost of compressing the gel at *fixed* volume fraction depends on the bulk modulus of the gel at that volume fraction which is much larger than the shear modulus μ, often one or two orders of magnitude for hydrogel [37] and up to four for actual rubber [14]. We can therefore regard changes in volume fraction as costly compared with shear deformations and quench all *local* volume changes with the constraint

$$\det \epsilon = 1 \, . \tag{2.36}$$

By fixing the volume fraction of the gel locally as well as globally, we require by the lever rule Eq. (2.6) that the fraction of solvent-poor region, f is fixed. As f is set

by the thickness $h = a - b$ of the solvent poor region, fixing f places a restriction on the interface shape $b = b_0(1 + \Gamma(\theta))$. Restricting our attention to breaking coaxial symmetry of the cross-section rather than longitudinal, "peristaltic" modes [38], the constraint on Γ is, to leading order,

$$\int_0^{2\pi} \mathrm{d}\theta \, \Gamma(\theta) = 0 \, . \tag{2.37}$$

It is therefore convenient to expand Γ in Fourier modes

$$\begin{aligned} \Gamma(\theta) &= \sum_{m=1}^{\infty} \Gamma_m(\theta) \\ \Gamma_m(\theta) &= \left[\int_0^{2\pi} \frac{\mathrm{d}\varphi}{\pi} \, \Gamma(\varphi) \cos(\varphi) \right] \cos\theta + \left[\int_0^{2\pi} \frac{\mathrm{d}\varphi}{\pi} \, \Gamma(\varphi) \sin(\varphi) \right] \sin\theta \end{aligned} \tag{2.38}$$

where Eq. (2.37) is satisfied due to the exclusion of $m = 0$.

As the total volumes occupied by two phases of gel are unchanged and the portion of the free-energy density that depends on volume fraction alone is also unchanged, the total free-energy may be written $F = F_0 + \Delta F$ where

$$F_0 = V \left\{ (1 - f) \left[\mathcal{F}_{\mathrm{rem}}(\phi_r) + p \left(\frac{\phi_h}{\phi_r} - 1 \right) \right] + f \left[\mathcal{F}_{\mathrm{rem}}(\phi_p) + p \left(\frac{\phi_h}{\phi_p} - 1 \right) \right] \right\} \tag{2.39}$$

is the free-energy of the symmetric cylinder and ΔF is the free-energy change due to symmetry breaking. Expanding the free-energy to quadratic order in ϵ requires that the incompressibility constraint be expanded to quadratic order. The result of expanding the determinant to quadratic order in ϵ, performed in Appendix C, is

$$\mathrm{tr}\ \epsilon \approx \frac{1}{2} \mathrm{tr}\ \epsilon^2 - (\mathrm{tr}\ \epsilon)^2 + \mathcal{O}(\epsilon^3) \tag{2.40}$$

which can be iterated once, resulting in

$$\mathrm{tr}\ \epsilon \approx \frac{1}{2}\mathrm{tr}\ \epsilon^2 + \mathcal{O}(\epsilon^3)\ . \tag{2.41}$$

Therefore, certain linear terms in ΔF are replaced in order to satisfy the incompressibility constraint [14]; we choose

$$\begin{aligned} \epsilon_{11} + \epsilon_{22} &\approx -\epsilon_{33} + \frac{1}{2}\mathrm{tr}\ \epsilon^2 \quad \text{in } \mathcal{R}_r \\ \epsilon_{NN} &\approx -\epsilon_{TT} - \epsilon_{33} + \frac{1}{2}(\epsilon_{NN}^2 + \epsilon_{TT}^2 + 2\,\epsilon_{T3}^2 + \epsilon_{33}^2) \\ &\approx -\epsilon_{TT} - \epsilon_{33} + \epsilon_{TT}^2 + \epsilon_{T3}^2 + \epsilon_{33}^2 + \epsilon_{TT}\,\epsilon_{33} \quad \text{in } \mathcal{R}_p \end{aligned} \tag{2.42}$$

where we have solved for ϵ_{NN} through a second iteration of the volume constraint.

2.3.5 free-energy change due to symmetry-breaking

Enforcing the incompressibility constraints of Eq. (2.42), the free-energy change ΔF can be written in linear elastic form as

$$\begin{aligned} \Delta F = \int_0^L \mathrm{d}s \Bigg\{ & \int_{\mathcal{R}_r^{xs}} \mathrm{d}^2x\,\gamma \left[\mu\,(\Lambda_\ell^2 - \Lambda_t^2)\,\epsilon_{33} + \frac{1}{2}c_{AB}^r\,\epsilon_A\,\epsilon_B\right] \\ & + \int_0^{2\pi} \mathrm{d}\theta\,b\,h\,\gamma_b \left[\mu\,(\Lambda_\ell^2 - \Lambda_n^2)\,\epsilon_{33} + \mu\,(\Lambda_t^2 - \Lambda_n^2)\,\epsilon_{TT} + \frac{1}{2}c_{\alpha\beta}^p\,\epsilon_\alpha\,\epsilon_\beta\right]\Bigg\} \end{aligned} \tag{2.43}$$

where c^r_{AB} is an elastic constant tensor, expressed using the Voigt convention, $A, B \in \{11, 22, 33, 23, 13, 12\}$, and is given by

$$c^r_{AB} = \mu \begin{Bmatrix} 2\Lambda_t^2 & 0 & 0 & 0 & 0 & 0 \\ 0 & 2\Lambda_t^2 & 0 & 0 & 0 & 0 \\ 0 & 0 & \Lambda_l^2 + \Lambda_t^2 & 0 & 0 & 0 \\ 0 & 0 & 0 & \Lambda_l^2 + 3\Lambda_t^2 & 0 & 0 \\ 0 & 0 & 0 & 0 & \Lambda_l^2 + 3\Lambda_t^2 & 0 \\ 0 & 0 & 0 & 0 & 0 & 4\Lambda_t^2 \end{Bmatrix} \tag{2.44}$$

and similarly for the solvent-poor region, the interface-tangent Voigt indices are $\{\alpha, \beta\} \in \{TT, 33, T3\}$ and the elastic constant tensor is

$$c^p_{\alpha\beta} = \mu \begin{Bmatrix} \Lambda_t^2 + 3\Lambda_n^2 & 2\Lambda_n^2 & 0 \\ 2\Lambda_n^2 & \Lambda_l^2 + 3\Lambda_n^2 & 0 \\ 0 & 0 & \Lambda_l^2 + \Lambda_t^2 + 2\Lambda_n^2 \end{Bmatrix} . \tag{2.45}$$

We have thus arrived at a *linear elastic* description of a composite system composed of two materials with different elastic structures, characterized by elastic constant tensors c^r and c^p, that are stretched from their rest shape due to inhomogeneous strain $\epsilon_{33} \neq 0$. To simplify the problem of determining the equilibrium displacement field $\mathbf{u}$, we approximate the integration region in Eq. (2.43) as a straight cylinder so $\gamma \approx 1$, which can be taken as long as $\kappa\, a \ll 1$.

Now, we seek the equilibrium internal displacement field $\mathbf{u}$ that makes the free-

energy stationary:

$$\delta\Delta F = 0 = \int_0^L \mathrm{d}s \Bigg\{ \int_{\mathcal{R}_r^{xs}} \mathrm{d}^2x \Big[\mu \left(\Lambda_\ell^2 - \Lambda_t^2\right) \delta\epsilon_{\mathrm{int},33} + c^r_{AB}\, \epsilon_B\, \delta\epsilon_{\mathrm{int},A} \Big] + \int_0^{2\pi} \mathrm{d}\theta\, b\, h \left[\mu \left(\Lambda_\ell^2 - \Lambda_n^2\right) \delta\epsilon_{\mathrm{int},33} + \mu \left(\Lambda_t^2 - \Lambda_n^2\right) \delta\epsilon_{\mathrm{int},TT} + c^p_{\alpha\beta}\, \epsilon_\beta\, \delta\epsilon_{\mathrm{int},\alpha} \right] \Bigg\} \tag{2.46}$$

where we have noted that $\delta\epsilon = \delta\epsilon_{\mathrm{int}}$ as variations are taken with respect to the internal displacement field $\mathbf{u}$. As the integration region is approximated as a straight cylinder, we can approximate the internal strain as

$$\begin{aligned} \epsilon_{\mathrm{int},\mu\nu} &= \frac{1}{2}\left(\nabla'_\mu u_\nu + \nabla'_\nu u_\mu\right) = \frac{1}{2}\left(\partial'_\mu u_\nu + \partial'_\nu u_\mu - 2\Omega^\lambda_{\mu\nu}\, u_\lambda\right) \\ &\approx \frac{1}{2}\left(\partial'_\mu u_\nu + \partial'_\nu u_\mu\right) \end{aligned} \tag{2.47}$$

where $\Omega^\lambda_{\mu\nu}$ are the Christoffel symbols of the curved tube (see Appendix B), so that variations are given by

$$\delta\epsilon_{\mathrm{int},\mu\nu} \approx \frac{1}{2}\left(\partial'_\mu \delta u_\nu + \partial'_\nu \delta u_\mu\right) \ . \tag{2.48}$$

Defining symmetric stress tensors σ^r and σ^p with components

$$\begin{aligned} \sigma^r_{mn} &= 2\,\mu\,\Lambda_t^2\,\epsilon_{mn} \\ \sigma^r_{m3} &= \mu\left(\Lambda_\ell^2 + 3\Lambda_t^2\right)\epsilon_{m3} \\ \sigma^r_{33} &= \mu\left(\Lambda_\ell^2 + \Lambda_t^2\right)\epsilon_{33} \\ \sigma^p_{TT} &= \mu\left[\left(\Lambda_t^2 + 3\Lambda_n^2\right)\epsilon_{TT} + 2\,\Lambda_n^2\,\epsilon_{33}\right] \\ \sigma^p_{T3} &= \frac{1}{2}\,\mu\left(\Lambda_\ell^2 + \Lambda_t^2 + 2\,\Lambda_n^2\right)\epsilon_{T3} \\ \sigma^p_{33} &= \mu\left[\left(\Lambda_\ell^2 + 3\,\Lambda_n^2\right)\epsilon_{33} + 2\,\Lambda_n^2\,\epsilon_{TT}\right] \end{aligned} \tag{2.49}$$

the variation of the free-energy can be written as

$$\delta\Delta F = \int_0^L \mathrm{d}s \left\{ \int_{\mathcal{R}'^{xs}_r} \frac{\mathrm{d}^2x'}{\Lambda_t^2}\, \sigma^r_{\mu\nu}\, \partial'_\nu \delta u_\mu + \int_0^{2\pi} \mathrm{d}\theta' \, \frac{b'\, h'}{\Lambda_t\, \Lambda_n}\, \sigma^p_{\alpha\beta}\, \partial'_\beta \delta u_\alpha \right\} \tag{2.50}$$

where we have transformed to the intermediate reference space $\mathcal{R}'$ by taking $\mathrm{d}^2x = \mathrm{d}^2x'/\Lambda_t^2$ and $b = b'/\Lambda_t$, $h = h'/\Lambda_n$. Note that the solvent-poor free-energy is similar to that of a thin plate which is dominated by in-plane stresses; $\alpha, \beta \in \{T, 3\}$. Integrating by parts,

$$\begin{aligned}
\delta\Delta F = \int_0^L \mathrm{d}s \Bigg\{ & \left[\int_0^{2\pi} \mathrm{d}\theta' \, \frac{b'\, h'}{\Lambda_t\, \Lambda_n} (\sigma^p_{T3}\, \delta u_T + \sigma^p_{33}\, \delta u_3) + \int_{\mathcal{R}^{xs}_r} \frac{\mathrm{d}^2x'}{\Lambda_t^2}\, \sigma^r_{\mu 3}\, \delta u_\mu \right]_0^L \\
& + \int_0^{2\pi} \mathrm{d}\theta' \, b' \left[\left(\sigma^r_{NN} + \frac{h'}{b'} (1 - \partial_{\theta\theta}\Gamma) \sigma^p_{TT} \right) \delta u_N + (\sigma^r_{TN} - \partial'_T\, h'\, \sigma^p_{TT})\, \delta u_T \right. \\
& \left. + (\sigma^r_{N3} - \partial'_T\, h'\, \sigma^p_{T3})\, \delta u_3 \right] - \int_{\mathcal{R}^{xs}_r} \frac{\mathrm{d}^2x'}{\Lambda_t^2}\, \delta u_\mu\, \partial'_\nu \sigma^r_{\mu\nu} \Bigg\}
\end{aligned} \tag{2.51}$$

where the first line results from integration over the endcaps at $s = 0, L$. Thus, the equilibrium equations and boundary conditions are provided by setting the integrands in Eq. (2.51) equal to zero.

In the slender rod limit, variations of the strain along the arclength are small compared with the variations in the cross-section. Appealing to this separation of scales, we can make a "quasistatic" approximation of the stress balance along the rod's arclength where variations of the displacement field along s are ignored, $\partial'_s u_\mu \ll \partial'_n u_\mu$ for $n = 1, 2$. The quasistatic equilibrium equations are

$$\partial'_n \sigma^r_{\mu n} = 0 \quad \text{for } \rho < b(\theta) \tag{2.52}$$

with cross-section boundary conditions

$$\left.\begin{aligned} \sigma^r_{NN} + \tfrac{h'}{b'}(1 - \partial_{\theta\theta}\Gamma)\sigma^p_{TT} &= 0 \\ \sigma^r_{TN} - \partial'_T\, h'\, \sigma^p_{TT} &= 0 \\ \sigma^r_{N3} - \partial'_T\, h'\, \sigma^p_{T3} &= 0 \end{aligned}\right\} \quad \text{for } \rho = b(\theta)\ . \tag{2.53}$$

The equilibrium strain field is determined in Appendix D. Due to the surface stress $h'\,\sigma^p_{TT}$, there is a Laplace-like pressure (see e.g., [36, 39]) that acts on the solvent rich region, balanced by normal stress σ^r_{NN}. The first boundary condition relates these two stresses, where $(1 - \partial_{\theta\theta}\Gamma)/b' \approx (1 - \Gamma - \partial_{\theta\theta}\Gamma)/b_0$ is the mean curvature of the interface (see Eq. (2.70)). Furthermore, changes in surfaces stress due to, for example, changes in solvent-poor thickness h must be balanced by traction of the solvent-rich region, provided by the other two boundary conditions which balance gradients in surface stresses $h'\,\sigma^p_{TT}$ and $h'\,\sigma^p_{T3}$ against solvent-rich region stresses σ^r_{TN} and σ^r_{N3}. Such gradients of surface stress are similar to the Marangoni force in fluids [39], an effect arising from gradients in surface tension that leads to flow of viscous fluids.

2.3.6 An effective rod model

By determining the equilibrium displacement field $\mathbf{u}$ in terms of constrained rod shape parameters $\Delta\kappa$ and $\Delta\tau$, as well as constrained interface shape $\Gamma(\theta)$, we can now develop a reduced deformation free-energy ΔF due to to maintaining these constraints. We have effectively integrated out all other degrees of freedom of the rod, resulting in an effective description in terms of fewer fields. This method is completely general in physics; for example, the Helmholtz free-energy of a thermodynamic system is obtained by integrating out all microscopic degrees of freedom consistent with a constrained temperature, volume, and number of particles (e.g., [23]). By determining the equilibrium strain (Eqs. (D.20)) to linear order in the constrained parameters, we therefore obtain a quadratic free-energy.

Inserting the equilibrium strain into the ΔF in Eq. (2.43), we are left with an integrand that varies over the solvent-rich region cross-section $\mathcal{R}_r^{xs}$ as well as the phase interface. The integrand depends solely on powers of x_m and therefore integration over $\mathcal{R}_r^{xs}$ involves calculating moments of area

$$\begin{aligned}\underbrace{\langle x_m\, x_n \cdots x_p \rangle}_{N} &\equiv \int_0^{2\pi} \mathrm{d}\theta \int_0^{b(\theta)} \mathrm{d}\rho\, \rho^{N+1}\, \hat{\rho}_m\, \hat{\rho}_n \cdots \hat{\rho}_p \\ &= \frac{b_0^{N+2}}{N+2} \int_0^{2\pi} \mathrm{d}\theta (1+\Gamma(\theta))^{N+2}\, \hat{\rho}_m\, \hat{\rho}_n \cdots \hat{\rho}_p\ .\end{aligned} \tag{2.54}$$

We note that

$$\varepsilon_{pq3}\,(\Delta\kappa_p + \dots)\ \langle x_q \rangle = b_0^3\, \varepsilon_{pq3}\,(\Delta\kappa_p + \dots) \int_0^{2\pi} \mathrm{d}\theta\ \left(\Gamma_1(\theta)\, \hat{\rho}_q + \mathcal{O}(\Gamma^3)\right) \tag{2.55}$$

$$\varepsilon_{pq3}\,\varepsilon_{rs3}\,(\Delta\kappa_p + \dots)(\Delta\kappa_r + \dots)\ \langle x_q x_s \rangle \approx \frac{\pi}{4}\, b_0^4 \left| \Delta\boldsymbol{\kappa} + \frac{\Lambda_t - 1}{\Lambda_t} \boldsymbol{\kappa} \right|^2 (1 + \mathcal{O}(\Gamma^2)) \tag{2.56}$$

where Eq. (2.55) couples the curvature and the center of mass of the solvent-rich region and Eq. (2.56) results in the structure of the bending modulus which, while generally an anisotropic tensor, is isotropic to leading order. The center of mass $\langle x_m \rangle$ is non-zero only if $\Gamma_1 \neq 0$ and therefore serves as an indication of symmetry breaking. It is convenient to expand $\Gamma(\theta)$ as

$$\Gamma(\theta) = \boldsymbol{\psi} \cdot \hat{\boldsymbol{\rho}}(\theta) + \sum_{m=2}^{\infty} \left(\Psi_m e^{i\, m\, \theta} + \Psi_m^* e^{-i\, m\, \theta} \right) \tag{2.57}$$

where $\boldsymbol{\psi}$ is a vector parameter describing the magnitude and direction of the displacement of the centers of mass of the solvent-rich core and solvent-poor shell relative to one another, as given by

$$\langle x_m \rangle = b_0^3 \int_0^{2\pi} \mathrm{d}\theta\, \Gamma_1(\theta)\, \hat{\rho}_m \equiv \pi\, b_0^3\, \psi_m, . \tag{2.58}$$

In analogy to the displacement between atomic nucleus and electron cloud brought

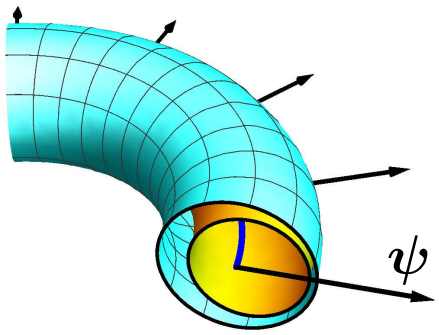

Figure 2.8: Symmetry broken rod in which the solvent-rich and solvent-poor regions do not share a common center of mass but are instead shifted relative to one another, described by polarization $\boldsymbol{\psi}$.

on by an external electric field, we will refer to $\boldsymbol{\psi}$ as a "polarization" of the core and shell (see Fig. 2.8). Other modes of interface shape deformation are represented in terms of complex Fourier amplitudes Ψ_m.

After integration, the total reduced free-energy is

$$\begin{aligned}\Delta F = \frac{1}{2}\int_0^L \mathrm{d}s \Big\{ E\,\eta^2 + B\left|\Delta\boldsymbol{\kappa} + \frac{\Lambda_t - 1}{\Lambda_t}\boldsymbol{\kappa}\right|^2 + J\left(\Delta\tau + \frac{\Lambda_\ell - 1}{\Lambda_\ell}\tau\right)^2 \\ -2\,k\,\varepsilon_{pq3}\left(\Delta\kappa_p + \frac{\Lambda_t - 1}{\Lambda_t}\kappa_p\right)\psi_q - r_1|\boldsymbol{\psi}|^2 - \sum_{m=2}^{\infty} r_m\,|\Psi_m|^2 \Big\}\end{aligned} \tag{2.59}$$

with coefficients given below:

$$\begin{aligned} E &= \mu\pi b_0^2\left[\Lambda_\ell^2 + 2\Lambda_t^2 + \frac{h_0}{2b_0}\left(4\Lambda_\ell^2 + \Lambda_t^2 + 7\Lambda_n^2\right)\right] \\ B &= \frac{1}{4}\mu\pi b_0^4\left[\Lambda_\ell^2 + 2\Lambda_t^2 + \frac{h_0}{b_0}\left(4\Lambda_\ell^2 + \Lambda_t^2 + 7\Lambda_n^2\right)\right] \\ J &= \frac{1}{8}\mu\pi b_0^4\left[\Lambda_\ell^2 + 3\Lambda_t^2 + 4\frac{h_0}{b_0}\left(\Lambda_\ell^2 + \Lambda_t^2 + 2\Lambda_n^2\right)\right] \\ r_m &= \frac{1}{2}\mu\pi b_0^2 m\frac{(\Lambda_t^2 - \Lambda_n^2)^2}{\Lambda_t^2}\left[1 + \frac{h_0}{2b_0}\left(3\frac{\Lambda_t^2 - \Lambda_n^2}{\Lambda_t^2}m - 4\right)\right] \\ k &= \frac{1}{2}\mu\pi b_0^3\Lambda_t\left[\Lambda_t^2 - \Lambda_n^2 + \frac{h_0}{b_0}\left(\frac{(\Lambda_t^2 - \Lambda_n^2)^2}{\Lambda_t^2} + \Lambda_t^2 + \Lambda_n^2 - 2\Lambda_\ell^2\right)\right] \end{aligned} \tag{2.60}$$

As with the classical rod theory, the cost of extensile deformation, $E\,\eta^2$ is much larger

than the cost of bending and twisting deformations as long as $\kappa\, b_0, \tau\, b_0 \ll 1$. Thus, we can consider the slender rod as inextensible, able to only bend and twist at constant length [36].

2.4 Phase interface and bending instability of phase-coexistent rods

Examining the reduced deformation free-energy Eq. (2.59), we find that

$$\frac{\delta^2 \Delta F}{\delta \Psi_m^2} = -r_m \tag{2.61}$$

where $r_m > 0$ for small enough h_0/b_0. Therefore, even initially straight rods are unstable to *spontaneous symmetry breaking* of the interface shape. In particular, the polarization $\boldsymbol{\psi}$ acquires a non-zero value, pointing is some undetermined direction transverse to the rod's centerline. Due to the coupling with $\Delta\boldsymbol{\kappa}$, we see that the straight rod is therefore *unstable to spontaneous bending* in an undetermined direction. The mechanical origin of this spontaneous bending is due to a *swelling moment*, a torque on the centerline due to the swelling stress of the solvent-rich region on one side and the deswelling stress of the solvent-poor region on the other, as shown in Fig. 2.8. This effect is also seen in the heating of bimetallic strips [40] composed of two laminated metals of different thermal expansion coefficients, leading to a thermal stress differential that results in a bent strip.

However, if the rod is initially curved so that $\kappa_p \neq 0$ then the free-energy is lowered if

$$\varepsilon_{pq3}\, \kappa_p\, \psi_q > 0 \tag{2.62}$$

which is maximized if

$$\boldsymbol{\psi} \propto \hat{\mathbf{d}}_{\mathbf{3}} \times \boldsymbol{\kappa}\ . \tag{2.63}$$

Therefore, we may regard the initial curvature $\boldsymbol{\kappa}$ as an *external aligning field* on the

polarization direction $\boldsymbol{\psi}$ in a manner analogous to a magnetic field acting on a spin system in a *ferromagnetic phase*, a relation that we shall further explore in the next section.

2.4.1 Stabilization of the phase interface

The instability of all Fourier modes of Γ is an artifact of adapting a homogeneous free-energy density, namely Eq. (2.2), to describe an inhomogeneous gel. Our rationale for doing this is that we are concerned with macroscopic deformations of the gel arising from two well-defined regions corresponding with solvent-rich and solvent-poor gel, each of homogeneous volume fraction. Smaller details, such as variation of ϕ across the width of the phase interface, require an inhomogeneous description of the gel. According to the program of Landau theory, the microscopic variation of the volume fraction should be penalized with a gradient-squared term, resulting in an inhomogeneous free-energy

$$F_{\text{inh}} = \int_{\mathcal{R}} \mathrm{d}^3 r \left[\frac{1}{2}\mu \ \text{tr}\ \Lambda^T \Lambda + \frac{1}{2} C \ |\boldsymbol{\nabla}\phi|^2 + \mathcal{F}_{\text{rem}}(\phi) \right] \tag{2.64}$$

that is required for describing interface shape [41].

In systems undergoing spinodal decomposition, the spatial modulations of ϕ are unstable for all wavenumbers q less than a upper cutoff wavenumber q_c, set by the rigidity of microscopic variation C [20, 27, 42]. Modulations of the phase interface for the coaxial phase coexistent rod should similarly be stabilized at some large Fourier mode through the introduction of a missing inhomogeneous contribution to the free-energy which contribute to an interfacial free-energy. Following [20], the interfacial free-energy has a phenomenological form which depends on the (i) surface tension c_0,

the (ii) mean curvature H_{int}, and (iii) the Gaussian curvature K_{int}:

$$F_{\text{int}} = \int_{\text{int}} \mathrm{d}S \left[c_0 + \frac{1}{2} c_1 H^2 + \frac{1}{2} c_2 K \right] . \tag{2.65}$$

In our theory, the interface is described within our tube coordinates as a surface of radius $b(\theta)$, which we give the parametric form

$$\boldsymbol{\sigma}(\theta, s) = \boldsymbol{\ell}(s) + b(\theta)\hat{\boldsymbol{\rho}} \tag{2.66}$$

and is thus a *diffeomorphism*, a smooth mapping, of a cylinder. By the Gauss-Bonnet theorem (see e.g., [43]), the integral of the Gaussian curvature K and therefore contributes a constant to Eq. (2.65).

Furthermore, by adopting the "quasistatic" approximation of the rod equilibrium, variations of the surface area and mean curvature are due to Γ alone. To calculate the surface area and the mean curvature, we require the surface metric

$$g_{\alpha\beta} = \partial_\alpha \boldsymbol{\sigma} \cdot \partial_\beta \boldsymbol{\sigma} \approx \left\{ \begin{array}{cc} b_0^2((1+\Gamma)^2 + (\partial_\theta \Gamma)^2) & 0 \\ 0 & 1 \end{array} \right\} \tag{2.67}$$

describing lengths on the surface and the second fundamental form $B_{\alpha\beta}$

$$B_{\alpha\beta} = \partial_{\alpha\beta} \boldsymbol{\sigma} \cdot \hat{\mathbf{N}} \approx \left\{ \begin{array}{cc} b_0(\partial_{\theta\theta}\Gamma - (1+\Gamma) - 2(\partial_\theta \Gamma)^2) & 0 \\ 0 & 0 \end{array} \right\} \tag{2.68}$$

characterizing a local parabolic profile near surface points [44]. The surface area is

$$A_{\text{int}} = \int_0^L \mathrm{d}s \int_0^{2\pi} \mathrm{d}\theta \sqrt{\det\, g_{\alpha\beta}} \approx A_{\text{int},0} + \mathcal{O}(\Gamma^2) \tag{2.69}$$

and the mean curvature is given by the trace of the second fundamental form (or,

Weingarten's equation [43, 44])

$$H = B^{\alpha}{}_{\alpha} \approx -1 + \Gamma + \partial_{\theta\theta}\Gamma + \mathcal{O}(\Gamma^2) \, . \tag{2.70}$$

Thus, the free-energy change due to interface deformation is

$$\Delta F_{\text{int}} \approx \frac{c_1}{2b_0^2} \int_0^L \mathrm{d}s \int_0^{2\pi} \mathrm{d}\theta \, (\partial_{\theta\theta}\Gamma + \Gamma)^2 \approx \frac{c_1}{2b_0^2} \int_0^L \mathrm{d}s \sum_{m=1}^{\infty} (m^2 - 1)^2 \, |\Psi_m|^2 \tag{2.71}$$

where we have used the Fourier expansion of Γ. Importantly, the $m = 1$ mode does not contribute to the deformation free-energy of the interface because it is a simple translation of the interface about the rod's centerline. Deformation to higher modes, however, are penalized by an energy that scales as m^4. As this scaling is a higher power than the m^2 of the coefficient r_m in Eq. (2.60), deformations of the interface stabilized at a cutoff wavenumber $m_c > 1$. Thus, the $m = 1$ mode is *always* unstable in the low h_0/b_0 whilst higher-order modes are potentially stabilized by the interfacial energy.

CHAPTER 3
EQUILIBRIUM OF PHASE-SEPARATED GEL ROD

3.1 Equilibrium description via Landau Theory

In the previous section, we showed that the hydrogel rod with coaxial phase coexistence of solvent-rich and solvent-poor regions is unstable to symmetry breaking. This results in spontaneous polarization of the coaxial arrangement and internal swelling stress that leads to a bent rod. We have found that the essential physics is captured by the interplay of the change in curvature of the centerline $\Delta\boldsymbol{\kappa}$ and the polarization $\boldsymbol{\psi}$ which plays the role of an order parameter describing the rod's broken symmetry. If the rod is originally curved when fabricated with curvature $\boldsymbol{\kappa}$ then, due to inhomogeneous internal stress, $\boldsymbol{\psi}$ is aligned with the curvature direction. Thus, $\boldsymbol{\kappa}$ acts as an external aligning field on $\boldsymbol{\psi}$. We will now use these observations to develop a Landau free-energy that describes the equilibrium shape of the rod, with the idea that *the three-dimensional structure of the hydrogel can be abstracted to a one-dimensional field theory.* The Landau approach was originally developed to capture the behavior of a system near a continuous phase transition [45] and has been used to make mean-field predictions regarding diverse phenomena including the celebrated Ginzburg-Landau theory of type-I superconductors [46] and the Landau-de Gennes theory of the isotropic-to-nematic transition of liquid crystals [47].

A Landau free-energy density $\mathcal{L}$ is an analytic function constructed from, in principle, all symmetry-preserving combinations of fields characterizing a system undergoing a phase transition [20, 48]. In practice, $\mathcal{L}$ is truncated as a finite power series, maintaining the minimal terms needed to describe key aspects of the system. First, consider the polarization order parameter $\boldsymbol{\psi}$ which is a vector field along the rod's

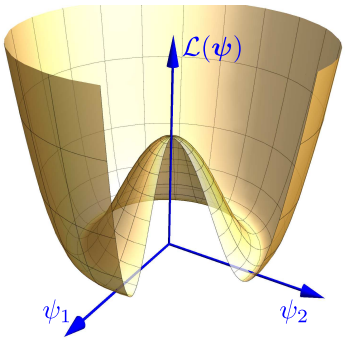

Figure 3.1: The "Mexican hat" profile of $\mathcal{L}(\boldsymbol{\psi})$

centerline, pointing in the transverse plane to the centerline at all points. In the absence of rod curvature, the free-energy should be invariant under SO(2) rotations of the order parameter and is thus given by

$$\mathcal{L} = \cdots - \frac{1}{2} r |\boldsymbol{\psi}|^2 + \frac{1}{4} u |\boldsymbol{\psi}|^4 + \mathcal{O}(|\boldsymbol{\psi}|^6) \tag{3.1}$$

where we truncate the expansion after the quartic term. Note that we exclude odd powers of $|\boldsymbol{\psi}| = \sqrt{\psi_1^2 + \psi_2^2}$ as they are non-analytic. Due to the results we obtained in the previous section, the quadratic term is typically negative resulting in instability of $\psi = 0$. However, the center of mass of the solvent-rich phase cannot be arbitrary far from the centerline and is limited by the gel's rigidity. The $|\boldsymbol{\psi}|^4$ term stabilizes the large-amplitude behavior of the free-energy, resulting in the classical "Mexican hat" profile for $\mathcal{L}(\boldsymbol{\psi})$, seen in Fig. 3.1. This feature is universal for systems that undergo a phase transition to a phase with a continuous symmetry encoded in degrees of freedom of the order parameter that are transverse to its magnitude.

In particular, we recognize that Eq. (3.1) belongs to the class of models that describe the physics of, for example, superfluids (via the Ginzburg-Landau theory) where the equilibrium at $|\boldsymbol{\psi}|^2 = r/u$ corresponds to the condensate density and the direction of $\boldsymbol{\psi}$ is an SO(2) rotational degree of freedom that is mapped to the unit circle in $\mathbb{C}^1$ and is thus a U(1) condensate phase. Finally, we introduce an external

field $\mathbf{H}$ which couples to $\boldsymbol{\psi}$ and selects an alignment direction

$$\mathcal{L} = \cdots - \frac{1}{2} r |\boldsymbol{\psi}|^2 + \frac{1}{4} u |\boldsymbol{\psi}|^4 - \mathbf{H} \cdot \boldsymbol{\psi} \ . \tag{3.2}$$

As we have previously shown, both the fabricated curvature $\boldsymbol{\kappa}$ and final curvature $\boldsymbol{\kappa'}$ of the rod couple to ψ. While the details of the curvature-polarization coupling is developed from the three-dimensional theory of the previous chapter, symmetry dictates the possible forms of the coupling. Requiring invariance under reversal of the rod's arclength coordinate $s \mapsto -s$, we find that $\boldsymbol{\kappa} \mapsto -\boldsymbol{\kappa}$ and $\hat{\mathbf{d}}_{\mathbf{3}} \mapsto -\hat{\mathbf{d}}_{\mathbf{3}}$ whereas $\boldsymbol{\psi} \mapsto \boldsymbol{\psi}$. Therefore, while the triple product $\hat{\mathbf{d}}_{\mathbf{3}} \cdot (\boldsymbol{\kappa} \times \boldsymbol{\psi}))$ is invariant, the scalar product $\boldsymbol{\kappa} \cdot \boldsymbol{\psi}$ is not and we recover the coupling

$$\mathbf{H} = \hat{\mathbf{d}}_{\mathbf{3}} \times (k_1 \Delta\boldsymbol{\kappa} + k_2 \boldsymbol{\kappa}) \tag{3.3}$$

where we use $\Delta\boldsymbol{\kappa} = \boldsymbol{\kappa'} - \boldsymbol{\kappa}$ without loss of generality.

So far, the Landau free-energy is a familiar complex ϕ^4 theory at fixed rod shape which acts as an external field on the polarization. We now allow the rod shape to vary, introducing additional terms. As we have argued, the rod is inextensible and it bends and twists at fixed length. For such rods, we can use the general deformation energy

$$\mathcal{L} = \frac{1}{2} B_{mn} \Delta\kappa_m \Delta\kappa_n + \frac{1}{2} J \Delta\tau^2 + \dots \tag{3.4}$$

where J is the torsional modulus and B_{mn} is a bending modulus matrix and is generally *anisotropic*. As this quadratic free-energy is taken to be positive-definite, higher order terms are not needed.

The bending modulus matrix B_{mn} can be decomposed as a sum of irreducible tensors [49]

$$B_{mn} = B^{(0)} \delta_{mn} + B^{(2)}_{mn} \tag{3.5}$$

where $B^{(0)}$ is the rank-0 tensor, or scalar, representing the isotropic part. The anisotropic contribution is given by $B^{(2)}_{mn}$, which a the rank-2 traceless, symmetric tensor. Note that if the rod is unpolarized then it is isotropic with $B_{mn} = B^{(0)}\delta_{mn}$. Therefore, we expect an expansion of the form

$$\begin{aligned} B^{(0)} &= B^{(0,0)} + B^{(0,2)}|\boldsymbol{\psi}|^2 + \dots \\ B^{(2)}_{mn} &= B^{(2,2)}(|\boldsymbol{\psi}|^2\delta_{mn} - 2\psi_m\psi_n) + \dots \end{aligned} \tag{3.6}$$

where the expansions are taken to $\mathcal{O}(\psi^2)$ and are required to have the above forms due to symmetry. Now, the bending modulus is determined by the second moment of area, weighted by a Young's modulus E [36] which generally varies over space; using notation where $\langle\,\cdot\,\rangle$ represents integration over the cross section, $B_{mn} = \langle E(\mathbf{x})x_p x_q\rangle\,\varepsilon_{mp3}\varepsilon_{nq3}$. If we consider a simple model where the rod is composed of solvent-rich and solvent-poor regions with Young's moduli E_r and E_p, then

$$B_{mn} = (E_r\,\langle x_p x_q\rangle_r + E_p\,\langle x_p x_q\rangle_P)\varepsilon_{mp3}\varepsilon_{nq3} \tag{3.7}$$

with the cross-section integration decomposed into integration over solvent-rich and solvent-poor regions. In the unpolarized case $\boldsymbol{\psi} \to 0$, these two regions share a common center of area and are both isotropic. The center of area for the solvent-rich region is $\langle\mathbf{x}\rangle_r = b\boldsymbol{\psi}$ and for the solvent-poor region is $\langle\mathbf{x}\rangle_p = -b\boldsymbol{\psi}$ for an appropriate length b. Moving to center of area coordinates $\delta\mathbf{x}^r = \mathbf{x} - b\boldsymbol{\psi}$ for the solvent-rich region and $\delta\mathbf{x}^p = \mathbf{x} + b\boldsymbol{\psi}$ for the solvent-poor region where $\langle\delta\mathbf{x}^r\rangle_r = \langle\delta\mathbf{x}^p\rangle_p = 0$, the second moments can be decomposed as

$$\begin{aligned} \langle x_p x_q\rangle_r &= b^2\psi_p\psi_q + I^r_{pq} \\ \langle x_p x_q\rangle_p &= b^2\psi_p\psi_q + I^p_{pq} \end{aligned} \tag{3.8}$$

where $I^{r/p}_{pq}$ are second moments of area in the frame of the respective centers of area.

If we assume that the polarization $\boldsymbol{\psi}$ describes a shift of the centers of the two regions and that any departures from isotropy are dominated by this shift then we can take $I^{r/p}_{pq} \approx I^{r/p}\delta_{pq}$ and

$$\begin{aligned} B_{mn} &\approx ((E_r I^r + E_p I^p \delta_{pq} + (E_r + E_p) b^2 \psi_p \psi_q)\varepsilon_{mp3}\varepsilon_{nq3} \\ &= B\delta_{mn} + \tilde{B}\psi_p\psi_q\varepsilon_{mp3}\varepsilon_{nq3} \end{aligned} \tag{3.9}$$

where the modulus $\tilde{B}$ characterizes the anisotropic bending rigidity due to polarization of the gel. However, the above form of the bending modulus matrix results in curvature-polarization coupling of the form $(\varepsilon_{mn3}\Delta\kappa_m\psi_n)^2$ which is higher order-than the linear coupling already present in $\mathcal{L}$. Therefore, we can regard the anisotropy in B_{mn} as *higher-order curvature-polarization coupling* which can be ignored in the context of Landau theory. Therefore, the final form for the Landau free-energy density is

$$\mathcal{L} = \frac{1}{2}B|\Delta\boldsymbol{\kappa}|^2 + \frac{1}{2}J\Delta\tau^2 - \frac{1}{2}r|\boldsymbol{\psi}|^2 + \frac{1}{4}u|\boldsymbol{\psi}|^4 - \varepsilon_{mn3}(k_1\Delta\kappa_m + k_2\kappa_m)\psi_n \ . \tag{3.10}$$

The full Landau free-energy L is an integral of the Landau free-energy density $\mathcal{L}$ over the rod's length along with gradients of the fields to penalize variation. Thus,

$$L = \int \mathrm{d}s \left[\frac{1}{2}C|\dot{\boldsymbol{\psi}}|^2 + \mathcal{L}\right] \tag{3.11}$$

where $\dot{\boldsymbol{\psi}}$ is taken to be an ordinary derivative with respect to s as the covariant form $\nabla_s\boldsymbol{\psi}$ yields additional couplings between rod shape and $\boldsymbol{\psi}$ that, like the anisotropic part of B_{mn}, are higher order contributions. Furthermore, it is important to note that curvature κ'_m and torsion τ' of the deformed rod already encompass elastic-like terms and thus do not require additional gradients. To see this, note that the general

Frenet-Serret equations Eq. (B.2) can be arranged as

$$\begin{aligned}\kappa_1' &= \hat{\mathbf{d}}_3' \cdot \nabla_s \hat{\mathbf{d}}_2' = -\hat{\mathbf{d}}_2' \cdot \nabla_s \hat{\mathbf{d}}_3' \\ \kappa_2' &= \hat{\mathbf{d}}_1' \cdot \nabla_s \hat{\mathbf{d}}_3' = -\hat{\mathbf{d}}_3' \cdot \nabla_s \hat{\mathbf{d}}_1' \\ \tau' &= \hat{\mathbf{d}}_2' \cdot \nabla_s \hat{\mathbf{d}}_1' = -\hat{\mathbf{d}}_1' \cdot \nabla_s \hat{\mathbf{d}}_2'\end{aligned} \tag{3.12}$$

from which we find

$$\begin{aligned}|\kappa'|^2 &= |\nabla_s \hat{\mathbf{d}}_3'|^2 \\ \tau'^2 &= |\hat{\mathbf{d}}_3' \times \nabla_s \hat{\mathbf{d}}_1'|^2 \\ \varepsilon_{mn3}\kappa_m \psi_n &= -\boldsymbol{\psi} \cdot \nabla_s \hat{\mathbf{d}}_3'\end{aligned} \tag{3.13}$$

so that the rod elasticity can be regarded as an O(3) nonlinear σ-model in one dimension, where the nonlinearity comes from fixing the unit magnitudes of $\{\hat{\mathbf{d}}_\mu'\}$ [50]. Thus, we get a glimpse of the complexity of the rod's Landau theory.

3.2 Equilibrium equations

In the rod's equilibrium configuration, the Landau free-energy is stationary, $\delta L = 0$, with respect to variations of the order parameter $\boldsymbol{\psi}$, as well as variations in the frame orientation, $\{\hat{\mathbf{d}}_\mu'\}$. Whilst variations of the order parameter lead to the equilibrium equation via the usual Euler-Lagrange equations [51]

$$c\ddot{\psi}_m + r\psi_m - u|\boldsymbol{\psi}|^2\psi_m - \varepsilon_{mn3}(k_1\Delta\kappa_m + k_2\kappa_m) = 0 \tag{3.14}$$

variations of the frame are more involved as the frame basis must remain orthonormal. Thus, the varied frame $\{\hat{\mathbf{d}}_\mu' + \delta\hat{\mathbf{d}}_\mu'\}$ must be accessed via SO(3) rotations of $\{\hat{\mathbf{d}}_\mu'\}$. We can define the rotation via a set of three angles $\{\delta\theta_\mu\}_0^3$, indicating a specific element of the three-dimensional rotation group SO(3), which may then be represented by a

rotation matrix $U(\delta\boldsymbol{\theta})$. The variation of the frame orientation is thus

$$\delta\hat{\mathbf{d}}'_\mu = (U_{\mu\nu}(\delta\boldsymbol{\theta}) - \delta_{\mu\nu})\hat{\mathbf{d}}'_\nu \, . \tag{3.15}$$

Taking $U = \exp \theta_\lambda T^{(\lambda)}$ where $T^{(\lambda)}_{\mu\nu} = -\varepsilon_{\lambda\mu\nu}$ forms a basis of the Lie algebra $\mathfrak{so}(3)$, we find

$$\delta\hat{\mathbf{d}}'_\mu = \delta\theta_\lambda T^{(\lambda)}_{\mu\nu}\hat{\mathbf{d}}'_\nu = \delta\boldsymbol{\theta} \times \hat{\mathbf{d}}'_\mu \, . \tag{3.16}$$

Variations of the frame orientation results in variations of curvature and torsion via Eq. (3.12), which correspond to the rate of rotation of the frame. If we make the dynamical analogy where the rod's shape represents the trajectory of an asymmetric top, where the arclength parameter s plays the role of time, then the curvature and torsion represent the top's angular momentum components. Thus, we can define conjugate rotational moments $\mathbf{M}$, given by

$$\mathbf{M} = \Delta\boldsymbol{\kappa} + J\Delta\tau\hat{\mathbf{d}}'_3 \tag{3.17}$$

as well as a "swelling moment" $\mathbf{M}_{\text{swell}}$

$$\mathbf{M}_{\text{swell}} = k_1\boldsymbol{\psi} \times \hat{\mathbf{d}}'_3 \tag{3.18}$$

which represents the torque exerted by swelling stresses due to the internal phase separation. Using the relations [52]

$$\begin{aligned} \Delta\kappa'_1 &= \hat{\mathbf{d}}'_1 \cdot \nabla_s\delta\boldsymbol{\theta} \\ \Delta\kappa'_2 &= \hat{\mathbf{d}}'_2 \cdot \nabla_s\delta\boldsymbol{\theta} \\ \Delta\tau' &= \hat{\mathbf{d}}'_3 \cdot \nabla_s\delta\boldsymbol{\theta} \end{aligned} \tag{3.19}$$

the rod shape set by $\boldsymbol{\kappa}'$ and τ' satisfies the Kirchhoff equations

$$\nabla_s(\mathbf{M}+\mathbf{M}_{\text{swell}}) = \dot{\mathbf{M}} + \dot{\mathbf{M}}_{\text{swell}} + (\boldsymbol{\kappa}' + \tau'\hat{\mathbf{d}}_{\mathbf{3}}) \times (\mathbf{M}+\mathbf{M}_{\text{swell}}) = 0 \; . \tag{3.20}$$

The Kirchhoff equations are a system of nonlinear, first-order differential equations that result from requiring balance of internal and applied, i.e. swelling, moments along a rod that is generally curved. In the special case of a symmetric rod with isotropic bending modulus, there are closed-form solutions, just as with the symmetric top. However, the rod equations incorporate an asymmetric bending modulus and much like the asymmetric top, we expect that Eq. (3.20) are non-integrable and can even have chaotic solutions [53, 54].

3.3 Buckling of phase-separated rings

We consider the simple case of the symmetric equilibrium of a planar, ring-like hydrogel toroid and its buckling instability, recovering the result of [35]. The planar ring initially has a centerline given by

$$\boldsymbol{\ell}(s) = R\left(\cos\frac{s}{R}\hat{\mathbf{e}}_{\mathbf{1}} + \sin\frac{s}{R}\hat{\mathbf{e}}_{\mathbf{2}}\right) \tag{3.21}$$

and we choose the frame to correspond to the usual Frenet-Serret frame

$$\begin{aligned}
\hat{\mathbf{d}}_{\mathbf{1}}(s) &= -\cos\frac{s}{R}\hat{\mathbf{e}}_{\mathbf{1}} - \sin\frac{s}{R}\hat{\mathbf{e}}_{\mathbf{2}} \\
\hat{\mathbf{d}}_{\mathbf{2}}(s) &= \hat{\mathbf{e}}_{\mathbf{3}} \\
\hat{\mathbf{d}}_{\mathbf{3}}(s) &= -\sin\frac{s}{R}\hat{\mathbf{e}}_{\mathbf{1}} + \cos\frac{s}{R}\hat{\mathbf{e}}_{\mathbf{2}}
\end{aligned} \tag{3.22}$$

as shown in Fig. 3.2. The initial curvature is therefore $\boldsymbol{\kappa} = (1/R)\hat{\mathbf{d}}_{\mathbf{2}}$ and, as the centerline lies in the plane, it is torsionless.

Now consider the equilibrium where the ring maintains uniform curvature and

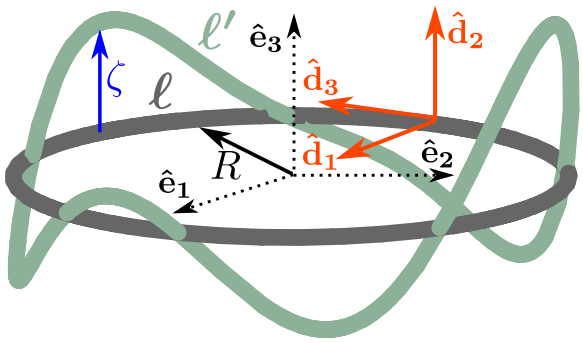

Figure 3.2: Planar ring $\boldsymbol{\ell}$ with a representative form of perturbed ring $\boldsymbol{\ell}' = \boldsymbol{\ell} + \zeta\hat{\mathbf{d}}_2$ defined in reference to a fixed basis $\{\hat{\mathbf{e}}_1, \hat{\mathbf{e}}_2, \hat{\mathbf{e}}_3\}$.

planar shape, only able to undergo *homogeneous* changes in radius $R \to R'$. However, as we are considering the extensible limit of rods, the circumference of the ring cannot change so we require that $R' = R$; thus, $\kappa' = \kappa$ and $\Delta\kappa = 0$. In this equilibrium,

$$L = \pi R \left[-r|\boldsymbol{\psi}|^2 + \frac{1}{2}u|\boldsymbol{\psi}|^4 + 2k_2\frac{1}{R}\psi_1 \right] \tag{3.23}$$

so $\boldsymbol{\psi}$ attains an equilibrium value

$$\boldsymbol{\psi}^* \approx -\left(\sqrt{\frac{r}{u}} + \frac{k_2}{2rR} + \mathcal{O}(R^{-2}) \right) \hat{\mathbf{d}}_1 \tag{3.24}$$

where, for simplicity, we take R to be large. We may regard this symmetric equilibrium as corresponding to an ordered polar phase of the ring where the initial curvature sets the alignment direction as $-\hat{\mathbf{d}}_1$.

To address the stability of this homogeneous equilibrium, we have to determine the free-energy change due to inhomogeneous variations of the fields about their equilibrium values. Observing that the free-energy is lowered only if

$$2k_1\psi_1^* \int_0^{2\pi R} \mathrm{d}s\Delta\kappa_2 < 0 \tag{3.25}$$

and that the arclength integral of the curvature of any simple closed planar curve is

2π (see e.g., [43]) the ring must therefore be linearly stable to planar deflection of the centerline. We therefore search for instabilities by considering non-planar deflections of the centerline

$$\boldsymbol{\ell'} = \boldsymbol{\ell} + \zeta(s)\hat{\mathbf{d}}_{\mathbf{2}} \tag{3.26}$$

as well as transverse fluctuations of $\boldsymbol{\psi}$

$$\boldsymbol{\psi} \approx |\boldsymbol{\psi}^*| \left[-\left(1 - \frac{1}{2}\varphi(s)^2\right)\hat{\mathbf{d}}_{\mathbf{1}} + \varphi(s)\hat{\mathbf{d}}_{\mathbf{2}} \right] \tag{3.27}$$

where we assume that the magnitude $|\boldsymbol{\psi}^*|$ remains fixed. The geometric curvature and geometric torsion, corresponding to the deformed Frenet-Serret frame $\{\hat{\mathbf{n}}', \hat{\mathbf{b}}', \hat{\mathbf{t}}'\}$, as in Appendix B, are given by

$$\kappa_{\text{geo}} \approx \frac{1}{R}\left(1 + \frac{1}{2}R^2\ddot{\zeta}^2 - \dot{\zeta}^2\right) \tag{3.28}$$

$$\tau_{\text{geo}} \approx \frac{1}{R}\left(R^2\dddot{\zeta} + \dot{\zeta}\right) \ . \tag{3.29}$$

Finally, we assume that the transverse frame $\{\hat{\mathbf{d}}_{\mathbf{1}}', \hat{\mathbf{d}}_{\mathbf{2}}'\}$ can undergo an additional rotation by $\xi(s)$, from the Frenet-Serret frame, resulting in a transformation of curvature and torsion (see Eq. (B.8)):

$$\begin{aligned} \Delta\kappa_1 &= \kappa_{\text{geo}} \sin\chi \approx \frac{1}{R}\chi \\ \Delta\kappa_2 &= \kappa_{\text{geo}} \cos\chi \approx \frac{1}{R}\left(-\frac{1}{2}\chi^2 + \frac{1}{2}R^2\ddot{\zeta}^2 - \dot{\zeta}^2\right) \\ \Delta\tau &= \tau_{\text{geo}} + \dot{\chi} \approx \frac{1}{R}\left(R^2\dddot{\zeta} + \dot{\zeta}\right) + \dot{\chi} \end{aligned} \tag{3.30}$$

The second variation of the Landau free-energy is therefore given by

$$\begin{aligned} \delta^2 L = \frac{1}{2}\int_0^{2\pi R} \mathrm{d}s \Bigg[& B\frac{1}{R^2}\chi^2 + J\left(\frac{1}{R}(R^2\dddot{\zeta} + \dot{\zeta}) + \dot{\chi}\right)^2 \\ & + C|\psi_1^*|^2\dot{\varphi}^2 + \frac{k_2|\psi_1^*|}{R}\varphi^2 - \frac{k_1|\psi_1^*|}{R}(R^2\ddot{\zeta}^2 - 2\dot{\zeta}^2 - \chi^2 + 2\chi\varphi)\Bigg] \ . \end{aligned} \tag{3.31}$$

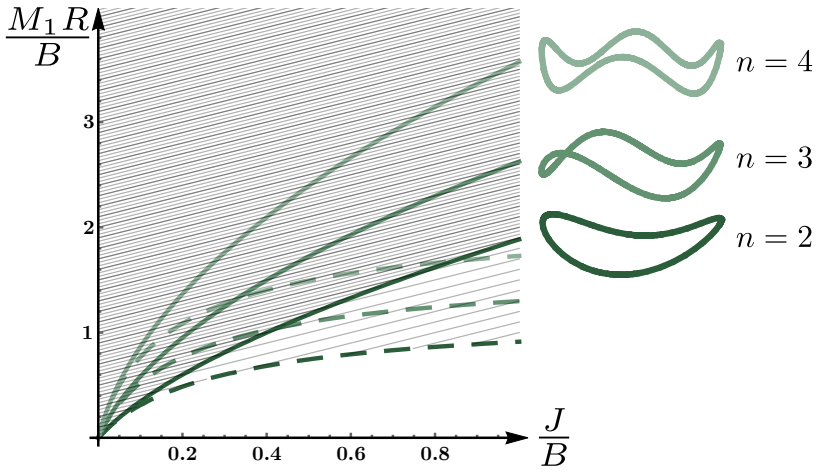

Figure 3.3: Buckling thresholds shown for dimensionless stress $M_1 R/B$ versus dimensionless torsional rigidity J/B; hatched regions are unstable. Solid lines represent the case in which fluctuations in $\boldsymbol{\psi}$ is quenched, reproducing Fig. 3 from [35]. Dashed lines include effect of fluctuating $\boldsymbol{\psi}$, with $C'/B = M_2 R/B = 1$.

After performing a Fourier expansion in each of the perturbing fields (see Appendix E), we find buckling thresholds for each of the modes, indexed by n, as shown in Fig. 3.3. Two cases are shown: solid lines represent the result when variations of $\boldsymbol{\psi}$ are quenched, recovering the result of [35]; dashed lines show the effect of including variations of $\boldsymbol{\psi}$. Modes $n \geq 2$ are shown as the first Fourier mode corresponds to a rigid rotation of the ring and is thus excluded from our analysis. The lowest mode to go unstable is $n = 2$, resulting in the "Pringle" shape that is characteristic of ring buckling. Note that allowing $\boldsymbol{\psi}$ to fluctuate decreases the buckling threshold for all modes. This is not surprising as quenching fluctuations is tantamount to constraining degrees of freedom, thus making the rod more rigid.

3.4 Spin and twist: Goldstone modes of hydrogel rods

The case of an initially straight rod is special as it is unstable to *spontantous* symmetry breaking to a state of constant $\boldsymbol{\psi}$ and $\Delta\boldsymbol{\kappa} = \boldsymbol{\kappa'}$ which solve the equilibrium equations (Eqs. (3.14),(3.20) and (3.14)) but whose direction is not uniquely specified, and thus results in a spontaneously chosen direction, which we may specify by as a

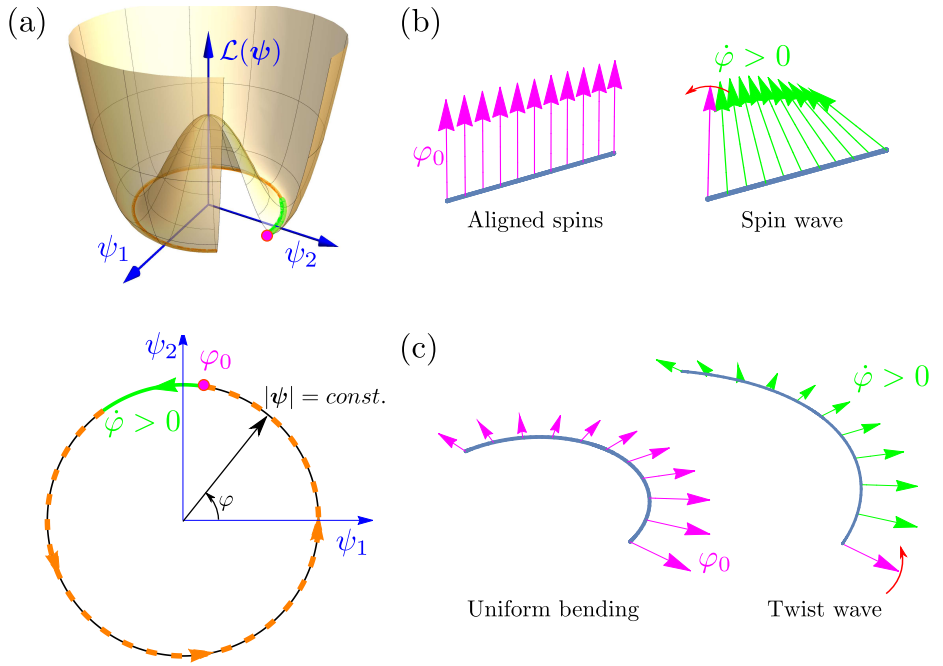

Figure 3.4: (a) Minimium of the quartic potential $\mathcal{L}(\boldsymbol{\psi})$ has continuous rotational symmetry of phase field $\delta\phi$ at fixed $|\boldsymbol{\psi}|$. (b) A spin chain that possesses an aligned phase with spontaneous phase φ_0 has spin wave Goldstone modes with modulated phase φ. (c) The polarized rod with spontaneous bending direction set by φ_0 has "twist wave" Goldstone modes with modulated bending direction.

phase φ of the polarization $\boldsymbol{\psi}$, as in Fig. 3.4a. In this way, the initially straight rod resembles a spin chain that spontaneously forms an ordered phase of aligned spins, or a ferromagnetic phase whose magnetization order parameter, defined as the average orientation of the spins, attains a fixed value but points in an arbitrary direction, as shown in Fig. 3.4b. As this ordering breaks a *continuous* symmetry, a long wavelength modulation of the orientation known as a "spin wave" [55] has an energetic cost that vanishes as wavenumber $k \to 0$, corresponding to the limit of a global rotation of the orientation and are thus "gapless." The Landau free-energy models the cost of such a deformation and for small enough k, only the quadratic order term is kept so $L_{\text{spin}-\text{wave}} \propto k^2$.

In general, any system that spontaneously breaks a continuous symmetry supports these gapless excitations [56, 57], also called Nambu-Goldstone modes. With

the characteristic $\propto k^2$ energy cost, Goldstone modes provide the foundation for elasticity of condensed matter systems: the proportionality constant is known as the rigidity of the modes [20]. This is easily seen in crystalline systems where the position of a lattice breaks the continuous translational symmetry and modulations of the lattice position, low-frequency acoustic phonons, are Goldstone modes of the system. Rigidity from broken continuous symmetry is, however, perhaps best exemplified by liquid crystals, "mesophase" systems possessing both liquid and crystalline characteristics [47]. In the case of nematic liquid crystals, the orientation of the molecules, defined similarly to the magnetization of a spin chain, is spontaneously broken and distortions of this "director field" away from a uniform orientation are characterized as twist, splay, and bend deformations with their respective rigidities. Furthermore, due to the vanishingly small energy cost of Goldstone modes, they are susceptible to thermal fluctuations and thus, by the Fluctuation-Dissipation theorem [58], play an important role in energy dissipation [20].

Goldstone modes of the straight rod, much like spin waves, correspond to the rod whose orientation undergoes a long wavelength rotation about the centerline as shown in Fig. 3.4c. In the limit where the orientation of the symmetry-broken rod is modulated very little along the rod's length, we may once again consider a "quasistatic" treatment where the rod is in equilibrium at all points along its length, independent of all other points, despite the imposed rotation of the bending direction. Fixing the magnitudes of $\boldsymbol{\psi}$ and $\boldsymbol{\kappa'}$, we note that the moment balance Eq. (3.20) requires that $\boldsymbol{\kappa'} || \boldsymbol{\psi} \times \hat{\mathbf{d}}'_{\mathbf{3}}$ so

$$\begin{aligned} \boldsymbol{\psi} &= |\boldsymbol{\psi}|(\hat{\mathbf{d}}'_{\mathbf{1}} \cos\varphi(s) + \hat{\mathbf{d}}'_{\mathbf{2}} \sin\varphi(s)) = -|\boldsymbol{\psi}|\hat{\mathbf{n}}'(s) \\ \boldsymbol{\kappa'} &= |\boldsymbol{\kappa'}|\hat{\mathbf{b}}'(s) \end{aligned} \tag{3.32}$$

where $\varphi(s)$ describes the modulation of the rod's orientation. The rotation of $\boldsymbol{\psi}$ in going from $s \to s + \delta s$ is therefore $\delta\boldsymbol{\psi} = \delta\varphi\ \hat{\mathbf{d}}'_{\mathbf{3}}$. As $\boldsymbol{\psi}$ always points in $-\hat{\mathbf{n}}$ and $\boldsymbol{\kappa'}$

always points in $\hat{\mathbf{b}}$ we have

$$\delta\hat{\mathbf{n}} = \delta\varphi\ \hat{\mathbf{d}}'_{\mathbf{3}} \times \hat{\mathbf{n}} = \delta\varphi\ \hat{\mathbf{b}};\ \ \delta\hat{\mathbf{b}} = -\delta\varphi\ \hat{\mathbf{n}}\ . \tag{3.33}$$

Thus, we see that by the Frenet-Serret equations Eq. (B.5), the torsion is $\tau' = \dot{\varphi}$. Therefore, the change in the Landau free-energy due to slow modulation is,

$$\Delta L = \frac{1}{2}\int \mathrm{d}s(J + C|\boldsymbol{\psi}|^2)\dot{\varphi}^2\ . \tag{3.34}$$

We find that by representing the orientation ϑ in Fourier space

$$\varphi(s) = \int \text{đ}k\ \hat{\varphi}(k)e^{iks} \tag{3.35}$$

borrowing $\text{đ}k = \mathrm{d}k/2\pi$ [48], that the free-energy per mode is $(1/2)C_{\mathrm{tw}}k^2$ which is indeed proportional to k^2, with "twist wave" rigidity $C_{\mathrm{tw}} = J + C|\boldsymbol{\psi}|^2$. In addition to the "spin wave"-like mode corresponding with rotations of $\boldsymbol{\psi}$, contributing a rigidity $C|\boldsymbol{\psi}|^2$, there there is an accompanying torsion of the rod contributing a rigidity J. By introducing torsion to a rod of fixed curvature, the full rod becomes a non-planar structure, locally described as part of a helix [43].

Now, in assuming that the rod's modulation is varied slowly, we have implicitly introduced a lower length scale cutoff $\Lambda_<$, defining the size of the region for which the quasistatic approximation holds, providing an upper cutoff for $k \sim \Lambda_<^{-1}$. On the other end, the rod is assumed to be long but is practically finite and thus has an upper length scale $\Lambda_>$ which introduces a lower cutoff for $k \sim \Lambda_>^{-1}$. As we shall show in the next chapter, the effect of fluctuations of the field φ at a point s on some other point s' is characterized by the fluctuation correlation function G:

$$G(s - s') = \int_{\Lambda_>^{-1}}^{\Lambda_<^{-1}} \text{đ}k\ \frac{e^{ik(s-s')}}{k^2}\ . \tag{3.36}$$

While the upper limit doesn't give us any trouble, the k^2 denominator diverges for small k and we find that G has an *infrared divergence*, $G \sim \Lambda_>$. Therefore, the effect of a fluctuation *grows* along the rod and, in the case of long rods, results in the breakdown of long-range order. In general, the Mermin-Wagner theorem tells us that long range order can only exist in systems with a dimension $d > 2$ [48]: in higher dimensions, $đ^d k \propto |k|^{d-1} \mathrm{d}|k|$ so that the integrand scales as $|k|^{d-3}$ and thus has a removable singularity for $d > 2$. We therefore conclude that while a segment straight rod may spontaneously bend in a well-defined direction and thus lie on a plane, a very long rod will be a non-planar object. Note, however, that a planar bent rod that is long enough will always intersect itself and that this theory does not take into account the nonlocal effects of self-interaction.

3.5 Using internal phase separation for actuating deformations of hydrogel rods

One way to validate our model is to observe spontaneous bending of slender hydrogel rods along with a clear distinction between solvent-rich and solvent-poor phases that are polarized orthogonal to the bending direction. However, as straight rods have been shown in experiments to undergo a large variety of instabilities upon heating, including the surface "ballooning" seen in spherical samples, it may be difficult to observe the ordered polarization that we predict. On the other hand, there is evidence of this polarization picture in toroid-shaped samples of hydrogel [35]. The homogeneous ring curvature of the toroid provides a uniform aligning field on the polarization within our model. We therefore propose that rapid heating experiments on curved rods may provide a good test of our predictions.

An S-shaped rod, for example, undergoes a an abrupt flip in the direction of $\boldsymbol{\kappa}$ at an inflection point, as seen in Fig. 3.5a. The behavior of the polarization at this inflection point could either (i) resemble a domain wall between regions of oppositely aligned $\boldsymbol{\psi}$

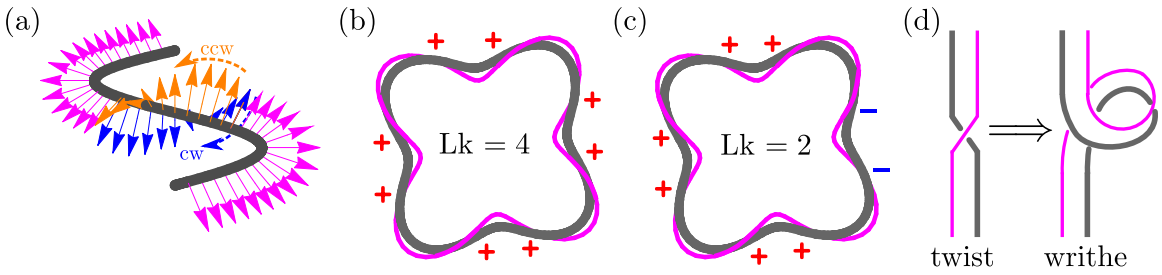

Figure 3.5: (a) An S-shaped portion of a rod with possible clockwise (cw) or counterclockwise (ccw) twist in the inflection region; (b) example planar ring with eight inflection points and "positively" crossings leading to a linking number of 4; (c) the same ring but in a configuration that includes 2 "negative" crossings and a linking number of 2; (d) interconversion between twist and write.

or (ii) undergo a rotation. The case of a rotation is expected if the inflection section is expanded into a length of gel with $\boldsymbol{\kappa} = 0$. Much like the "twist-wave" Goldstone modes, we expect a rotation of $\boldsymbol{\psi}$ to exert an internal torque that twists the rod. Therefore, such inflection points could be incorporated in the design of a hydrogel rod to yield non-planar deformations that are actuated upon rapid heating.

Polarization rotations in inflection regions can either be clockwise or counterclockwise as shown in Fig. 3.5a. This has an interesting consequence for closed rings with multiple inflection regions. As $\boldsymbol{\psi}$ obeys periodic boundary conditions in rings, there is the possibility that the phase of the polarization, φ, can be wound around the ring such that it can't be unwound without changing $|\boldsymbol{\psi}|$. Therefore, rings can support *topologically distinct* configurations of φ, two of which are shown in Fig. 3.5b,c. The number of topologically distinct windings of the polarization can be enumerated once we note that as the ring is topologically equivalent to S^1 and that the phase is a mapping $\varphi : S^1 \to S^1$. The topologically distinct configurations are thus enumerated by the first fundamental group $\pi_1(S^1) = \mathbf{Z}$, and can be described by a single integer, the winding number. Much like in other ordered materials, such as liquid crystals and crystalline solids, we find that the order that results from internal phase separation in hydrogel rods can be globally classified using the notion of a topological charge, i.e. the winding number. Equivalently, the polarization traces out a ring-like path that

winds about the centerline such that the top down projection in Fig. 3.5b,c shows crossings, which can be assigned a value of ± 1. The equivalent topological characterization of two rings is the linking number (Lk) which is computed as the sum over the crossing values, divided by 2. This number can alternatively be expressed as the sum over two geometric (i.e., non-topological) quantities, known as the twist and writhe [59]. As constant linking number, there can be an interconversion between twist and writhe, shown in Fig. 3.5d, dictating the allowable configurations of the equilibrium ring. Thus, we can expect that the stress due to a twisting polarization of the phase separated regions will be relieved through writhing, similar to how the twist in DNA double helices is converted to writhe and leads to "supercoiling" [60].

CHAPTER 4
CONTINUUM MODEL OF FLUCTUATION-ALLOSTERIC REGULATION

4.1 Introduction to allostery

The capacity for proteins to alter binding affinity due to changes in environment is essential to many biological processes. Allosteric regulation, in which binding at a certain active site on a protein is modified by the presence of an effector ligand, bound to a regulatory site on the protein, allows for such a response. Effector ligands may be either inducers, increasing the binding affinity at active site, or inhibitors, decreasing binding affinity. The traditional, textbook notion of allostery is a based on the two-state model of Monod, *et al.* [61] where effector binding triggers conformational changes of the protein, altering the geometry of the active site and thus binding ability. However, it is now recognized that effector binding does not necessarily change single protein behavior; rather, it can affect the statistics of an *ensemble* of proteins [62, 63]. Furthermore, there is evidence [64] that allostery does not require protein conformational change but may occur via changes in protein dynamics. We consider one version of dynamical allostery in which the sole effect of ligand binding is the alteration of protein vibrational normal modes, thus changing its entropy without altering its mean conformation. It has been demonstrated [65] that only a few normal modes need undergo a modest frequency adjustment to achieve a measurable entropy change.

Slow modes, characterized by long wavelength deformations, have proven to play the dominant role in fluctuation allostery as disorder in the protein's small scale structure tends to localize fast modes [66]. This observation has led to the development of

simplified models of proteins where only the large-scale features are retained [66, 67], resulting in free-energy estimates of the fluctuation-allosteric effect that are consistent with measurements. It also offers the opportunity to develop continuum elastic models of proteins based on coarse-grained descriptions of protein structures, averaged over some cutoff length scale, which may be obtained experimentally, e.g., via x-ray diffraction [68]. Proof-of-principle continuum models have shown that in order to obtain a substantial free-energy change from remote binding, there must be a high degree of inhomogeneity present [69, 70]. However, spatial modulations of rigidity of an elastic protein is not the only source of inhomogneity: the boundary of a continuum breaks translational symmetry so protein shape may be regarded prescribing an inhomogeneity.

Shape plays an important role in determining the vibrational properties of continua with an impact on the density of states of waves [71]; conversely, the vibrational spectrum may provide clues about the shape of the continuum in the inverse problem of "hearing the shape of a drumhead" [72]. In this work, we use a continuum elastic description of protein fluctuations to demonstrate that changes in coarse-grained protein shape due to ligand binding can result in fluctuation-allosteric regulation. In particular, in order to diagnose the effect of shape change on remote signal, we develop a method of computing the change in fluctuation correlations and show how this change can lead to cooperative binding effects.

4.2 Continuum Model of Coarse-Grained Protein

Consider a coarse-grained, continuum representation of a protein's shape which we'll label Ω where the resolution of the protein has been cut off at some coarse-graining length scale a. Instead of characterizing the protein by a sequence of atomic coordi-

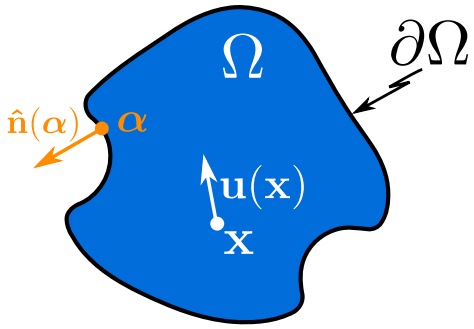

Figure 4.1: Schematic of the protein's continuum shape $\Omega \ni \mathbf{x}$, along with displacement field $\mathbf{u}$, and boundary $\partial\Omega \ni \boldsymbol{\alpha}$ with outer normal $\hat{\mathbf{n}}$

nates $\{\mathbf{x}_i\}$ and the corresponding pairwise interactions

$$\sum_{i<j} V(|\mathbf{x}_i - \mathbf{x}_j|) \tag{4.1}$$

the atomic positions are averaged, blurred out over a volume a^3, resulting in a smooth density profile $\rho(\mathbf{x})$, as well as an energy functional $V[\rho]$ which is likewise smooth. This standard coarse-graining procedure provides the basis for developing continuum theories (see e.g., [39]) and has also been used to characterize large-scale protein structure [68].

With a continuum representation of the protein in hand, we now consider a continuum linear elastic description of small deformations. Starting from an equilibrium conformation where the protein has a fixed mean shape Ω, a small shape change displaces points $\mathbf{x} \to \mathbf{x} + \mathbf{u}(\mathbf{x})$ where $\mathbf{u}$ is a displacement field, depicted in Fig. 4.1. Assuming an interaction of the form Eq. (4.1), the protein's energy changes only if inter-atomic lengths are changed. The change in continuum intervals $|\mathrm{d}\mathbf{x}|^2$ is

$$\begin{aligned} |\mathrm{d}\mathbf{x} + \mathrm{d}\mathbf{u}|^2 - |\mathrm{d}\mathbf{x}|^2 &= \mathrm{d}\mathbf{x} \cdot \mathrm{d}\mathbf{u} + \mathrm{d}\mathbf{u} \cdot \mathrm{d}\mathbf{x} + |\mathrm{d}\mathbf{u}|^2 \\ &= (\partial_i u_j + \partial_j u_i + \partial_i \mathbf{u} \cdot \partial_j \mathbf{u}) \mathrm{d}x^i \mathrm{d}x^j \equiv 2u_{ij} \mathrm{d}x^i \mathrm{d}x^j \end{aligned} \tag{4.2}$$

where the strain tensor u_{ij} is symmetric, reflecting invariance under rotation. By

considering small fluctuations of the protein's shape, we approximate the strain tensor to leading order in $\mathbf{u}$

$$u_{ij} \approx \frac{1}{2}(\partial_i u_j + \partial_j u_i) \; . \tag{4.3}$$

Expanding the energetic cost of small deformations about an equilibrium conformation leads to a general form for the elastic energy

$$H = \frac{1}{2}\int_\Omega \mathrm{d}V_x \; C_{ijkl}(\mathbf{x}) u_{ij}(\mathbf{x}) u_{kl}(\mathbf{x}) = \frac{1}{2}\int_\Omega \mathrm{d}V_x \; C_{ijkl}(\mathbf{x}) \; \partial_i u_j \; \partial_k u_l \tag{4.4}$$

where the elastic constant tensor C is generally inhomogeneous and anisotropic but, owing to the symmetry of the strain tensor $u_{ij} = u_{ji}$, must have the following symmetries

$$C_{ijkl} = C_{jikl} = C_{ijlk} = C_{klij} \tag{4.5}$$

which reduces the number of independent components from $3^4 = 81$ to 21 [73]. In the case of an isotropic continuum, the elastic constant tensor is further reduced

$$C_{ijkl} = \mu(\delta_{ik}\delta_{jl} + \delta_{il}\delta_{jk}) + \lambda\delta_{ij}\delta_{kl} \tag{4.6}$$

where μ is the shear modulus and λ is the Lamé parameter related to the bulk modulus K via $\lambda = K - \frac{2}{3}\mu$.

Integrating Eq. (4.7) by parts and applying Stokes' theorem,

$$H = \frac{1}{2}\oint_{\partial\Omega} \mathrm{d}S_\alpha \; u_i(\boldsymbol{\alpha})\hat{n}_j(\boldsymbol{\alpha}) C_{ijkl}(\boldsymbol{\alpha}) \frac{\partial}{\partial \alpha^k} u_l(\boldsymbol{\alpha}) - \frac{1}{2}\int_\Omega \mathrm{d}V_x \; u_j \partial_j C_{ijkl}(\mathbf{x}) \; \partial_k u_l \tag{4.7}$$

the equilibrium condition $\delta H = 0$ yields the equilibrium equation

$$-\partial_j C_{ijkl} \partial_k u_l \equiv \hat{\mathcal{H}}_{il} u_l = 0 \;\; \text{for } \mathbf{x} \in \Omega \tag{4.8}$$

with zero-traction boundary conditions

$$\hat{n}_j(\boldsymbol{\alpha})C_{ijkl}(\boldsymbol{\alpha})\frac{\partial}{\partial\alpha^k}u_l(\boldsymbol{\alpha}) = 0 \text{ for } \boldsymbol{\alpha} \in \partial\Omega \tag{4.9}$$

due to the free variations of δu at the boundary and is equivalent to specifying that the protein is fluctuating at *constant hydrostatic pressure* P. The equilibrium elasticity operator $\hat{\mathcal{H}}_{ij}$ defined in Eq. (4.8) along with the zero-traction boundary conditions specifies the vibrational spectrum of the protein. The spectrum is defined through the eigenvalue problem

$$(\hat{\mathcal{H}} - \epsilon_n \mathbb{1})\boldsymbol{\eta}_n = 0 \tag{4.10}$$

where the eigenfunctions $\boldsymbol{\eta}_n$ obey the zero-traction boundary conditions and are continuum normal modes of the elastic medium. Importantly, the eigenfunctions form a complete set

$$\sum_{n=0}^{\infty} \eta_{n,i}(\mathbf{x})\eta_{n,j}(\mathbf{y}) = \delta_{ij}\delta(\mathbf{x}-\mathbf{y}) \tag{4.11}$$

and can be taken to be orthonormal

$$\int_\Omega \mathrm{d}V_x \boldsymbol{\eta}_m \cdot \boldsymbol{\eta}_n = \delta_{mn} \, . \tag{4.12}$$

4.3 Shape fluctuations calculated via ensemble theory

Recall that we seek to study allosteric regulation as a change in protein statistic rather than a deterministic effect on a single protein. To this end, consider an ensemble of proteins of the same continuum shape Ω in a thermal reservoir at temperature $k_BT = \beta^{-1}$; averages of the deformation field $\mathbf{u}$ are calculated by sampling proteins from this ensemble, each of which generally has a unique displacement field, representing a unique microstate σ. Within this *canonical ensemble* [23], the probability of observing

a certain microstate σ is proportional to a Boltzmann factor

$$P(\sigma) = \frac{1}{Z} e^{-\beta H(\sigma)} \tag{4.13}$$

where the proportionality constant $1/Z$ normalizes the distribution, $\sum_\sigma P = 1$, so

$$Z = \sum_\sigma e^{-\beta H(\sigma)} \tag{4.14}$$

which is the canonical partition function. As the microstate specified by a given deformation field, the partition function is a sum over field configurations

$$Z = \int \mathcal{D}\mathbf{u} e^{-\beta H[\mathbf{u}]} = e^{-\beta G} \tag{4.15}$$

where $H[\mathbf{u}]$ is the energy functional Eq. (4.7) and we have introduced the Gibbs free-energy G which is the thermodynamic potential that characterizes the system at fixed constraints of temperature T, pressure P (c.f. the boundary condition Eq. (4.9)), and number of atoms N. The functional integral is a field generalization of the Feynman path integral [74] and can similarly be evaluated by subdividing Ω into N regions, with $N \to \infty$, indexed by $\mathbf{x}_n$, as shown in Fig. 4.2. The displacement field evaluated at one of these points $\mathbf{u}_n = \mathbf{u}(\mathbf{x}_n)$ is then integrated over $\mathbb{R}^3$, independently of its neighboring points, so

$$\int \mathcal{D}\mathbf{u} = \lim_{N\to\infty} \underbrace{\int_{\mathbb{R}^3} \int_{\mathbb{R}^3} \cdots \int_{\mathbb{R}^3}}_{N} \prod_{n=1}^{N} [\mathrm{d}\mathbf{u}_n] \, . \tag{4.16}$$

Note that uniform translations and rotations of Ω do not stretch the protein in any way so $u_{ij} = 0$ and thus the elastic energy Eq. (4.7) disappears, leading to diverging contributions to Z. This is a problem manifest in gauge theories where H has some gauge symmetry and is solved by a process of gauge fixing. Thus, we restrict the set

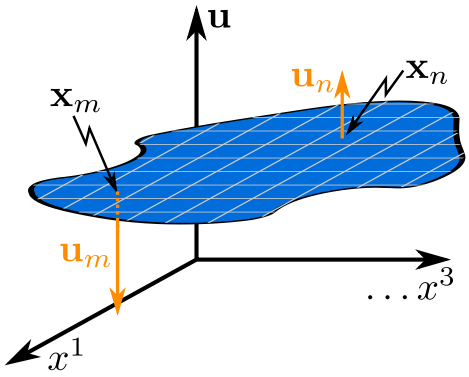

Figure 4.2: Continuum subdivided into small volumes, indexed by points $\mathbf{x}_n$ with a displacement vector $\mathbf{u}_n$ for $n \in \{1 \ldots N\}$.

of permissible deformations to the space of *located shapes*

$$Z = \int_{(\text{loc})} \mathcal{D}\mathbf{u}\; e^{-\beta H[u]} \tag{4.17}$$

that have fixed center of mass and orientation, borrowing the term from the theory of gauge kinematics [75]. However, this restriction isn't easily made using the definition of the functional integral in Eq. (4.16) as it is a coordinated restriction between all of the points in Ω. Following [76], we instead use a system of collective coordinates $\{b_n\}$ with a basis provided by the normal modes,

$$\mathbf{u}(\mathbf{x}) = \sum_{\alpha=1}^{6} b_0^{(\alpha)} \boldsymbol{\eta}_0^{(\alpha)}(\mathbf{x}) + \sum_{n=1}^{\infty} b_n \boldsymbol{\eta}_n(\mathbf{x}) \tag{4.18}$$

where $\{\boldsymbol{\eta}_0^{(1)}, \ldots, \boldsymbol{\eta}_0^{(6)}\}$ is the set of zero-modes, forming a degenerate subspace with $\epsilon_0 \equiv 0$, i.e. a set of $d = 3$ translations along with a set of rotations, and $\boldsymbol{\eta}_{n>1}$ modes that are transverse to the zero-modes subspace, which we show schematically in Fig. 4.3. The functional integration restricted to the space of located shapes is thus conveniently given by

$$\int_{(\text{loc})} \mathcal{D}\mathbf{u} = \int_{-\infty}^{\infty} \cdots \int_{-\infty}^{\infty} \prod_{n=1}^{\infty} [\mathrm{d}b_n] \tag{4.19}$$

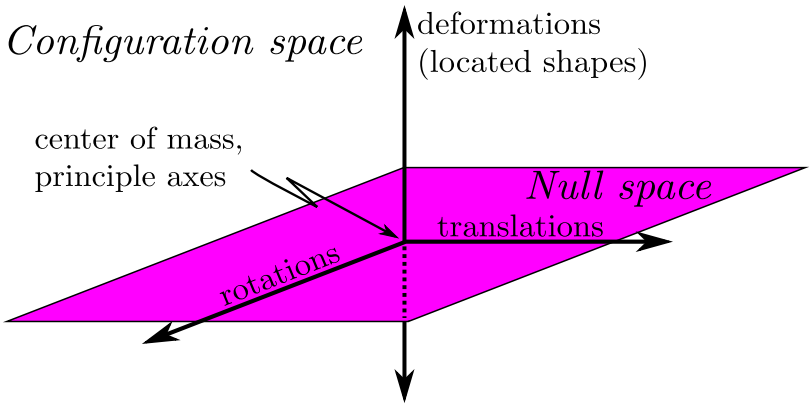

Figure 4.3: Partitioning of configuration space into the null space, spanned by zero-modes of the elasticity operator and its complement, the space of located shapes. Deformations are taken in reference to the protein's center of mass and principle axes of intertia.

where $b_n \in (-\infty, \infty)$. As the energy is quadratic in b_n,

$$H = \frac{1}{2} \sum_{n=1}^{\infty} b_n^2 \epsilon_n \tag{4.20}$$

the partition function is easily evaluated as a product of Gaussian integrals

$$Z = \prod_{n=1}^{\infty} \int_{-\infty}^{\infty} \mathrm{d}b_n \; e^{-\frac{1}{2}\beta\epsilon_n b_n^2} = \prod_{n=1}^{\infty} \sqrt{\frac{2\pi}{\beta\epsilon_n}} = \mathcal{N} \left(\det{}' \; \beta\hat{\mathcal{H}} \right)^{-1/2} \tag{4.21}$$

where we have identified the product of non-zero eigenmodes as the determinant of the operator $\hat{\mathcal{H}}$, restricted to the space transverse to the null space.

To measure the degree to which shape fluctuations in different locations of the protein are related, consider the fluctuation correlation function

$$\langle u_i(\mathbf{x}) u_j(\mathbf{y}) \rangle = \frac{1}{Z} \int_{(\mathrm{loc})} \mathcal{D}\mathbf{u} \; e^{-\beta H[\mathbf{u}]} u_i(\mathbf{x}) u_j(\mathbf{y}). \tag{4.22}$$

Using the collective coordinate representation, we find that

$$\langle u_i(\mathbf{x}) u_j(\mathbf{y}) \rangle = k_B T \sum_{n=1}^{\infty} \frac{\eta_{n,i}(\mathbf{x}) \eta_{n,j}(\mathbf{y})}{\epsilon_n} \tag{4.23}$$

Therefore, $\langle u_i(\mathbf{x})u_j(\mathbf{y})\rangle = k_BT\Gamma_{ij}(\mathbf{x},\mathbf{y})$ where Γ is a *Green's function* satisfying

$$\begin{aligned}\hat{\mathcal{H}}_{ij}(\mathbf{x})\Gamma_{jk}(\mathbf{x},\mathbf{y}) &= \tilde{\delta}_{ik}(\mathbf{x},\mathbf{y}) \ \text{ for } \mathbf{x},\mathbf{y}\in\Omega \\ \hat{n}_j(\boldsymbol{\alpha})C_{ijkl}(\boldsymbol{\alpha})\frac{\partial}{\partial\alpha^k}\Gamma_{lm}(\boldsymbol{\alpha},\cdot) &= 0 \ \text{ for } \boldsymbol{\alpha}\in\partial\Omega\end{aligned} \tag{4.24}$$

where $\tilde{\delta}$ is the identity in the space transverse to the zero-mode subspace and Γ is referred to as the Moore-Penrose pseudoinverse of $\hat{\mathcal{H}}$; for more details, refer to Appendix F.

4.4 Change in elastic Green's function due to shape variation

Consider the addition of a small, continuum shape ω, representing a bound ligand to the larger protein shape Ω at a region $\Sigma \subset \partial\Omega$ representing a binding site, as shown in Fig. 4.4. Assuming that such an addition doesn't change the equilibrium conformation of the protein, the ligand-bound protein can be regarded as a continuum with a slightly different domain Ω'. It is essential that Ω' is *not a deformation* of Ω but should be treated as a completely different equilibrium protein of shape Ω'. To determine difference in shape fluctuations between the protein Ω and ligand-bound protein Ω, we determine the change in their elastic Green's functions Γ' and Γ. As Γ' and Γ are functions on two different spaces, we have to be careful about defining their difference $\Delta\Gamma = \Gamma' - \Gamma$. However, as $\Omega' = \Omega \cup \omega$, we can consider $\Gamma'_{ij}(\mathbf{x},\mathbf{y})$ as a *restriction* of the full function $\Gamma'_{ij}(\mathbf{x}',\mathbf{y}')$ to the protein part of the protein-ligand whole, so we can define

$$\Delta\Gamma_{ij}(\mathbf{x},\mathbf{y}) \equiv \Gamma'_{ij}(\mathbf{x},\mathbf{y}) - \Gamma_{ij}(\mathbf{x},\mathbf{y}) \text{ for } \mathbf{x},\mathbf{y}\in\Omega\ . \tag{4.25}$$

We seek a perturbative calculation of $\Gamma' = \Gamma + \Delta\Gamma$ in terms of a small parameter that scales with the size of the ligand ω. Thus we need a formalism where the Green's function equation Eq. (4.24) for Γ' can be expressed in terms of the equation for Γ,

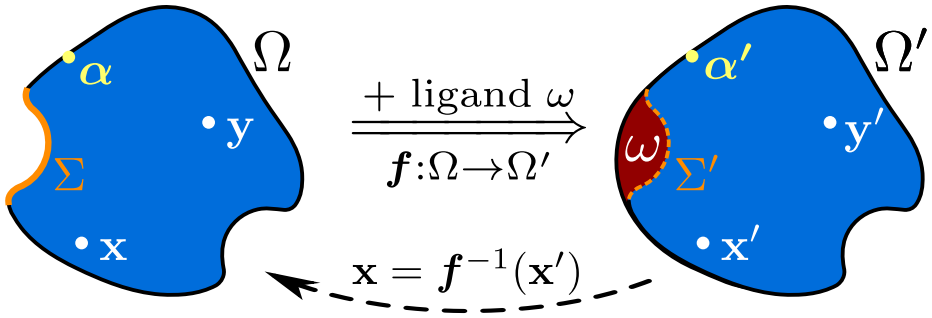

Figure 4.4: The addition of a small ligand ω at boundary location Σ results in a new protein domain Ω'. If the two shapes are diffeomorphic then $\mathbf{f}$ is a mapping between the two shapes.

plus a small correction. However, we face a problem where the form of the equilibrium elastic operator

$$\hat{\mathcal{H}}_{il} = -\partial_j C_{ijkl} \partial_k \tag{4.26}$$

remains unchanged but the change comes in through the specification of the *domain* and thus the boundary conditions as well. Equivalently, $\hat{\mathcal{H}}$ has different spectral forms due to the different eigenvalues and eigenfunctions in the two domains; even the zero modes $\boldsymbol{\eta}_0^{(\alpha)}$ are different as the orthonormal condition requires integration over different domains Ω' and Ω. This problem therefore lies outside of the familiar Schrödinger perturbation theory and is reminiscent of the problem of solving for the eigenstates of a particle, well known in a spherical potential, in a slightly ellipsoidal potential. A method of solving this problem involving a coordinate transformation that maps the ellipsoid onto the sphere was developed by Migdal [77] in the context of computing nuclear moments of inertial. This coordinate transformation alters the Hamiltonian, so that the result is then obtainable via Schrödinger perturbation theory [78] and provides a program for our calculation.

Problems of *domain variation* are important within the field of shape optimization and the study of moving surfaces [79]. In particular, the *Hadamard variational formula* provides $\Delta\Gamma$ in the case of Laplace's equation [80]. The method that we will use here is based on the approach of *interior variation* similar to that of [81, 82] and

relies on a diffeomorphism

$$\begin{array}{rccc} \boldsymbol{f}: & \Omega & \longrightarrow & \Omega' \\ & \mathbf{x} & \mapsto & \mathbf{x}' \end{array}$$

which results in a *pullback* of the operator $\hat{\mathcal{H}}$ on Ω' to a new operator $\hat{\mathcal{H}}'$ on Ω, analogous to the change in the Hamiltonian in Migdal's method.

Rather than taking the approach of Hadamard and others where a transformed Green's function equation Eq. (4.24) is found, we take a field-theory approach, calculating Γ' as

$$k_B T \Gamma'_{ij}(\mathbf{x}', \mathbf{y}') = \frac{\int_{(\mathrm{loc})} \mathcal{D}\mathbf{u}' \exp\{-\beta \int_{\Omega'} \mathrm{d}V_{z'}\ \mathcal{H}'(\mathbf{u}')\} u'_i(\mathbf{x}') u'_j(\mathbf{y}')}{\int_{(\mathrm{loc})} \mathcal{D}\mathbf{u}' \exp\{-\beta \int_{\Omega'} \mathrm{d}V_{z'}\ \mathcal{H}'(\mathbf{u}')\}} \tag{4.27}$$

where

$$\mathcal{H}' = \frac{1}{2} C_{ijkl}(\mathbf{z}')\ \partial'_i u'_j\ \partial'_k u'_l \tag{4.28}$$

is the energy density in Ω'. Now let $\mathbf{x}' = \boldsymbol{f}(\mathbf{x}) \equiv \mathbf{x} + \mathbf{s}(\mathbf{x})$ where $\mathbf{s}$ is a vector field describing the deformation that *would be required* to take $\Omega \to \Omega'$. Expanding the integrals in Eq. (4.27) to leading order in $\mathbf{s}$, we find that

$$\begin{aligned} k_B T \Delta\Gamma_{ij}(\mathbf{x}, \mathbf{y}) \approx -k_B T \int_\Sigma \mathrm{d}S_\alpha\ \zeta(\boldsymbol{\alpha}) \Big\{ & C_{klmn}(\boldsymbol{\alpha}) \frac{\partial \Gamma_{ik}(\mathbf{x}, \boldsymbol{\alpha})}{\partial \alpha^l} \frac{\partial \Gamma_{nj}(\boldsymbol{\alpha}, \mathbf{y})}{\partial \alpha^m} \\ & + K_{ik}(\mathbf{x}, \boldsymbol{\alpha}) \Gamma_{kj}(\boldsymbol{\alpha}, \mathbf{y}) + \Gamma_{ik}(\mathbf{x}, \boldsymbol{\alpha}) K_{kj}(\boldsymbol{\alpha}, \mathbf{y}) \Big\} \end{aligned} \tag{4.29}$$

where $\zeta(\boldsymbol{\alpha}) = \hat{\mathbf{n}} \cdot \mathbf{s}(\boldsymbol{\alpha})$ describes the depth of the perturbation and the null-space projection kernel K is given by Eq. (F.9); see Appendix G for full calculation details. It is important to note that Eq. (G.16) is a linear elastic version of Hadamard's result for Laplace Green's functions [79–82]. Furthermore, this leading order perturbative correction to the only involves single "scattering" off of the binding site boundary and that the magnitude of the correction scales with the volume of the ligand as illustrated

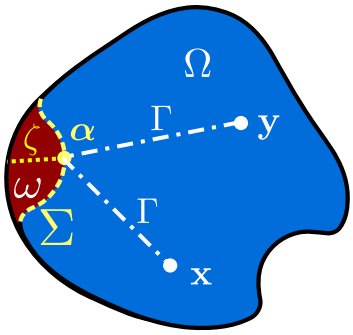

Figure 4.5: Graphical representation of the change in the Green's function as a scattering off of the binding site Σ, weighted with ligand depth ζ, with bare Green's function Γ.

in Fig. 4.5. The last two terms are required to ensure that the new Green's function Γ' is orthogonal to the zero-modes of the new protein shape. Finally, the formula holds for either ligand additions, which increase protein volume, ligand detachments or "scooping out" volume, or combinations of both. Importantly, this feature means that by varying the form of shape alteration, described by ζ, one can tune the fluctuation correlations.

4.5 Implications for Allostery

As strain quantifies anisotropic stretching of a material, the strain fluctuation correlations

$$\langle u_{ij}(\mathbf{x})u_{kl}(\mathbf{y})\rangle = \frac{1}{4}k_BT\bigg(\frac{\partial^2\Gamma_{jl}(\mathbf{x},\mathbf{y})}{\partial x^i\partial y^k}+\frac{\partial^2\Gamma_{il}(\mathbf{x},\mathbf{y})}{\partial x^j\partial y^k} + \frac{\partial^2\Gamma_{jk}(\mathbf{x},\mathbf{y})}{\partial x^i\partial y^l}+\frac{\partial^2\Gamma_{ik}(\mathbf{x},\mathbf{y})}{\partial x^j\partial y^l}\bigg) \tag{4.30}$$

detail the degree to which *shape deformations* of two regions in the protein are related. Taking the appropriate derivatives of Eq. (G.16), we find that the change in strain fluctuation correlations is given by

$$\Delta\langle u_{ij}(\mathbf{x})u_{kl}(\mathbf{y})\rangle \approx -\beta\int_\Sigma \mathrm{d}S_\alpha\ \zeta(\boldsymbol{\alpha})C_{mnpq}(\boldsymbol{\alpha})\ \langle u_{ij}(\mathbf{x})u_{mn}(\boldsymbol{\alpha})\rangle\langle u_{pq}(\boldsymbol{\alpha})u_{kl}(\mathbf{y})\rangle \tag{4.31}$$

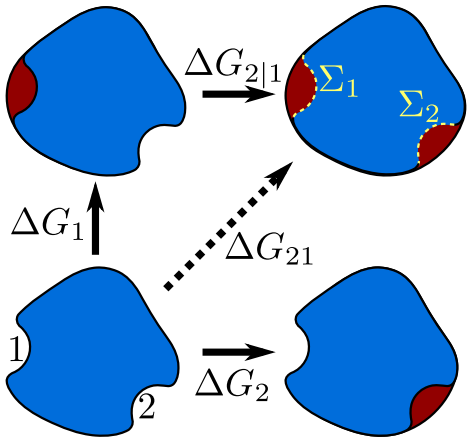

Figure 4.6: Sketch of cooperative binding with two binding sites, labeled 1 and 2, on the protein boundary locations Σ_1 and Σ_2. Process without regulator ligand attachment results in free-energy change ΔG_2 whereas the presence of a ligand at site 1 results in $\Delta G_{2|1}$, which may be obtained from the free-energy change of binding to site 1, ΔG_1, and the net free-energy change ΔG_{21}.

where the null-space projector K disappears as it is strain-less. Single-point strain fluctuations describe mean-squared fluctuations of material lengths and thus characterize the material's rigidity. We see from Eq.(4.31) that strain fluctuations decrease for added volume, meaning that ligand binding is expected to increase protein rigidity, to leading order; the magnitude of this increase is controlled by the degree of fluctuation correlations with the binding site. This is our central result and it can importantly be measured in crystallographic data as the width of Bragg peaks, characterized by the Debye-Waller 'B' factor [20].

In equilibrium, we can assume that the distribution of populations of proteins with and without bound ligands is set by the Gibbs free-energy change due to binding, ΔG. In cooperative (inhibitive) binding processes, the presence of an effector ligand decreases (increases) the binding free-energy, altering the equilibrium distribution. Cooperative effects are quantified by monitoring $\Delta\Delta G = \Delta G_{2|1} - \Delta G_2$, the difference in the free-energy of binding at site 2, given the presence of a bound effector ligand at site 1, $\Delta G_{2|1}$, and without a bound effector ligand ΔG_2. Referring to Fig. 4.6, the free-energy change of binding both ligands, ΔG_{21}, is equal to the *net* free-energy

change of binding the effector ligand at site 1 and then binding at site 2, $\Delta G_1 + \Delta G_{2|1}$. Therefore, $\Delta\Delta G = \Delta G_{21} - \Delta G_2 - \Delta G_1$ measures cooperativity by subtracting off the effects of individual binding processes.

Consider the case in which the effect of ligand binding is dominated by changes in vibrational entropy. The free-energy change is computed using the relation from Eq. (4.15), $G = -k_B T \ln Z$:

$$\Delta G = -k_B T \ln Z'/Z = \frac{1}{2} k_B T \ln \left(\frac{\det' \beta \hat{\mathcal{H}}'}{\det' \beta \hat{\mathcal{H}}} \right) \tag{4.32}$$

where the functional determinant was introduced in Eq. (4.21). As Γ is the pseudoinverse of $\hat{\mathcal{H}}$ in the null-space's complement, the restriction on the determinant can safely be dropped, so

$$\Delta G = \frac{1}{2} k_B \, T \ln \left(\frac{\det \beta \, \Gamma'^{-1}}{\det \beta \, \Gamma^{-1}} \right) = -\frac{1}{2} k_B \, T \ln \left(\frac{\det \Gamma'}{\det \Gamma} \right) \ . \tag{4.33}$$

Using the identity $\ln (\det \Gamma) = \mathrm{tr} \, (\ln \Gamma)$ (see Appendix C) and expanding $\Gamma' = \Gamma + \Delta\Gamma$, where $\Delta\Gamma$ is once again restricted to Ω,

$$\Delta G = -\frac{1}{2} k_B \, T \, \mathrm{tr} \ln (1 + \Gamma^{-1} \Delta\Gamma) \ . \tag{4.34}$$

To calculate $\Delta\Delta G$, let Γ_1, Γ_2, and Γ_{21} represent Green's functions with bound ligands at, respectively, site 1, site 2, and sites 1 and 2. Introducing ϵ as a small bookkeeping parameter for the expansion, we can represent Γ_1 and Γ_2 in the following way

$$\begin{aligned} \Gamma_1 &= \Gamma_0 + \epsilon \Delta\Gamma_1 = \Gamma_0 + \epsilon \Delta^{(1)} \Gamma_1[\Gamma_0] + \epsilon^2 \Phi_1[\Gamma_0] \\ \Gamma_2 &= \Gamma_0 + \epsilon \Delta\Gamma_2 = \Gamma_0 + \epsilon \Delta^{(1)} \Gamma_2[\Gamma_0] + \epsilon^2 \Phi_2[\Gamma_0] \end{aligned} \tag{4.35}$$

where $\Delta^{(1)}\Gamma_1[\Gamma_0]$ and $\Delta^{(1)}\Gamma_2[\Gamma_0]$ are the leading order corrections due to single scat-

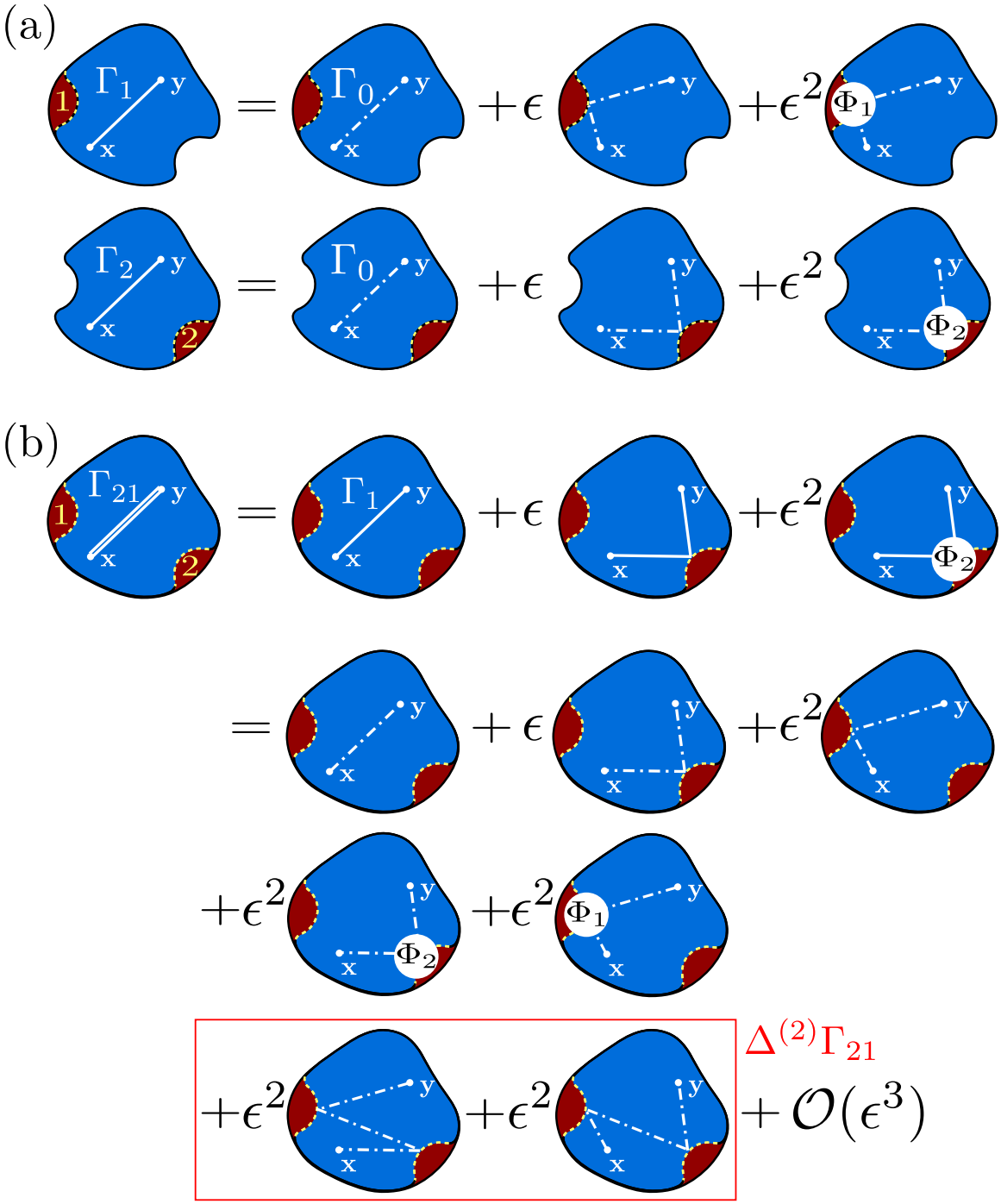

Figure 4.7: (a) Diagrams for calculating Γ_1 and Γ_2 are shown where Φ_1 and Φ_2 generate all $\mathcal{O}(\epsilon^2)$ corrections. (b) Calculation of the total propagator Γ_{21} can be written in terms of diagrams for Γ_1 and Γ_2 along with the leading order scattering diagrams between both ligands, given as $\Delta^{(2)}\Gamma_{21}$.

tering, given by Eq. (G.16), and $\Phi_1[\Gamma_0]$ and $\Phi_2[\Gamma_0]$ are higher order terms that involve interactions with the boundary; see Fig. 4.7a for a diagrammatic representation. Now, the Green's function Γ_{21} is expected to involve all scattering terms involving ligands 1 and 2 individually as well as scattering between the two ligands. To generate the expansion, it is convenient to compute Γ_{21} by imagining that Γ_1 has been computed and to determine the effect of introducing ligand 2, which can be determined via the expansion for Γ_2 using a dressed propagator:

$$\Gamma_{21} = \Gamma_0 + \epsilon\Delta\Gamma_{21} = \Gamma_1 + \epsilon\Delta^{(1)}\Gamma_2[\Gamma_1] + \epsilon\Phi_2[\Gamma_1] \; . \tag{4.36}$$

Expanding Γ_1, we find that

$$\epsilon\Delta\Gamma_{21} = \epsilon\Delta\Gamma_1[\Gamma_0] + \epsilon\Delta\Gamma_2[\Gamma_0] + \epsilon^2\Delta^{(2)}\Gamma_{21}[\Gamma_0] + \mathcal{O}(\epsilon^3) \tag{4.37}$$

where $\Delta^{(2)}\Gamma_{21}$ is defined diagrammatically in Fig. 4.7b and represents the lowest order mutual scattering between ligands 1 and 2. Writing $\Delta\Delta G$ in terms of the change in Green's functions by using Eq. (4.34),

$$\Delta\Delta G = -\frac{1}{2}k_BT\mathrm{tr}\left(\ln\frac{1+\epsilon\Gamma_0^{-1}\Delta\Gamma_{21}}{(1+\epsilon\Gamma_0^{-1}\Delta\Gamma_2)(1+\epsilon\Gamma_0^{-1}\Delta\Gamma_1)}\right) \; . \tag{4.38}$$

Expanding to ϵ^2 and evaluating with Eq 4.37, we find that

$$\Delta\Delta G \approx -\frac{\epsilon^2}{2}k_BT\mathrm{tr}\left(\Gamma_0^{-1}\Delta^{(2)}\Gamma_{21} - \Gamma_0^{-1}\Delta\Gamma_2\Gamma_0^{-1}\Delta\Gamma_1\right) \tag{4.39}$$

where if we use the spectral representation for Γ_0, we recognize that the second term

evaluates to half of the first, leading to the result

$$\Delta\Delta G \approx -\frac{1}{2}\beta \int_{\Sigma_1} \mathrm{d}S_\alpha \zeta(\boldsymbol{\alpha}) \int_{\Sigma_2} \mathrm{d}S_\beta \zeta(\boldsymbol{\beta})\, C_{pqij}(\boldsymbol{\alpha})\, \langle u_{ij}(\boldsymbol{\alpha}) u_{kl}(\boldsymbol{\beta})\rangle \times C_{klmn}(\boldsymbol{\beta})\, \langle u_{mn}(\boldsymbol{\beta}) u_{pq}(\boldsymbol{\alpha})\rangle \ . \tag{4.40}$$

Evidently, when the perturbation lengths ζ are of the same sign (i.e., positive for added ligands), the result is a cooperative interaction, a decrease in free-energy. It confirms the expectation that cooperativity is greatest when binding sites have large strain fluctuation correlations. Furthermore, this result is independent of binding order meaning that binding at site 2 can also regulate binding at site 1.

Considering that our result is a leading order effect, we expect that the possibility of inhibitive allostery via entropic changes alone occurs at higher order. For higher order terms to become important, the leading order term must be small, which occurs in the case of marginally correlated binding sites. Even if the magnitude of the correlation function is small, gradients need not be. This suggests that inflection points of correlation, which we expect to be more sensitive to ligand shape, are candidate allosteric sites. Alternatively, if there is a mismatch between binding site shape and ligand shape, then binding deforms both the ligand and the binding site. As the leading order effect of ligand attachment is a stiffening of the protein, fluctuation allostery is inhibitive for such "induced-fit" requirements.

4.6 Conclusion

Much of the development of fluctuation allosteric regulation has been centered on the premise that ligand binding alters the protein's elastic rigidity, altering its vibrational spectrum. By modeling the protein and ligand as elastic continua, we have shown that the allosteric effect of cooperative binding can occur even in the limit of homogeneous elastic moduli. In our model, the shape of the protein's boundary

plays a key role in determining the vibrational spectrum. The ligand alters vibration through adjustment of this boundary geometry and thus the allosteric effect relies on "hearing" the shape of the protein. Furthermore, we have shown that to leading order, the change in vibrational free-energy due to binding depends on the status of other binding sites, revealing a cooperative effect.

To conclude, we note that the notion of allostery has lately found its way into condensed matter physics. It has been demonstrated, through simulation, that mechanical lattices can be designed, with varying fidelity, to respond with a desired strain at one location on the boundary due to a prescribed strain elsewhere on the boundary [83, 84]. Interestingly, the method, which involves patterning inhomogeneities in the mechanical lattice, has shown that there is an optimal pattern in which a soft region, shaped like a trumpet's bell, connects the two sites and is surrounded by a more rigid region. However, the role of the lattice's boundary shape has not yet been explored. Our results might be used to help guide development of optimal geometries for such "allosteric materials."

CHAPTER 5

CONCLUSIONS: EXTREME STATISTICAL MECHANICS

As we have demonstrated, the *function* of a material, e.g., how it responds to changes in external controlling conditions such as temperature or pH, can be controlled by its *form*, meaning its large-scale geometry or topology and, possibly, internal constitution. First, we have shown that rapidly heated hydrogel rods undergo phase separation, forming solvent-rich and solvent-poor regions whose spatial arrangement is governed by rod shape. Because the internal stress due to phase separation bends the rod, rapid heating may be used to actuate large mechanical deformations. Second, We have shown that allosteric regulation, the process by which the ability of a protein to bind smaller biomolecules is modified by the attachment of a regulator ligand molecule to the protein, can be influenced by the overall shape of the protein. Changes in boundary geometry due to, e.g., the addition of a regulator molecule at one binding site on the protein alters correlations between thermal-fluctuation-induced elastic deformations of the protein, regarded as an elastic continuum. In both cases, hydrogel rods and allosteric proteins, some key aspects of the material's thermodynamics is determined by its overall shape.

There is currently much interest withing the soft matter physics and mechanical engineering communities in materials whose deformations are controlled by prescribed patterns of mechanical instability; such materials are said to exhibit "extreme mechanics" [85, 86]. For example, incompressible materials, such as rubber, can be made much more compressible, even auxetic[1], at the macroscopic scale through imprinting certain failure modes [87]. Another example is origami, where creases are

[1] i.e., having negative Poisson's ratio so that a bar of the material will become thinner when compressed at the ends

patterned in paper in such a way that they facilitate folding to non-flat, often complex, shapes [86]. The hydrogel rod, on the other hand, achieves large deformations through a *thermodynamic* instability and associated phase transition, placing it in a rather different category than materials that rely on mechanical instability.

The idea of actuation of shape change via phase transitions of materials, "extreme statistical mechanics," gives rise to further questions, most notably: What other systems exhibit a similar coupling between shape and thermodynamics and what practical, or even commercial, applications might they have. Closely related are the well-studied and quite beautiful couplings between elasticity and liquid crystalline order found in liquid crystal elastomers (see e.g., [14]). Furthermore, a number of interesting questions can be addressed for the hydrogel rod. For example, how do the hydrodynamics of the polarized solvent-poor shell and solvent-rich core regions affect the rod's equilibration dynamics? What does rapid heating do to other rod topologies, such as a two-hole doughnut (or a figure-of-eight)? And how does the polarization order parameter generalize to higher dimensions, e.g., in rapid heating of two-dimensional hydrogel slabs?[2] Additionally, it would be interesting to study critical phenomena (anomalous exponents, scaling, etc.) in deformable geometries. I look forward with excitement to see how these ideas are developed.

[2]These questions were raised by my committee (see title page) and Prof. Andrew Zangwill, whom I thank for their valuable input.

Appendices

APPENDIX A
PHASE COEXISTENCE AND THE COMMON TANGENT CONSTRUCTION

Consider a system of N particles with volume V held at temperature T. With these state functions, it is natural to describe the equilibrium of the system by the Helmholtz free-energy $F(T, V, N)$. As the free-energy is is a homogeneous function of first order,

$$F(T, V, N) = VF\left(T, 1, \frac{N}{V}\right) \equiv V\tilde{F}(T, \rho) \tag{A.1}$$

where $\rho = N/V$ is the number density of the particles. Consider a case in which the system has two coexistent phases. We will derive a set of equations that describe the phase-coexistent equilibrium, viz. the common tangent construction and the lever rule, and show that the free-energy density $\tilde{F}$ must have two equilibrium states.

Let the system phase separate into two phases 'A' and 'B' with densities ρ_A and ρ_B, occupying volumes V_A and V_B. Note that as

$$V_A + V_B = V \tag{A.2}$$

we can define a fraction $f \equiv V_A/V$ so the partitioning of the system implies that $V_B/V = 1 - f$. Furthermore, the total number of particles is conserved

$$N = N_A + N_B = V_A\rho_A + V_B\rho_B = V[f\rho_A + (1 - f)\rho_B] \,. \tag{A.3}$$

But the number of particles N is the same prior to separation into the two phases; we

can therefore set $N = \rho_h V$ where ρ_h is the density of the homogeneous phase. Thus,

$$\rho_h = f\rho_A + (1-f)\rho_B \tag{A.4}$$

and then we solve for f yielding the *lever rule*

$$f = \frac{\rho_h - \rho_B}{\rho_A - \rho_B} \; . \tag{A.5}$$

If ρ_A is much denser than ρ_B and ρ_h, then we expect that almost all of the volume is occupied by the less dense phase, phase 'B', resulting in small f. Note that the lever rule is a consequence of volume and number constraints alone and does not depend on the details of the system's thermodynamics.

To derive the other equilibrium equations, we write the total free-energy as the sum of free energies for each of the individual phases, $F = F_A + F_B$. In terms of free-energy densities,

$$\begin{aligned} F(T, V, \{\rho_A, \rho_B\}, f, \lambda)/V = f\tilde{F}(T, \rho_A) + (1-f)\tilde{F}(T, \rho_B) \\ + \lambda[f\rho_A + (1-f)\rho_B - \rho_h] \end{aligned} \tag{A.6}$$

where the total number constraint is enforced by introducing a Lagrange multiplier λ. Holding T and V constant, we can vary F with respect to ρ_A, ρ_B, f, and λ:

$$\begin{aligned} \delta F/V = 0 = f\left\{ \left.\frac{\partial \tilde{F}}{\partial \rho}\right|_{\rho_A} + \lambda \right\}\delta\rho_A + (1-f)\left\{ \left.\frac{\partial \tilde{F}}{\partial \rho}\right|_{\rho_B} + \lambda \right\}\delta\rho_B \\ + \{\tilde{F}(\rho_A) - \tilde{F}(\rho_B) + \lambda(\rho_A - \rho_B)\}\delta f \\ + \{f\rho_A + (1-f)\rho_B - \rho_h\}\delta\lambda \; . \end{aligned} \tag{A.7}$$

The equation obtained from varying with respect to λ yields the lever rule Eq.(A).

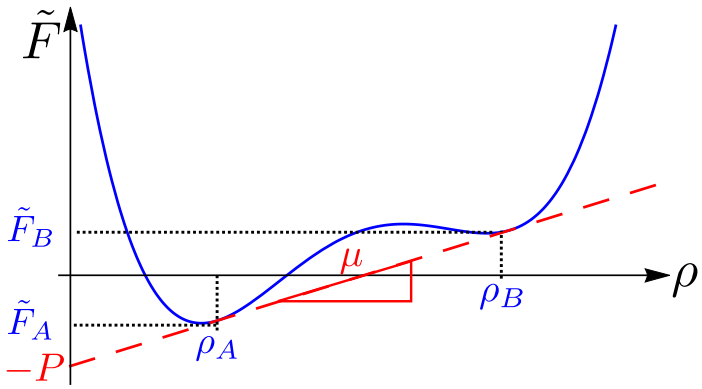

Figure A.1: free-energy density with quartic form is plotted along with the unique common tangent line, graphically determining equilibrium densities ρ_A and ρ_B.

Varying with respect to ρ_A and ρ_B yields a chemical potential balance

$$\mu_A = \left.\frac{\partial \tilde{F}}{\partial \rho}\right|_{\rho_A} = \left.\frac{\partial \tilde{F}}{\partial \rho}\right|_{\rho_B} = \mu_B \ . \tag{A.8}$$

Graphically, on a plot of $\tilde{F}(\rho)$, the chemical equilibrium implies that the slope of $\tilde{F}$ at $\rho = \rho_A$ is the same as the slope at $\rho = \rho_B$. Importantly, this is only true if the function $\tilde{F}(\rho)$ is not convex everywhere so that its Legendre transformation $\rho \to \partial \tilde{F}/\partial \rho$ is multivalued [13]. This only happens if there are multiple extrema, i.e. multiple equilibria, each equilibrium corresponding to a distinct phase.

Finally, variation with respect to F yields the condition

$$\tilde{F}(\rho_A) - \tilde{F}(\rho_B) + \lambda(\rho_A - \rho_B) = 0 \tag{A.9}$$

where, by virtue of the chemical equilibrium conditions,

$$\tilde{F}(\rho_A) - \tilde{F}(\rho_B) - \left(\left.\frac{\partial \tilde{F}}{\partial \rho}\right|_{\rho_A} \rho_A - \left.\frac{\partial \tilde{F}}{\partial \rho}\right|_{\rho_B} \rho_B \right) = 0 \ . \tag{A.10}$$

However, the above equation can be rewritten using the identity

$$\tilde{F} - \frac{\partial \tilde{F}}{\partial \rho}\rho = \tilde{F} - \mu\rho = -P \tag{A.11}$$

and is thus equivalent to a pressure balance $-P_A + P_B = 0$. Rewriting as

$$\tilde{F}(\rho_B) = \tilde{F}(\rho_A) + \left.\frac{\partial \tilde{F}}{\partial \rho}\right|_{\rho_A} (\rho_B - \rho_A) \tag{A.12}$$

shows that ρ_A and ρ_B must lie along the same line whose slope is given by the tangent to $\tilde{F}$ at both points, hence the "common tangent construction," shown schematically in Fig. A.1. Note that the slope of the tangent line is the chemical potential of the two phases and the intercept is the pressure.

APPENDIX B
DIFFERENTIAL GEOMETRY OF CURVES & TUBE COORDINATES

We review basic results of the differential geometry of space curves and then discuss the "tube" coordinate system that can be used to describe points near a curve.

B.1 Space curves

Let $\boldsymbol{\ell}(s)$ be a space curve of length L parametrized by arclengh parameter $s \in [0, L]$ so that

$$\frac{\mathrm{d}\boldsymbol{\ell}}{\mathrm{d}s} = \hat{\mathbf{t}}(s) \tag{B.1}$$

where $\hat{\mathbf{t}}(s)$ is the unit tangent vector. In three dimensions, we can define two unit vectors $\hat{\mathbf{d}}_\mathbf{1}$ and $\hat{\mathbf{d}}_\mathbf{2}$ so that the collection $\{\hat{\mathbf{d}}_\mathbf{1}, \hat{\mathbf{d}}_\mathbf{2}, \hat{\mathbf{t}}\}$ forms an orthonormal triad for each point s; we will designate $\hat{\mathbf{d}}_\mathbf{3} \equiv \hat{\mathbf{t}}$, which we show in Fig. B.1. In general, the frame at two different points can be related by a SO(3) rotation matrix.

Under an infinitesimal translation along the arclength, the frame undergoes an infinitesimal rotation that is described by an antisymmetric matrix, a general element of the Lie algebra $\mathfrak{so}(3)$. The evolution of the frame is therefore given by a generalized form of the Frenet-Serret equations

$$\nabla_s \begin{pmatrix} \hat{\mathbf{d}}_\mathbf{1} \\ \hat{\mathbf{d}}_\mathbf{2} \\ \hat{\mathbf{d}}_\mathbf{3} \end{pmatrix} = \begin{pmatrix} 0 & \tau & -\kappa_2 \\ -\tau & 0 & \kappa_1 \\ \kappa_2 & -\kappa_1 & 0 \end{pmatrix} \begin{pmatrix} \hat{\mathbf{d}}_\mathbf{1} \\ \hat{\mathbf{d}}_\mathbf{2} \\ \hat{\mathbf{d}}_\mathbf{3} \end{pmatrix} \tag{B.2}$$

where κ_1 and κ_2 are components of a curvature vector $\boldsymbol{\kappa}$ and τ is a torsion. The curvature and torsion here is generally different from what we'll refer to as the "geometric" curvature and torsion of a curve, κ_{geo} and τ_{geo}. One principle difference is that

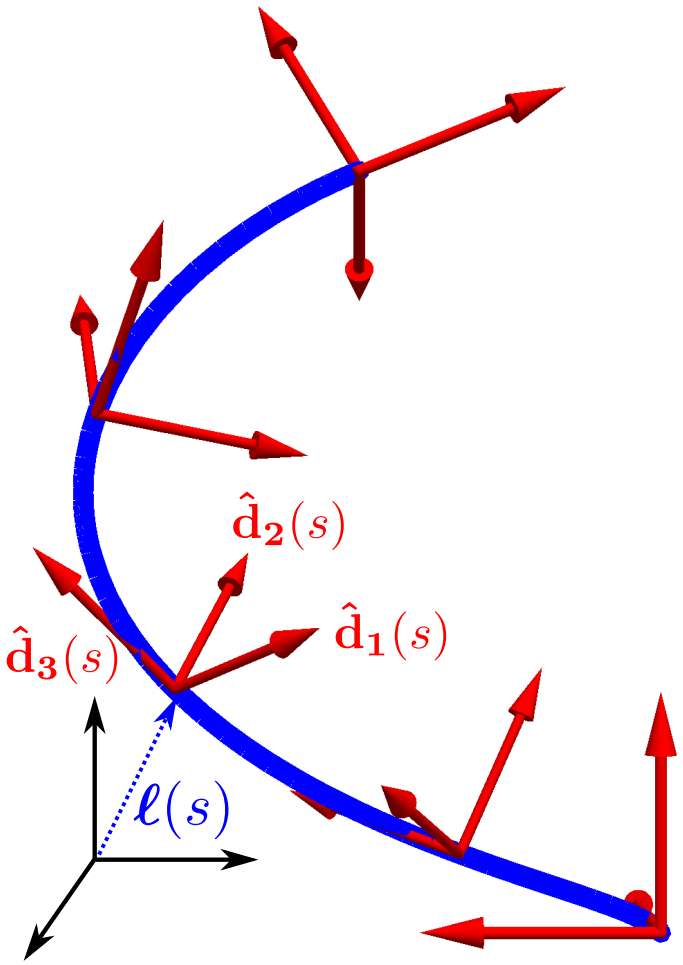

Figure B.1: Parametric space curve $\boldsymbol{\ell}(s)$ with orthonormal triad $\{\hat{\mathbf{d}}_1, \hat{\mathbf{d}}_2, \hat{\mathbf{d}}_3\}$

the curvature calculated in Eq. (B.2) is a vector rather than a scalar. The geometric curvature and torsion are related to the geometry of the centerline $\boldsymbol{\ell}$ *without* need of specifying a frame. They can be calculated with the equations [43]

$$\kappa_{\text{geo}} = \frac{|\ddot{\boldsymbol{\ell}} \times \dot{\boldsymbol{\ell}}|}{|\dot{\boldsymbol{\ell}}|^3} \tag{B.3}$$

$$\tau_{\text{geo}} = \frac{(\dot{\boldsymbol{\ell}} \times \ddot{\boldsymbol{\ell}}) \cdot \dddot{\boldsymbol{\ell}}}{|\dot{\boldsymbol{\ell}} \times \ddot{\boldsymbol{\ell}}|^2} \tag{B.4}$$

where the centerline $\boldsymbol{\ell}$ need not be in arclength (unit speed) parameterization. The Frenet-Serret frame is a unique frame that evolves according to the geometric curvature and torsion alone:

$$\nabla_s \begin{pmatrix} \hat{\mathbf{n}} \\ \hat{\mathbf{b}} \\ \hat{\mathbf{t}} \end{pmatrix} = \begin{pmatrix} 0 & \tau_{\text{geo}} & -\kappa_{\text{geo}} \\ -\tau_{\text{geo}} & 0 & 0 \\ \kappa_{\text{geo}} & 0 & 0 \end{pmatrix} \begin{pmatrix} \hat{\mathbf{n}} \\ \hat{\mathbf{b}} \\ \hat{\mathbf{t}} \end{pmatrix} \tag{B.5}$$

where $\hat{\mathbf{n}}$ is the normal, $\hat{\mathbf{b}}$ is the binormal, and $\hat{\mathbf{t}}$ is the tangent. The extra curvature in Eq. (B.2) comes from the freedom of choosing a transverse frame that is rotated from the $\hat{\mathbf{n}}$ and $\hat{\mathbf{b}}$ directions. Thus, $\boldsymbol{\kappa}$ encodes both κ_{geo} and the orientation of the frame relative to the Frenet-Serret frame. We find it useful to express the components of the curvature vector in the following way:

$$\kappa_1 = \kappa_{\text{geo}} \sin\chi, \quad \kappa_2 = \kappa_{\text{geo}} \cos\chi \tag{B.6}$$

where χ encodes the angle of the chosen frame relative to the Frenet-Serret frame:

$$\begin{pmatrix} \hat{\mathbf{d}}_1 \\ \hat{\mathbf{d}}_2 \\ \hat{\mathbf{d}}_3 \end{pmatrix} = \begin{pmatrix} \cos\chi & \sin\chi & 0 \\ -\sin\chi & \cos\chi & 0 \\ 0 & 0 & 1 \end{pmatrix} \begin{pmatrix} \hat{\mathbf{n}} \\ \hat{\mathbf{b}} \\ \hat{\mathbf{t}} \end{pmatrix} \equiv U(\chi) \begin{pmatrix} \hat{\mathbf{n}} \\ \hat{\mathbf{b}} \\ \hat{\mathbf{t}} \end{pmatrix} . \tag{B.7}$$

Differentiating the above transformation equation yields

$$\begin{aligned}\nabla_s \begin{pmatrix} \hat{\mathbf{d}}_1 \\ \hat{\mathbf{d}}_2 \\ \hat{\mathbf{d}}_3 \end{pmatrix} &= \left[\dot{U}U^{-1} + U \begin{pmatrix} 0 & \tau_{\text{geo}} & -\kappa_{\text{geo}} \\ -\tau_{\text{geo}} & 0 & 0 \\ \kappa_{\text{geo}} & 0 & 0 \end{pmatrix} U^{-1} \right] \begin{pmatrix} \hat{\mathbf{d}}_1 \\ \hat{\mathbf{d}}_2 \\ \hat{\mathbf{d}}_3 \end{pmatrix} \\ &= \begin{pmatrix} 0 & \tau_{\text{geo}} + \dot{\chi} & -\kappa_{\text{geo}} \cos\chi \\ -\tau_{\text{geo}} - \dot{\chi} & 0 & \kappa_{\text{geo}} \sin\chi \\ \kappa_{\text{geo}} \cos\chi & -\kappa_{\text{geo}} \sin\chi & 0 \end{pmatrix} \begin{pmatrix} \hat{\mathbf{d}}_1 \\ \hat{\mathbf{d}}_2 \\ \hat{\mathbf{d}}_3 \end{pmatrix}\end{aligned} \tag{B.8}$$

so we find that by rotating the transverse frame, the torsion in the rotated frame is gains an additional term

$$\tau = \tau_{\text{geo}} + \dot{\chi} \, . \tag{B.9}$$

This term appears due to the covariant piece of the transformation, namely $\dot{U}U^{-1}$.

B.2 Tube coordinates

Given a parametric curve in arc-length parametrization, $\boldsymbol{\ell}(s)$, we can define a cross-section plane at each value of s that is perpendicular to the tangent vector $\hat{\mathbf{d}}_3(s)$. Vectors in the cross-section planes can be written in the basis of unit vectors $\left\{ \hat{\mathbf{d}}_1(s), \hat{\mathbf{d}}_2(s) \right\}$. In general, position vector $\mathbf{r}$ may intersect *many* of these planes. However, it is often possible to find a unique point $\boldsymbol{\ell}(s)$ corresponding to the minimal distance between the point and the curve, $|\mathbf{r} - \boldsymbol{\ell}|$; it can be shown that $\mathbf{r}$ always lies within the corresponding cross-sectional plane. Choosing this minimal distance point, let

$$\mathbf{r}(x_1, x_2, s) = \boldsymbol{\ell}(s) + x_1 \hat{\mathbf{d}}_1(s) + x_2 \hat{\mathbf{d}}_2(s) \tag{B.10}$$

We will show later that the tuple (x_1, x_2, s) provides a consistent parametrization for $\mathbf{r}$ as long as $|\mathbf{x}| < \kappa^{-1}(s)$.

For generality, let $x_1 = x_1(q^1, q^2)$ and $x_2 = x_2(q^1, q^2)$ and define $\partial_m = \frac{\partial}{\partial q^m}$ for $m \in \{1, 2\}$. The coordinate basis is given by

$$\begin{aligned} \mathbf{r_3} &= \partial_s \mathbf{r} = (1 + \varepsilon_{mn3}\kappa_m x_n)\hat{\mathbf{d}}_\mathbf{3} + \tau \hat{\mathbf{d}}_\mathbf{3} \times \mathbf{x} \\ \mathbf{r_m} &= \partial_m \mathbf{r} = \partial_m \mathbf{x} \equiv \mathbf{x_m} \end{aligned} \tag{B.11}$$

Using this coordinate basis, we can express any vector $\mathbf{v}$ located at (q^1, q^2, s) as $\mathbf{v} = v^\mu \mathbf{r}_\mu$ for $\mu \in \{1, 2, 3\}$. Note that we will use Greek letters to index the full basis and Latin letters to index the cross-section basis.

For convenience, introduce $q^3 \equiv s$ so the lengths of intervals $\mathrm{d}q^\mu$ can be computed as:

$$|\mathrm{d}\mathbf{r}|^2 = (\partial_\mu \mathbf{r}\, \mathrm{d}q^\mu) \cdot (\partial_\nu \mathbf{r}\, \mathrm{d}q^\nu) = \mathbf{r}_\mu \cdot \mathbf{r}_\nu\, \mathrm{d}q^\mu \mathrm{d}q^\nu \equiv g_{\mu\nu} \mathrm{d}q^\mu \mathrm{d}q^\nu \tag{B.12}$$

The metric tensor $g_{\mu\nu}$ is therefore given in matrix form by

$$g_{\mu\nu} = \left\{ \begin{array}{cc|c} \mathbf{x_1} \cdot \mathbf{x_1} & \mathbf{x_1} \cdot \mathbf{x_2} & -\tau(\hat{\mathbf{d}}_\mathbf{3} \times \mathbf{x}) \cdot \mathbf{x_1} \\ \mathbf{x_2} \cdot \mathbf{x_1} & \mathbf{x_2} \cdot \mathbf{x_2} & \tau(\hat{\mathbf{d}}_\mathbf{3} \times \mathbf{x}) \cdot \mathbf{x_2} \\ \hline -\tau(\hat{\mathbf{d}}_\mathbf{3} \times \mathbf{x}) \cdot \mathbf{x_1} & \tau(\hat{\mathbf{d}}_\mathbf{3} \times \mathbf{x}) \cdot \mathbf{x_2} & \gamma^2 + \tau^2 |\mathbf{x}|^2 \end{array} \right\} \tag{B.13}$$

where we have defined, $\gamma \equiv 1 + \varepsilon_{mn3}\kappa_m x_n$. Note that we can define the cross-section block of the metric tensor as $\hat{g}_{mn} = \mathbf{x_m} \cdot \mathbf{x_n}$ so that the Jacobian of the coordinate transformation $\mathbf{r} \to q^\mu$ determines volume elements and is given by $\sqrt{\det g_{\mu\nu}} = \gamma\sqrt{\det \hat{g}_{mn}}$. Evidently, the determinant of the metric tensor has a risk of disappearing at points a distance $|\kappa|^{-1}$ from the centerline. This means, by the inverse function theorem, that while points close to the centerline are invertible $q^\mu \to \mathbf{r}$, there is always a breakdown of invertibility sufficiently far from the centerline of a curve. Restricting

our attention close to the centerline, define the inverse metric by $g^{\mu\nu}g_{\nu\rho} = \delta^{\mu}{}_{\rho}$:

$$g^{\mu\nu} = \left\{ \begin{array}{c|c} \hat{g}^{mn} + \gamma^{-2} g^{m3} g^{3n} & -\tau\gamma^{-2}(\hat{\mathbf{d}}_{\mathbf{3}} \times \mathbf{x}) \cdot \mathbf{x^m} \\ \hline -\tau\gamma^{-2}(\hat{\mathbf{d}}_{\mathbf{3}} \times \mathbf{x}) \cdot \mathbf{x^n} & \gamma^{-2} \end{array} \right\}. \tag{B.14}$$

where we define $\mathbf{x^m} \equiv \hat{g}^{mn}\mathbf{x_n}$.

With the metric tensor and the inverse in hand, we can define a covariant basis $\mathbf{r}^{\mu} = g^{\mu\nu}\mathbf{r}_{\nu}$, so that vectors may also be written $\mathbf{v} = v_{\mu}\mathbf{r}^{\mu}$. The covariant coordinate basis is:

$$\begin{aligned} \mathbf{r^3} &= \frac{1}{\gamma}\hat{\mathbf{d}}_{\mathbf{3}} \\ \mathbf{r^m} &= \mathbf{x^m} - \tau\frac{(\hat{\mathbf{d}}_{\mathbf{3}} \times \mathbf{x}) \cdot \mathbf{x^m}}{\gamma}\hat{\mathbf{d}}_{\mathbf{3}} \end{aligned} \tag{B.15}$$

The gradient $\boldsymbol{\nabla} = \frac{\partial}{\partial \mathbf{r}}$ can be written in terms of the tube coordinates using the chain rule

$$\boldsymbol{\nabla} = \mathbf{r}^{\mu}\partial_{\mu} = \frac{1}{\gamma}(\hat{\mathbf{d}}_{\mathbf{3}}\partial_s - \tau\mathbf{x} \times \boldsymbol{\nabla}_{\boldsymbol{t}}) + \boldsymbol{\nabla}_{\boldsymbol{t}} \tag{B.16}$$

where $\boldsymbol{\nabla}_{\boldsymbol{t}} \equiv \mathbf{x^m}\partial_m$ is the part of the gradient transverse to the centerline. Derivatives of vector fields are given by

$$\begin{aligned} \boldsymbol{\nabla} \otimes \mathbf{v} = \mathbf{r}^{\mu} \otimes \partial_{\mu} v^{\nu} \mathbf{r}_{\nu} &= \mathbf{r}^{\mu} \otimes \mathbf{r}_{\nu}\partial_{\mu}v^{\nu} + \mathbf{r}^{\mu} \otimes (\partial_{\mu}\mathbf{r}_{\nu})v^{\nu} \\ &= \mathbf{r}^{\mu} \otimes \mathbf{r}_{\nu}\left(\partial_{\mu}v^{\nu} + \Gamma^{\nu}{}_{\mu\lambda}v^{\lambda}\right) \end{aligned} \tag{B.17}$$

where the Christoffel symbols are defined by

$$\Gamma^{\nu}{}_{\mu\lambda} \equiv \mathbf{r}^{\nu} \cdot \partial_{\mu}\mathbf{r}_{\lambda} = \mathbf{r}^{\nu} \cdot \partial_{\lambda}\mathbf{r}_{\mu}\ . \tag{B.18}$$

Thus, we can define covariant differentiation ∇_μ of tensor field components by [44]

$$\begin{aligned}\nabla_\mu T^{\alpha\beta\ldots}{}_{\rho\sigma\ldots} \equiv \partial_\mu T^{\alpha\beta\ldots}{}_{\rho\sigma\ldots} &+ \Gamma^\alpha{}_{\mu\nu} T^{\nu\beta\ldots}{}_{\rho\sigma\ldots} + \Gamma^\beta{}_{\mu\nu} T^{\alpha\nu\ldots}{}_{\rho\sigma\ldots} + \ldots \\ &- \Gamma^\nu{}_{\mu\rho} T^{\alpha\beta\ldots}{}_{\nu\sigma\ldots} - \Gamma^\nu{}_{\mu\sigma} T^{\alpha\beta\ldots}{}_{\rho\nu\ldots} - \ldots\end{aligned} \tag{B.19}$$

Now, the covariant differentiation involves contributions due to (i) rod curvature and torsion and (ii) choice of cross-section coordinate system. We can isolate the effect of rod curvature by using Cartesian coordinates in the cross section so $q^m = x_m$ and $\hat{g} = \mathbb{1}$. Defining rod Christoffel symbols $\Omega^\lambda{}_{\mu\nu}$ through Eq. (B.18), evaluated with Cartesian coodinates, we find

$$\begin{aligned}\Omega^l{}_{m3} &= -\tau(\varepsilon_{lm3} + \gamma^{-1}(\mathbf{x}\cdot\boldsymbol{\kappa}\delta_{lm} - \kappa_l x_m)) \\ \Omega^l{}_{33} &= \gamma\varepsilon_{lm3}\kappa_m - \tau^2(x_l + \gamma^{-1}(\mathbf{x}\cdot\boldsymbol{\kappa})\varepsilon_{ml3}x_m) + (\dot{\tau} - \gamma^{-1}\tau\varepsilon_{mn3}\dot{\kappa}_m x_n)\varepsilon_{pl3}x_p \\ \Omega^3{}_{3m} &= -\gamma^{-1}\varepsilon_{mn3}\kappa_n \\ \Omega^3{}_{33} &= \gamma^{-1}\varepsilon_{mn3}\dot{\kappa}_m x_n + \gamma^{-1}\tau\boldsymbol{\kappa}\cdot\mathbf{x}\end{aligned} \tag{B.20}$$

where all other components are 0.

APPENDIX C
EXPANSION OF THE DETERMINANT

As it occurs several times in this document, let us consider the expansion of the determinant of a matrix, or more generally, an operator. Consider an invertible matrix or operator A (such that $\det A \neq 0$) that has a small addition $\epsilon\delta A$, where ϵ sets the scale of the addition and is taken to be small. Then

$$\det(A + \epsilon\delta A) = \det A \det(1 + \epsilon A^{-1}\delta A) \tag{C.1}$$

where we have used the decomposition of determinants $\det AB = \det A \det B$. Now, using the identity

$$\log \det A = \mathrm{tr} \ln A \tag{C.2}$$

we find

$$\det(A + \epsilon\delta A) = \det A \, e^{\mathrm{tr} \ln(1+\epsilon A^{-1}\delta A)} \, . \tag{C.3}$$

Using the power series representation for the matrix logarithm, we find

$$\begin{aligned} \det(A + \epsilon\delta A) &= \det A \, e^{\mathrm{tr} \ln(1+\epsilon A^{-1}\delta A)} \\ &= \det A \, e^{\mathrm{tr} \left(\epsilon A^{-1}\delta A - (1/2)\epsilon^2 (A^{-1}\delta A)^2 + \ldots\right)} \\ &= \det A \, e^{\epsilon \mathrm{tr} \, A^{-1}\delta A - (1/2)\epsilon^2 \mathrm{tr} \, (A^{-1}\delta A)^2 + \ldots} \, . \end{aligned} \tag{C.4}$$

Finally, Taylor expanding the exponential, we obtain the final result

$$\det(A + \epsilon\delta A) = (\det A)\left(1 + \epsilon \mathrm{tr} \, A^{-1}\delta A + \frac{1}{2}\epsilon^2((\mathrm{tr} \, A^{-1}\delta A)^2 - \mathrm{tr} \, (A^{-1}\delta A)^2) + \ldots\right) \tag{C.5}$$

where, in the special case that A is the metric tensor $g_{\mu\nu}$ and δA is the strain tensor $2u_{\mu\nu}$ that results from a deformation, the above result can be compactly written using Einstein notation $u^{\lambda}{}_{\nu} = g^{\lambda\mu}u_{\mu\nu}$ as

$$\det(g + 2u) = (\det\, g)\left(1 + 2u^{\mu}{}_{\mu} + 2u^{\mu}_{\mu}u^{\nu}{}_{\nu} - u^{\mu\nu}u_{\mu\nu} + \dots\right) \ . \tag{C.6}$$

APPENDIX D

SOLVING FOR THE EQUILIBRIUM INTERNAL DISPLACEMENT FIELD

We solve the quasistatic elastic equilibrium equations

$$\partial'_n \sigma^r_{\mu n} = 0 \quad \text{for } \rho < b(\theta) \tag{D.1}$$

with boundary conditions

$$\partial'_n \sigma^r_{\mu n} = 0 \quad \text{for } \rho < b(\theta) \tag{D.2}$$

with cross-section boundary conditions

$$\left.\begin{aligned} \sigma^r_{NN} + \tfrac{h'}{b'}(1 - \partial_{\theta\theta}\Gamma)\sigma^p_{TT} &= 0 \\ \sigma^r_{TN} - \partial'_T h' \sigma^p_{TT} &= 0 \\ \sigma^r_{N3} - \partial'_T h' \sigma^p_{T3} &= 0 \end{aligned}\right\} \quad \text{for } \rho = b(\theta)\ . \tag{D.3}$$

To solve, first note that the above system of equations is augmented by the incompressibility condition on the strain

$$\text{tr } \epsilon = 0\ . \tag{D.4}$$

However, with this extra condition, the system of 3 differential equations for the strain is now overspecified and can lead to inconsistent results.

To overcome this problem, we regularize the problem by adding a term that pe-

nalizes compression to the free-energy ΔF,

$$\Delta F = \int_0^L \mathrm{d}s \left\{ \cdots + \int_{\mathcal{R}_r^{xs}} \mathrm{d}^2x \left[\cdots + K(\mathrm{tr}\ \epsilon)^2 \right] \right\} \tag{D.5}$$

where K is a fixed bulk modulus. The regularized constitutive equations are

$$\begin{aligned}
\sigma^r_{mn} &= 2\mu\Lambda_t^2\epsilon_{mn} + K\Lambda_t^2\delta_{mn}\mathrm{tr}\ \epsilon \\
\sigma^r_{m3} &= \mu(\Lambda_\ell^2 + 3\Lambda_t^2)\epsilon_{m3} \\
\sigma^r_{33} &= \mu(\Lambda_\ell^2 + \Lambda_t^2)\epsilon_{33} + K\Lambda_t^2\mathrm{tr}\ \epsilon \\
\sigma^p_{TT} &= \mu[(\Lambda_t^2 + 3\Lambda_n^2)\epsilon_{TT} + 2\Lambda_n^2\epsilon_{33}] \\
\sigma^p_{T3} &= \frac{1}{2}\mu(\Lambda_\ell^2 + \Lambda_t^2 + 2\Lambda_n^2)\epsilon_{T3} \\
\sigma^p_{33} &= \mu[(\Lambda_\ell^2 + 3\Lambda_n^2)\epsilon_{33} + 2\Lambda_n^2\epsilon_{TT}]
\end{aligned} \tag{D.6}$$

which resemble the result for a linear, isotropic elastic medium in the case of a homogeneous gel where $\Lambda_0 = \mathbb{1}$. With the regularization parameter K introduced, we solve the system of equilibrium equations with boundary conditions, taking $K \to \infty$ limit at the end of the calculation, resulting in an infinitely high cost of compressing the gel. Thus, the incompressible solutions are obtained *as a limit* of the more general solutions with finite K.

Applying the constitutive relations, the equilibrium equations are

$$\begin{aligned}
2\mu\partial'_n\epsilon_{mn} + K\partial'_m\mathrm{tr}\ \epsilon = 0 \\
\partial'_m\epsilon_{m3} = 0
\end{aligned} \tag{D.7}$$

where the deformation matrix elements conveniently drop out, leading to isotropic elasticity equations. Recall that the strain ϵ is a superposition of strain due to external constraints, ϵ_{ext}, and strain that is the result of an internal displacement field allowed

to attain equilibrium under the constraints, ϵ_{int}, and is thus

$$\begin{aligned}
\epsilon_{mn} &= \frac{1}{2}(\partial'_m u_n + \partial'_n u_m) \\
\epsilon_{m3} &= \frac{1}{2}\varepsilon_{mn3}\left(\Delta\tau + \frac{\Lambda_\ell - 1}{\Lambda_\ell}\right) x'_n + \frac{1}{2}\partial_m u_3 \\
\epsilon_{33} &= \varepsilon_{pq3}\left(\Delta\kappa_p + \frac{\Lambda_t - 1}{\Lambda_t}\kappa_p\right) x'_q + \eta
\end{aligned} \tag{D.8}$$

where under the quasistatic approximation, $\partial_s u_m \approx 0$ and $\partial_s u_3 \equiv \eta$, where η is an extensile strain of the rod. In terms of the displacement field, the equilibrium equations are given by

$$\begin{gathered}
\mu\nabla_t^2 u_m + (\mu + K)\partial'_m\partial'_n u_n = K\varepsilon_{mn3}\left(\Delta\kappa_n + \frac{\Lambda_t - 1}{\Lambda_t}\kappa_n\right) \\
\nabla_t^2 u_3 = 0
\end{gathered} \tag{D.9}$$

with transverse Laplacian $\nabla_t^2 \equiv \partial'_{mm}$. In cylindrical coordinates,

$$\begin{aligned}
&\left[(2\mu + K)\left(\frac{1}{\rho'}\partial'_\rho\rho'\partial'_\rho - \frac{1}{\rho'^2}\right) + \mu\frac{1}{\rho'^2}\partial'_{\theta\theta}\right] u_\rho \\
&\quad + \left[-(3\mu + K)\frac{1}{\rho'^2}\partial'_\theta + (\mu + K)\frac{1}{\rho'}\partial'_{\rho\theta}\right] u_\theta = K\left(\Delta\kappa_n + \frac{\Lambda_t - 1}{\Lambda_t}\kappa_n\right)\hat{\theta}'_n \\
&\left[(2\mu + K)\frac{1}{\rho'^2}\partial'_{\theta\theta} + \mu\left(\frac{1}{\rho'}\partial'_\rho\rho'\partial'_\rho - \frac{1}{\rho'^2}\right)\right] u_\theta \\
&\quad + \left[(3\mu + K)\frac{1}{\rho'^2}\partial'_\theta + (\mu + K)\frac{1}{\rho'}\partial'_{\rho\theta}\right] u_\rho = -K\left(\Delta\kappa_n + \frac{\Lambda_t - 1}{\Lambda_t}\kappa_n\right)\hat{\rho}'_n \\
&\left[\frac{1}{\rho'}\partial'_\rho\rho'\partial'_\rho + \frac{1}{\rho'^2}\partial'_{\theta\theta}\right] u_3 = 0\ .
\end{aligned} \tag{D.10}$$

To solve, we assume a series solution

$$u_i = \sum_{m,n=0}^{\infty} \rho'^n \left(\alpha_i^{mn}\cos m\theta' + \beta_i^{mn}\sin m\theta'\right) \tag{D.11}$$

which is periodic in θ' and finite as $\rho' \to 0$. Plugging our Ansatz into the equilibrium

equations Eq. (D.10) yields general solutions

$$
\begin{aligned}
u_\rho &= \rho' \alpha_\rho^{01} + \left(\alpha_\theta^{10} + \frac{\rho'^2}{5\mu + 3K} (-K(\Delta\kappa_2 + \dots) + (K-\mu)\alpha_\theta^{12}) \right) \sin\theta' \\
&\quad - \left(\beta_\theta^{10} + \rho'^2 (-K(\Delta\kappa_3 + \dots) + (K-\mu)\beta_\theta^{12}) \right) \cos\theta' \\
&\quad + \sum_{m>1} \Bigg[\left(\rho'^{m-1} \alpha_\theta^{m,m-1} + \rho'^{m+1} \frac{(\mu+K)m - 2\mu}{(\mu+K)m + 2(2\mu+K)} \alpha_\theta^{m,m+1} \right) \sin m\theta' \\
&\quad - \left(\rho'^{m-1} \beta_\theta^{m,m-1} + \rho'^{m+1} \frac{(\mu+K)m - 2\mu}{(\mu+K)m + 2(2\mu+K)} \beta_\theta^{m,m+1} \right) \cos m\theta' \Bigg] \\
u_\theta &= \rho' \alpha_\theta^{01} + \sum_{m=1} \Bigg[\left(\rho'^{m-1} \alpha_\theta^{m,m-1} + \rho'^{m+1} \alpha_\theta^{m,m+1} \right) \cos m\theta' \\
&\quad + \left(\rho'^{m-1} \beta_\theta^{m,m-1} + \rho'^{m+1} \beta_\theta^{m,m+1} \right) \sin m\theta' \Bigg] \\
u_3 &= \alpha_3^0 + \sum_{n=1} \rho'^n \left(\alpha_3^n \cos n\theta' + \beta_3^n \sin n\theta' \right)
\end{aligned}
\tag{D.12}
$$

where the $\Delta\kappa_m + \dots$ is shorthand for $\Delta\kappa_m + ((\Lambda_t - 1)/\Lambda_t)\kappa_m$. The general strain is thus

$$
\begin{aligned}
\epsilon_{\rho\rho} &= \alpha_\rho^{01} - \frac{2\rho'}{5\mu + 3K} (-K(\Delta\kappa_3 + \dots) + (K-\mu)\beta_\theta^{12}) \cos\theta' \\
&\quad + \frac{2\rho'}{5\mu + 3K} (-K(\Delta\kappa_2 + \dots) + (K-\mu)\alpha_\theta^{12}) \sin\theta' \\
&\quad + \sum_{m>1} \rho'^m \Bigg[- \left(\frac{m-1}{\rho'^2} \beta_\theta^{m,m-1} + \frac{(m+1)((\mu+K)m - 2\mu)}{(\mu+K)m + 2(2\mu+K)} \beta_\theta^{m,m+1} \right) \cos m\theta' \\
&\quad + \left(\frac{m-1}{\rho'^2} \alpha_\theta^{m,m-1} + (m+1) \frac{(m+1)((\mu+K)m - 2\mu)}{(\mu+K)m + 2(2\mu+K)} \alpha_\theta^{m,m+1} \right) \sin m\theta' \Bigg]
\end{aligned}
\tag{D.13}
$$

$$
\begin{aligned}
\epsilon_{\rho\theta} &= \frac{\rho'}{10\mu + 6K} (-K(\Delta\kappa_2 + \dots) + 4(\mu+K)\alpha_\theta^{12}) \cos\theta' \\
&\quad + \frac{\rho'}{10\mu + 6K} (-K(\Delta\kappa_3 + \dots) + 4(\mu+K)\beta_\theta^{12}) \sin\theta' \\
&\quad + \sum_{m>1} \rho'^m \Bigg[\left(\frac{m-1}{\rho'^2} \alpha_\theta^{m,m-1} + \frac{(m+1)m(\mu+K)}{(\mu+K)m + 2(2\mu+K)} \alpha_\theta^{m,m+1} \right) \cos m\theta' \\
&\quad + \left(\frac{m-1}{\rho'^2} \beta_\theta^{m,m-1} + \frac{(m+1)m(\mu+K)}{(\mu+K)m + 2(2\mu+K)} \beta_\theta^{m,m+1} \right) \sin m\theta' \Bigg]
\end{aligned}
\tag{D.14}
$$

$$
\begin{aligned}
\epsilon_{\theta\theta} &= \alpha_\rho^{01} + \frac{\rho'}{5\mu+3K}(K(\Delta\kappa_3+\dots)+2(3\mu+K)\beta_\theta^{12})\cos\theta' \\
&- \frac{\rho'}{5\mu+3K}(K(\Delta\kappa_2+\dots)+2(3\mu+K)\alpha_\theta^{12})\sin\theta' \\
&+ \sum_{m>1}\rho'^m\Bigg[\left(\frac{m-1}{\rho'^2}\beta_\theta^{m,m-1}+\frac{(m+1)((\mu+K)m+2\mu)}{(\mu+K)m+2(2\mu+K)}\beta_\theta^{m,m+1}\right)\cos m\theta' \\
&- \left(\frac{m-1}{\rho'^2}\alpha_\theta^{m,m-1}+(m+1)\frac{(m+1)((\mu+K)m+2\mu)}{(\mu+K)m+2(2\mu+K)}\alpha_\theta^{m,m+1}\right)\sin m\theta'\Bigg]
\end{aligned}
\tag{D.15}
$$

$$
\epsilon_{\rho 3} = \frac{1}{2}\sum_{n=0}\rho'^n(n+1)\left[\alpha_3^{n+1}\cos(n+1)\theta' + \beta_3^{n+1}\sin(n+1)\theta'\right] \tag{D.16}
$$

$$
\begin{aligned}
\epsilon_{\theta 3} &= \frac{1}{2}\left(\Delta\tau + \frac{\Lambda_\ell - 1}{\Lambda_\ell}\right) \\
&+ \frac{1}{2}\sum_{n=0}\rho'^n(n+1)\left[-\alpha_3^{n+1}\sin(n+1)\theta' + \beta_3^{n+1}\cos(n+1)\theta'\right]
\end{aligned}
\tag{D.17}
$$

$$
\epsilon_{33} = \eta + \epsilon_{pq3}\left(\Delta\kappa_p + \frac{\Lambda_t - 1}{\Lambda_t}\kappa_p\right)x_q' \tag{D.18}
$$

with unknown coefficients that are determined by the stress boundary conditions.

The boundary conditions supplied by Eqs. (D.3) are in terms of components of the stress tensor that are tangential and normal to the boundary and are thus rotated from polar directions $\hat{\boldsymbol{\rho}}$ and $\hat{\boldsymbol{\theta}}$ by an small angle that scales with $\partial_\theta\Gamma$. However, the interface displacement Γ results in a strain; we consider the leading order response so that ϵ, and thus σ, contains terms proportional to Γ. Thus, we can linearize the boundary conditions, keeping only leading order terms in Γ and ϵ, resulting in reduced

boundary conditions

$$
\begin{aligned}
&2\mu\epsilon_{\rho\rho} + K\,\mathrm{tr}\,\epsilon + \mu\frac{h_0}{b_0}\left(\frac{\Lambda_t^2+3\Lambda_n^2}{\Lambda_t^2}\epsilon_{\theta\theta} + 2\frac{\Lambda_n^2}{\Lambda_t^2}\epsilon_{33}\right) \\
&\qquad = \mu\frac{\Lambda_t^2-\Lambda_n^2}{\Lambda_t^2}\left(\frac{h_0}{b_0}(-1+\partial'_{\theta\theta}\Gamma+\Gamma)+\Gamma\right) \\
&2\epsilon_{\rho\theta} - \frac{h_0}{b_0}\left(\frac{\Lambda_t^2+3\Lambda_n^2}{\Lambda_t^2}\partial'_\theta\epsilon_{\theta\theta} + 2\frac{\Lambda_n^2}{\Lambda_t^2}\partial'_\theta\epsilon_{33}\right) = -\frac{\Lambda_t^2-\Lambda_n^2}{\Lambda_t^2}\partial'_\theta\Gamma \\
&2\epsilon_{\rho 3} - \frac{h_0}{b_0}\frac{\Lambda_\ell^2+\Lambda_t^2+2\Lambda_n^2}{\Lambda_\ell^2+3\Lambda_t^2}\partial'_\theta\epsilon_{\theta 3} = 0
\end{aligned}
\tag{D.19}
$$

where the Laplace pressure is clearly present in the first with mean curvature equal to the result of Eq. (2.70). The second equation involves a gradient Γ arising from a gradient of the surface stress, resulting in a Marangoni-like force.

Using Eq. D.19 to determine the unknown coefficients and taking limit $K \to \infty$

to recover the incompressibility constraint, we find

$$
\begin{aligned}
\epsilon_{\rho\rho} &= -\frac{1}{2}\epsilon_{33} - \frac{1}{4}\frac{h_0}{b_0}\frac{\Lambda_t^2-\Lambda_n^2}{\Lambda_t^2}\varepsilon_{pq3}\left(\Delta\kappa_p + \frac{\Lambda_t-1}{\Lambda_t}\kappa_p\right)x'_q \\
&\quad - \frac{1}{4}\frac{\Lambda_t-\Lambda_n^2}{\Lambda_t^2}\sum_{m=1} m\Bigg[(m+1)\left(1+\frac{1}{2}\frac{h_0}{b_0}\left(\frac{\Lambda_t^2-3\Lambda_n^2}{\Lambda_t^2}m-2\right)\right)\left(\frac{\rho'}{b'_0}\right)^m \\
&\qquad - (m-1)\left(1+\frac{1}{2}\frac{h_0}{b_0}\left(\frac{\Lambda_t^2-3\Lambda_n^2}{\Lambda_t^2}m-2\right)\right)\left(\frac{\rho'}{b'_0}\right)^{m-2}\Bigg]\Gamma_m(\theta') \\
\epsilon_{\rho\theta} &= -\frac{1}{4}\frac{h_0}{b_0}\frac{\Lambda_t^2-\Lambda_n^2}{\Lambda_t^2}\left(\Delta\kappa_p + \frac{\Lambda_t-1}{\Lambda_t}\kappa_p\right)x'_p \\
&\quad - \frac{1}{4}\frac{\Lambda_t-\Lambda_n^2}{\Lambda_t^2}\sum_{m=1} m\Bigg[(m+1)\left(1+\frac{1}{2}\frac{h_0}{b_0}\left(\frac{\Lambda_t^2-3\Lambda_n^2}{\Lambda_t^2}m-2\right)\right)\left(\frac{\rho'}{b'_0}\right)^m \\
&\qquad - (m-1)\left(1+\frac{1}{2}\frac{h_0}{b_0}\left(\frac{\Lambda_t^2-3\Lambda_n^2}{\Lambda_t^2}m-2\right)\right)\left(\frac{\rho'}{b'_0}\right)^{m-2}\Bigg]\partial'_\theta\Gamma_m(\theta') \\
\epsilon_{\theta\theta} &= -\frac{1}{2}\epsilon_{33} + \frac{1}{4}\frac{h_0}{b_0}\frac{\Lambda_t^2-\Lambda_n^2}{\Lambda_t^2}\varepsilon_{pq3}\left(\Delta\kappa_p + \frac{\Lambda_t-1}{\Lambda_t}\kappa_p\right)x'_q \\
&\quad + \frac{1}{4}\frac{\Lambda_t-\Lambda_n^2}{\Lambda_t^2}\sum_{m=1} m\Bigg[(m+1)\left(1+\frac{1}{2}\frac{h_0}{b_0}\left(\frac{\Lambda_t^2-3\Lambda_n^2}{\Lambda_t^2}m-2\right)\right)\left(\frac{\rho'}{b'_0}\right)^m \\
&\qquad - (m-1)\left(1+\frac{1}{2}\frac{h_0}{b_0}\left(\frac{\Lambda_t^2-3\Lambda_n^2}{\Lambda_t^2}m-2\right)\right)\left(\frac{\rho'}{b'_0}\right)^{m-2}\Bigg]\Gamma_m(\theta') \\
\epsilon_{\rho 3} &= 0 \\
\epsilon_{\theta 3} &= \frac{1}{2}\left(\Delta\tau + \frac{\Lambda_\ell-1}{\Lambda_\ell}\tau\right)\rho' \\
\epsilon_{33} &= \eta + \varepsilon_{pq3}\left(\Delta\kappa_p + \frac{\Lambda_t-1}{\Lambda_t}\kappa_p\right)x'_q
\end{aligned}
\tag{D.20}
$$

where $\Gamma_m(\theta')$ is the m^{th} mode of $\Gamma(\theta')$, as defined in Eq. 2.38. Note that Eqs. D.20 satisfy the incompressibility constraint $\epsilon_{\rho\rho} + \epsilon_{\theta\theta} + \epsilon_{33} = 0$. Furthermore, the effect of torsion only contributes to $\epsilon_{\theta 3}$ and $\epsilon_{\rho 3} = 0$, recovering the case of twisting a circular rod [36]. Finally, the form of ϵ_{33} also agrees with the rod theory prediction.

APPENDIX E

LINEAR STABILITY OF RING SYMMETRIC EQUILIBRIUM

Starting with the expansion of the Landau free-energy about the symmetric equilibrium of the planar toroid, Eq. (3.31) We make a change of variables $s = R\tilde{s}$ so that $\dot{f} \to \dot{f}/R$ and we take $\chi = \tilde{\chi} - (\ddot{\zeta} + \zeta)/R$ so

$$\begin{aligned}\delta^2 L = \frac{1}{2} R \int_0^{2\pi} \mathrm{d}\tilde{s} \Bigg[\left(B\frac{1}{R^2} + \frac{k_1|\psi_1^*|}{R} \right) \left(\frac{1}{R}(\ddot{\zeta} + \zeta) - \tilde{\chi} \right)^2 + \frac{J}{R^2}\dot{\tilde{\chi}}^2 + \frac{C|\psi_1^*|^2}{R^2}\dot{\varphi}^2 \\ + \frac{k_2|\psi_1^*|}{R}\varphi^2 - \frac{k_1|\psi_1^*|}{R} \left(\frac{1}{R^2}(\ddot{\zeta}^2 - 2\dot{\zeta}^2) - 2\left(\frac{1}{R}(\ddot{\zeta} + \zeta) - \tilde{\chi} \right) \varphi \right) \Bigg] .\end{aligned} \tag{E.1}$$

Now we expand each of the perturbing fields in Fourier modes

$$\begin{aligned}\zeta &= R \sum_{n=-\infty}^{\infty}{}' \hat{\zeta}_n e^{in\tilde{s}}, \quad \hat{\zeta}_{-n} = \hat{\zeta}_n^* \\ \tilde{\chi} &= \sum_{n=-\infty}^{\infty}{}' \hat{\tilde{\chi}}_n e^{in\tilde{s}}, \quad \hat{\tilde{\chi}}_{-n} = \hat{\tilde{\chi}}_n^* \\ \varphi &= \sum_{n=-\infty}^{\infty}{}' \hat{\varphi}_n e^{in\tilde{s}}, \quad \hat{\varphi}_{-n} = \hat{\varphi}_n^*\end{aligned} \tag{E.2}$$

where we use $\sum'$ to denote a sum with the restrictions that $n \neq 0$, removing homogeneous perturbations and we additionally require that each of the fields be real. As $\delta^2 L$ is quadratic in the perturbing fields, it is diagonalized in Fourier space and can be expressed as the sum of contributions from individual modes, $\sum_n' \delta^2 L_n$, where

$$\begin{aligned}\frac{\delta^2 L_n}{\pi R} = \left(B\frac{1}{R^2} + \frac{k_1|\psi_1^*|}{R} \right) \left[(n^2-1)^2 |\hat{\zeta}_n|^2 + |\hat{\tilde{\chi}}_n|^2 \right. \\ \left. + (n^2-1)(\hat{\zeta}_n^* \hat{\tilde{\chi}}_n + \hat{\zeta}_n \hat{\tilde{\chi}}_n^*) \right] + \frac{J}{R^2} n^2 |\hat{\tilde{\chi}}_n|^2 + \left(\frac{C|\psi_1^*|^2}{R^2} n^2 + \frac{k_2|\psi_1^*|}{R} \right) |\hat{\varphi}_n|^2 \\ - \frac{k_1|\psi_1^*|}{R} \left(n^2(n^2-2)|\hat{\zeta}_n|^2 + 2(n^2-1)(\hat{\zeta}_n^* \hat{\varphi}_n + \hat{\zeta}_n \hat{\varphi}_n{}^*) + 2(\hat{\tilde{\chi}}_n^* \hat{\varphi}_n + \hat{\tilde{\chi}}_n^* \hat{\varphi}_n) \right) .\end{aligned} \tag{E.3}$$

As $\delta^2 L_n$ is a quadratic form, it may be represented in matrix form as

$$\delta^2 L_n = \sigma_n^\dagger A^{(n)} \sigma_n \tag{E.4}$$

where $\sigma_n = (\hat{\zeta}_n, \hat{\bar{\chi}}_n, \hat{\varphi}_n)$, with $\sigma_n^\dagger$ the Hermitian conjugate, and

$$A^{(n)} = \frac{\pi}{R} \left(\begin{array}{cc|c} B(n^2-1)^2 + M_1 R & (B+M_1 R)(n^2-1) & -2M_1 R(n^2-1) \\ (B+M_1 R)(n^2-1) & B + M_1 R + Jn^2 & -M_1 R \\ \hline -2M_1 R(n^2-1) & -M_1 R & C' n^2 + M_2 R \end{array} \right) \tag{E.5}$$

where we have defined coefficients

$$\begin{aligned} C' &\equiv C|\psi_1^*|^2 \\ M_1 &\equiv k_1 |\psi_1^*| \\ M_2 &\equiv k_2 |\psi_1^*| \end{aligned} \tag{E.6}$$

Note that $A^{(n)}$ has a block form where the upper left matrix

$$\left(A^{(n)}\right)_\psi = \frac{\pi}{R} \left(\begin{array}{cc} B(n^2-1)^2 + M_1 R & (B+M_1 R)(n^2-1) \\ (B+M_1 R)(n^2-1) & B + M_1 R + Jn^2 \end{array} \right) \tag{E.7}$$

describes the effect of varying whilst holding $\boldsymbol{\psi}$ fixed.

Instability occurs if there are variations that result in a decrease of the free-energy. Noting that the eigenvalues of $A^{(n)}$ determine the extremal response to the variations, the condition for the loss of stability is $\det A^{(n)} = 0$.

APPENDIX F

MOORE-PENROSE GREEN'S FUNCTION

Consider spectral representations

$$\begin{aligned}\hat{\mathcal{H}} &= \sum_{n=0}^{\infty} \epsilon_n |n\rangle \langle n| = \sum_{n=1}^{\infty} \epsilon_n |n\rangle \langle n| \quad \text{as } \epsilon_0 \equiv 0 \\ \Gamma &= \sum_{n=1}^{\infty} \frac{1}{\epsilon_n} |n\rangle \langle n|\end{aligned} \tag{F.1}$$

where are using Dirac notation $\boldsymbol{\eta}_n = |n\rangle$ for convenience. Note that Γ is not a true inverse of $\hat{\mathcal{H}}$ as

$$\hat{\mathcal{H}}\Gamma = \sum_{n=1}^{\infty} |n\rangle \langle n| = \mathbb{1} - \sum_{\alpha=1}^{6} \left|0^{(\alpha)}\right\rangle \left\langle 0^{(\alpha)}\right| \tag{F.2}$$

where $\{\left|0^{(1)}\right\rangle, \ldots, \left|0^{(6)}\right\rangle\}$ is the set of zero-modes. We define

$$\begin{aligned}K &\equiv \sum_{\alpha=1}^{6} \left|0^{(\alpha)}\right\rangle \left\langle 0^{(\alpha)}\right| \\ \tilde{\mathbb{1}} &\equiv \mathbb{1} - K\end{aligned} \tag{F.3}$$

where K is a projection onto the null space of $\hat{\mathcal{H}}$ and $\tilde{\mathbb{1}}$ (which we call $\tilde{\delta}_{ij}(\mathbf{x}, \mathbf{y})$ in position representation) is the complement of K and describes an "identity" on the space transverse to the null space so that

$$\hat{\mathcal{H}}\Gamma = \tilde{\mathbb{1}} \tag{F.4}$$

provides us the interpretation of Γ as the inverse of $\hat{\mathcal{H}}$ in the complement of the null space.

Now, the Moore-Penrose pseudoinverse X of a matrix A, which may not be in-

vertible and need not be square, satisfies [88]

$$\text{(i)}\ \ AXA = A,$$

$$\text{(ii)}\ \ XAX = X,$$

$$\text{(iii)}\ \ (AX)^\dagger = AX,$$

$$\text{(iv)}\ \ (XA)^\dagger = XA,$$

where X is unique and a solution can be found to the above equations for any A. It is simple to show, using the spectral representations Eq. (F.1) that the above conditions are satisfied for $A = \hat{\mathcal{H}}$ and $X = \Gamma$. Thus, the Green's function Γ is a Moore-Penrose pseudoinverse of the operator $\hat{\mathcal{H}}$.

F.0.1 Representation of the null space projection kernel

The real-space representation of the projection kernel K requires specification of the 6 zero-modes $\boldsymbol{\eta}_0^{(\alpha)}$. We choose center of mass coordinates such that

$$\int_\Omega \mathrm{d}V\ \mathbf{x} = 0 \tag{F.5}$$

and basis $\{\hat{\mathbf{e}}_\mathbf{1}, \hat{\mathbf{e}}_\mathbf{2}, \hat{\mathbf{e}}_\mathbf{3}\}$ corresponding with the continuum's principle axes, where the inertia tensor

$$I \equiv \hat{\mathbf{e}}_\mu \otimes \hat{\mathbf{e}}_\nu \int_\Omega \mathrm{d}V\ (|\mathbf{x}|^2 \delta_{\mu\nu} - x_\mu x_\nu) = \hat{\mathbf{e}}_\mathbf{1} \otimes \hat{\mathbf{e}}_\mathbf{1} I_1 + \hat{\mathbf{e}}_\mathbf{2} \otimes \hat{\mathbf{e}}_\mathbf{2} I_2 + \hat{\mathbf{e}}_\mathbf{3} \otimes \hat{\mathbf{e}}_\mathbf{3} I_3 \tag{F.6}$$

is diagonal. An orthonormal zero mode basis is therefore given by

$$\boldsymbol{\eta}_0^{(\alpha)} = \begin{cases} \frac{1}{\sqrt{V}} \hat{\mathbf{e}}_\alpha & \text{for} \quad \alpha = 1, 2, 3 \\ \frac{1}{\sqrt{I_{\alpha-3}}} \hat{\mathbf{e}}_{\alpha-\mathbf{3}} \times \mathbf{x} & \text{for} \quad \alpha = 4, 5, 6 \end{cases} \tag{F.7}$$

Therefore, the null space projection kernel is

$$K(\mathbf{x},\mathbf{y}) = \frac{1}{V}\sum_{i=1}^{3}(\hat{\mathbf{e}}_\mathbf{i}\otimes\hat{\mathbf{e}}_\mathbf{i}) + \sum_{i=1}^{3}\frac{1}{I_i}(\hat{\mathbf{e}}_\mathbf{i}\times\mathbf{x})\otimes(\hat{\mathbf{e}}_\mathbf{i}\times\mathbf{y}) \tag{F.8}$$

which can be condensed as

$$K(\mathbf{x},\mathbf{y}) = \frac{1}{V}\mathbb{1} - \mathbf{x}\times I^{-1}\times\mathbf{y}\ . \tag{F.9}$$

Finally, the identity in the complement to the null space is

$$\tilde{\delta}_{ij}(\mathbf{x},\mathbf{y}) = \left(\delta(\mathbf{x}-\mathbf{y}) - \frac{1}{V}\right)\delta_{ij} - \varepsilon_{ikm}\varepsilon_{jln}I^{-1}_{kl}x^m y^n \tag{F.10}$$

where we note that $\delta(\mathbf{x}-\mathbf{y}) - 1/V$ is the modified identity used when solving for the Green's function for Laplace's equation with Neumann boundary conditions [89].

APPENDIX G
DEVELOPMENT OF THE GREEN'S FUNCTION DOMAIN PERTURBATION THEORY

Starting with Eq. (4.27), we need to determine the effect of the coordinate change $\mathbf{x}' = \mathbf{x} + \mathbf{s}(\mathbf{x})$. Note, however, that the restriction to the space of located shapes is a technical difficulty: as the two protein shapes Ω and Ω' have different null spaces, the domain of functional integration is different between the two. We overcome this difficulty by regularizing the zero modes with a "mass" m

$$\Gamma_m \equiv \sum_\alpha \frac{\left|0^{(\alpha)}\right\rangle \left\langle 0^{(\alpha)}\right|}{m^2} + \sum_{n\geq 1} \frac{|n\rangle \langle n|}{\epsilon_n} = \frac{1}{m^2} K + \Gamma \tag{G.1}$$

that is introduced in the elastic energy

$$\mathcal{H}_m = \frac{1}{2}\left(C_{ijkl}\, \partial_i u_j\, \partial_k u_l + m^2 |\mathbf{u}|^2\right) \tag{G.2}$$

with the idea that the perturbation expansion will be carried out with finite m, characterizing an energy penalty for translations and rotations, and then the $m \to 0$ limit will be taken at the end of the calculation. Note that K/m^2 is the singular part of Γ_m and Γ is the regular part.

Transforming from $\mathbf{x}'$ to $\mathbf{x}$, we can write the elastic energy density as

$$H'_m = \frac{1}{2}\int_\Omega \mathrm{d}V_x\, \sqrt{\det\, g}\left(C^{abcd}\, \nabla_a u_b\, \nabla_c u_d + m^2 g^{ab} u_a u_b\right) \tag{G.3}$$

where

$$\nabla_a u_b = \frac{\partial u_b}{\partial x^a} - \gamma^c{}_{ab} u_c \tag{G.4}$$

is a covariant derivative. Keeping up to linear order in s

$$\begin{aligned}\frac{\partial x'^i}{\partial x^a} &\approx \delta_{ai} + \partial_a s_i \\ \frac{\partial x^a}{\partial x'^i} &\approx \delta_{ai} - \partial_a s_i\end{aligned} \tag{G.5}$$

we we find that

$$\begin{aligned}C^{abcd}(\mathbf{x}) &= C_{ijkl}(\mathbf{x}'(\mathbf{x}))\frac{\partial x^a}{\partial x'^i}\frac{\partial x^b}{\partial x'^j}\frac{\partial x^c}{\partial x'^k}\frac{\partial x^d}{\partial x'^l} \\ &\approx (1+\mathbf{s}\cdot\boldsymbol{\nabla})C_{abcd} - C_{pbcd}\partial_p s_a - C_{apcd}\partial_p s_b - C_{abpd}\partial_p s_c - C_{abcp}\partial_p s_d \\ g_{ab} &= \frac{\partial \mathbf{x}'}{\partial x^a}\cdot\frac{\partial \mathbf{x}'}{\partial x^b} \approx \delta_{ab} + \partial_a s_b + \partial_b s_a \\ g^{ab} &= (g_{ab})^{-1} \approx \delta_{ab} - \partial_a s_b - \partial_b s_a \\ \gamma^c{}_{ab} &= g^{cd}(\partial_d \mathbf{x})\cdot\partial_{ab}\mathbf{x} \approx \partial_{ab}s_c\end{aligned} \tag{G.6}$$

Thus, the energy can be expressed as $H'_m \approx H_m + h_m$ where H_m is the elastic energy for Ω and

$$\begin{aligned}h_m = \frac{1}{2}\int_\Omega \mathrm{d}V_x \Big\{ &- C_{abcd}(\partial_{ab}s_r)u_r\partial_c u_d + (\partial_r s_r C_{abcd})(\partial_a u_b)(\partial_c u_d) \\ &- 2C_{abcd}(\partial_a s_q)\left[\partial_q u_b + \partial_b u_q\right]\partial_c u_d + m^2\left[(\boldsymbol{\nabla}\cdot\mathbf{s})|\mathbf{u}|^2 - 2(\partial_p s_q)u_p u_q\right]\Big\}.\end{aligned} \tag{G.7}$$

The functional integral Eq. (4.27) is transformed from integration over $\mathcal{D}\mathbf{u}'$ to $\mathcal{D}\mathbf{u}$

$$k_B T\Gamma'_{m,ij}(\mathbf{x}'(\mathbf{x}),\mathbf{y}'(\mathbf{y})) = \frac{\partial x^a}{\partial x'^i}\frac{\partial y^b}{\partial y'^j}\frac{\int \mathcal{D}\mathbf{u}\; e^{-\beta(H_m+h_m)}u_a(\mathbf{x})u_b(\mathbf{y})}{\int \mathcal{D}\mathbf{u}\; e^{-\beta(H_m+h_m)}} \tag{G.8}$$

which we expand to leading order in $\mathbf{s}$

$$\begin{aligned}k_B T\Gamma'_{m,ij}(\mathbf{x}'(\mathbf{x}),\mathbf{y}'(\mathbf{y})) \approx \frac{\partial x^a}{\partial x'^i}\frac{\partial y^b}{\partial y'^j}\big\{ &\left\langle u_a(\mathbf{x})u_b(\mathbf{y})\right\rangle_m \\ &- \beta\left\langle h_m u_a(\mathbf{x})u_b(\mathbf{y})\right\rangle_m + \beta\left\langle h_m\right\rangle_m\left\langle u_a(\mathbf{x})u_b(\mathbf{y})\right\rangle_m\big\}\end{aligned} \tag{G.9}$$

where averages are taken with respect to the bare energy H_m:

$$\langle \mathcal{O} \rangle_m \equiv \frac{\int \mathcal{D}\mathbf{u}\; e^{-\beta H_m} \mathcal{O}}{\int \mathcal{D}\mathbf{u}\; e^{-\beta H_m}} \; . \tag{G.10}$$

Noting that the perturbation h_m is quadratic in $\mathbf{u}$, we can expand $\langle h_m u_a(\mathbf{x}) u_b(\mathbf{y}) \rangle_m$ using Wick's theorem (see e.g., [50])

$$\langle u_a u_b u_c u_d \rangle_m = \langle u_a u_b \rangle_m \langle u_c u_d \rangle_m + \langle u_a u_c \rangle_m \langle u_b u_d \rangle_m + \langle u_a u_d \rangle_m \langle u_b u_c \rangle_m \; . \tag{G.11}$$

After simplifying the resulting expression by integrating by parts and using the modified Green's function equation

$$(-\partial_j C_{ijkl} \partial_k + m^2 \delta_{il}) \Gamma_{lm}(\mathbf{x}, \mathbf{y}) = \delta_{im} \delta(\mathbf{x} - \mathbf{y}) \tag{G.12}$$

we find

$$\begin{aligned} \Gamma'_{m,ij}(\mathbf{x}'(\mathbf{x}), \mathbf{y}'(\mathbf{y})) \approx \Gamma_{m,ij}(\mathbf{x}, \mathbf{y}) &+ (\mathbf{s}(\mathbf{x}) \cdot \boldsymbol{\nabla}_x + \mathbf{s}(\mathbf{y}) \cdot \boldsymbol{\nabla}_y) \Gamma_{m,ij}(\mathbf{x}, \mathbf{y}) \\ &- \oint_{\partial\Omega} \mathrm{d}S_\alpha \hat{\mathbf{n}} \cdot \mathbf{s} \Big\{ C_{abcd} \partial_a \Gamma_{m,bi}(\boldsymbol{\alpha}, \mathbf{x}) \; \partial_c \Gamma_{m,dj}(\boldsymbol{\alpha}, \mathbf{y}) \\ &\qquad + m^2 \Gamma_{m,bi}(\boldsymbol{\alpha}, \mathbf{x}) \Gamma_{m,bj}(\boldsymbol{\alpha}, \mathbf{y}) \Big\} \; . \end{aligned} \tag{G.13}$$

The right hand side can be shifted from $\mathbf{x} \to \mathbf{x}'$ using the Taylor expansion

$$\begin{aligned} \Gamma_{m,ij}(\mathbf{x}', \mathbf{y}') &= \Gamma_{m,ij}(\mathbf{x} + \mathbf{s}(\mathbf{x}), \mathbf{y} + \mathbf{s}(\mathbf{y})) \\ &\approx \Gamma_{m,ij}(\mathbf{x}, \mathbf{y}) + (\mathbf{s}(\mathbf{x}) \cdot \boldsymbol{\nabla}_x + \mathbf{s}(\mathbf{y}) \cdot \boldsymbol{\nabla}_y) \Gamma_{m,ij}(\mathbf{x}, \mathbf{y}) \end{aligned} \tag{G.14}$$

so that

$$\begin{aligned} \Gamma'_{m,ij}(\mathbf{x}', \mathbf{y}') \approx \Gamma_{m,ij}(\mathbf{x}', \mathbf{y}') - \int_\Sigma \mathrm{d}S_\alpha \hat{\mathbf{n}} \cdot \mathbf{s} \Big\{ & C_{abcd} \partial_a \Gamma_{m,bi}(\boldsymbol{\alpha}, \mathbf{x}') \; \partial_c \Gamma_{m,dj}(\boldsymbol{\alpha}, \mathbf{y}') \\ & + m^2 \Gamma_{m,bi}(\boldsymbol{\alpha}, \mathbf{x}') \Gamma_{m,bj}(\boldsymbol{\alpha}, \mathbf{y}') \Big\} \end{aligned} \tag{G.15}$$

where $\zeta(\boldsymbol{\alpha}) \equiv \hat{\mathbf{n}}(\boldsymbol{\alpha}) \cdot \mathbf{s}(\boldsymbol{\alpha})$ and the integration is taken over $\Sigma \subset \partial\Omega$, the region where $\zeta \neq 0$. Finally, using Eq. (G.1) to decompose Γ_m and Γ'_m into singular and regular parts yields, upon taking $m \to 0$, we find

$$\begin{aligned}
\Delta\Gamma_{ij}(\mathbf{x}, \mathbf{y}) \approx -\int_\Sigma \mathrm{d}S_\alpha \; \zeta(\boldsymbol{\alpha}) \Big\{ & C_{klmn}(\boldsymbol{\alpha}) \frac{\partial \Gamma_{ik}(\mathbf{x}, \boldsymbol{\alpha})}{\partial \alpha^l} \frac{\partial \Gamma_{nj}(\boldsymbol{\alpha}, \mathbf{y})}{\partial \alpha^m} \\
& + K_{ik}(\mathbf{x}, \boldsymbol{\alpha}) \Gamma_{kj}(\boldsymbol{\alpha}, \mathbf{y}) + \Gamma_{ik}(\mathbf{x}, \boldsymbol{\alpha}) K_{kj}(\boldsymbol{\alpha}, \mathbf{y}) \Big\} \qquad \text{(G.16)} \\
\Delta K_{ij}(\mathbf{x}, \mathbf{y}) \approx -\int_\Sigma \mathrm{d}S_\alpha \; & \zeta(\boldsymbol{\alpha}) \; K_{ib}(\mathbf{x}, \boldsymbol{\alpha}) K_{bj}(\boldsymbol{\alpha}, \mathbf{y})
\end{aligned}$$

where the $\Delta\Gamma$ equation is our central result. Furthermore, we are obtain a formula for the change in the null space projection kernel, ΔK.

REFERENCES

[1] P.-G. de Gennes. *Scaling Concepts in Polymer Physics*. Cornell University Press, 1979. ISBN: 9780801412035 (cit. on pp. 1, 2, 9, 11, 14, 16, 17).

[2] P. M. Goldbart, H. E. Castillo, and A. Zippelius. "Randomly crosslinked macromolecular systems: Vulcanization transition to and properties of the amorphous solid state". *Advances in Physics* 45.5 (1996), pp. 393–468 (cit. on p. 2).

[3] E. Sato Matsuo and T. Tanaka. "Kinetics of discontinuous volume-phase transition of gels". *The Journal of Chemical Physics* 89.3 (1988), pp. 1695–1703 (cit. on pp. 3, 19, 26, 30).

[4] T. Tanaka, S.-T. Sun, Y. Hirokawa, S. Katayama, J. Kucera, Y. Hirose, and T. Amiya. "Mechanical instability of gels at the phase transition". *Nature* 325.6107 (1987), pp. 796–798 (cit. on p. 3).

[5] M. K. Kang and R. Huang. "Effect of surface tension on swell-induced surface instability of substrate-confined hydrogel layers". *Soft Matter* 6 (22 2010), pp. 5736–5742 (cit. on p. 3).

[6] E. Efrati, E. Sharon, and R. Kupferman. "The metric description of elasticity in residually stressed soft materials". *Soft Matter* 9 (34 2013), pp. 8187–8197 (cit. on p. 3).

[7] M. Pezzulla, S. A. Shillig, P. Nardinocchi, and D. P. Holmes. "Morphing of geometric composites via residual swelling". *Soft Matter* 11 (29 2015), pp. 5812–5820 (cit. on p. 3).

[8] D. P. Holmes, M. Roche, T. Sinha, and H. A. Stone. "Bending and twisting of soft materials by non-homogenous swelling". *Soft Matter* 7.11 (2011), pp. 5188–5193 (cit. on p. 3).

[9] V. Trujillo, J. Kim, and R. C. Hayward. "Creasing instability of surface-attached hydrogels". *Soft Matter* 4 (3 2008), pp. 564–569 (cit. on p. 3).

[10] E. Hohlfeld and L. Mahadevan. "Unfolding the Sulcus". *Phys. Rev. Lett.* 106 (10 2011), p. 105702 (cit. on p. 3).

[11] D. Breid and A. J. Crosby. "Effect of stress state on wrinkle morphology". *Soft Matter* 7 (9 2011), pp. 4490–4496 (cit. on p. 3).

[12] A. Sydney Gladman, E. A. Matsumoto, R. G. Nuzzo, L. Mahadevan, and J. A. Lewis. "Biomimetic 4D printing". *Nat. Mater.* 15.4 (2016), pp. 413–418 (cit. on p. 3).

[13] H. B. Callen. *Thermodynamics and an Introduction to Thermostatistics*. Wiley, 1985. ISBN: 9780471862567 (cit. on pp. 5, 98).

[14] M. Warner and E. M. Terentjev. *Liquid Crystal Elastomers*. International Series of Monographs on Physics. OUP Oxford, 2003. ISBN: 9780191523632 (cit. on pp. 7, 8, 45, 47, 94).

[15] L. R. G. Treloar. *The Physics of Rubber Elasticity*. Monographs on the physics and chemistry of materials. Oxford University Press, USA, 1975. ISBN: 9780191523304 (cit. on p. 8).

[16] P. J. Flory and J. Rehner. "Statistical Mechanics of Cross-Linked Polymer Networks I. Rubberlike Elasticity". *The Journal of Chemical Physics* 11.11 (1943), pp. 512–520 (cit. on pp. 10, 17).

[17] P. J. Flory and J. Rehner. "Statistical Mechanics of Cross-Linked Polymer Networks II. Swelling". *The Journal of Chemical Physics* 11.11 (1943), pp. 521–526 (cit. on pp. 10, 12, 17).

[18] P. J. Flory. *Principles of polymer chemistry*. Cornell University Press, 1953 (cit. on pp. 12, 17).

[19] R. T. Deam and S. F. Edwards. "The Theory of Rubber Elasticity". *Philosophical Transactions of the Royal Society of London A: Mathematical, Physical and Engineering Sciences* 280.1296 (1976), pp. 317–353 (cit. on p. 13).

[20] P. M. Chaikin and T. C. Lubensky. *Principles of Condensed Matter Physics*. Cambridge: Cambridge University Press, 1995 (cit. on pp. 15, 55, 58, 70, 87).

[21] P. J. Flory. "Thermodynamics of High Polymer Solutions". *The Journal of Chemical Physics* 10.1 (1942), pp. 51–61 (cit. on p. 16).

[22] B. Erman and P. J. Flory. "Critical phenomena and transitions in swollen polymer networks and in linear macromolecules". *Macromolecules* 19.9 (1986), pp. 2342–2353 (cit. on pp. 18, 19, 30).

[23] M. Kardar. *Statistical Physics of Particles*. Cambridge University Press, 2007. ISBN: 9781139464871 (cit. on pp. 19, 51, 79).

[24] S. Hirotsu. "Static and time-dependent properties of polymer gels around the volume phase transition". *Phase Transitions* 47.3-4 (1994), pp. 183–240 (cit. on pp. 20, 30).

[25] S. Hirotsu. "Critical points of the volume phase transition in N-isopropylacrylamide gels". *The Journal of Chemical Physics* 88.1 (1988), pp. 427–431 (cit. on p. 20).

[26] A. Onuki. "Paradox in phase transitions with volume change". *Phys. Rev. A* 38 (4 1988), pp. 2192–2195 (cit. on p. 23).

[27] L. Golubović and T. C. Lubensky. "Nonlinear elasticity of amorphous solids". *Phys. Rev. Lett.* 63 (10 1989), pp. 1082–1085 (cit. on pp. 23, 55).

[28] W. H. Zurek. "Cosmological experiments in superfluid helium?" *Nature* 317.6037 (1985), pp. 505–508 (cit. on p. 26).

[29] T. W. B. Kibble. "Topology of cosmic domains and strings". *Journal of Physics A: Mathematical and General* 9.8 (1976), p. 1387 (cit. on p. 26).

[30] T. W. B. Kibble. "Some implications of a cosmological phase transition". *Physics Reports* 67.1 (1980), pp. 183 –199 (cit. on p. 26).

[31] I. Chuang, R. Durrer, N. Turok, and B. Yurke. "Cosmology in the Laboratory: Defect Dynamics in Liquid Crystals". *Science* 251.4999 (1991), pp. 1336–1342 (cit. on p. 26).

[32] M. J. Bowick, L. Chandar, E. A. Schiff, and A. M. Srivastava. "The Cosmological Kibble Mechanism in the Laboratory: String Formation in Liquid Crystals". *Science* 263.5149 (1994), pp. 943–945 (cit. on p. 26).

[33] M. Doi. "Gel Dynamics". *Journal of the Physical Society of Japan* 78.5 (2009), pp. 052001–052001 (cit. on p. 29).

[34] E. S. Matsuo and T. Tanaka. "Patterns in shrinking gels". *Nature* 358.6386 (1992), pp. 482–485 (cit. on p. 30).

[35] Y-W. Chang, M. S. Dimitriyev, A. Souslov, S. V. Nikolov, S. M. Marquez, A. Alexeev, P. M. Goldbart, A. Fernández-Nieves. (manuscript submitted) 2017. (cit. on pp. 31, 65, 68, 72).

[36] L. D. Landau, E. M. Lifshitz, A. M. Kosevich, and L. P. Pitaevskiĭ. *Theory of Elasticity*. Course of theoretical physics. Butterworth-Heinemann, 1986. ISBN: 9780750626330 (cit. on pp. 41, 51, 54, 61, 115).

[37] S. Hirotsu. "Softening of bulk modulus and negative Poisson's ratio near the volume phase transition of polymer gels". *The Journal of Chemical Physics* 94.5 (1991), pp. 3949–3957 (cit. on p. 45).

[38] B. Barrière, K. Sekimoto, and L. Leibler. "Peristaltic instability of cylindrical gels". *The Journal of Chemical Physics* 105.4 (1996), pp. 1735–1738 (cit. on p. 46).

[39] B. Lautrup. *Physics of Continuous Matter: Exotic and Everyday Phenomena in the Macroscopic World*. Taylor & Francis, 2004. ISBN: 9780750307529 (cit. on pp. 51, 77).

[40] S. Timoshenko. "Analysis of Bi-Metal Thermostats". *J. Opt. Soc. Am.* 11.3 (1925), pp. 233–255 (cit. on p. 54).

[41] A. Onuki. "Theory of phase transition in polymer gels". In: *Responsive Gels: Volume Transitions I*. Ed. by K. Dušek. Berlin, Heidelberg: Springer Berlin Heidelberg, 1993, pp. 63–121. ISBN: 978-3-540-47737-2 (cit. on p. 55).

[42] A. Onuki and S. Puri. "Spinodal decomposition in gels". *Phys. Rev. E* 59 (2 1999), R1331–R1334 (cit. on p. 55).

[43] A. Pressley. *Elementary differential geometry*. Springer undergraduate mathematics series. Springer, 2010. ISBN: 978-1-84882-890-2 (cit. on pp. 56, 57, 67, 71, 102).

[44] E. Kreyszig. *Differential Geometry*. Differential Geometry. University of Toronto Press, 1959. ISBN: 9780486667218 (cit. on pp. 56, 57, 106).

[45] L. D. Landau. "On the theory of phase transitions. I." *Phys. Z. Sowjet.* 11 (1937), p. 26 (cit. on p. 58).

[46] V. L. Ginzburg and L. D. Landau. "On the Theory of Superconductivity". In: *On Superconductivity and Superfluidity: A Scientific Autobiography*. Berlin, Heidelberg: Springer Berlin Heidelberg, 2009, pp. 113–137. ISBN: 978-3-540-68008-6 (cit. on p. 58).

[47] P.-G. de Gennes and J. Prost. *The Physics of Liquid Crystals*. International Series of Monographs on Physics. Clarendon Press, 1995. ISBN: 9780198517856 (cit. on pp. 58, 70).

[48] N. Goldenfeld. *Lectures on Phase Transitions and the Renormalization Group*. Frontiers in physics. Avalon Publishing, 1992. ISBN: 9780201554090 (cit. on pp. 58, 71, 72).

[49] M. Tinkham. *Group Theory and Quantum Mechanics*. Dover Books on Chemistry and Earth Sciences. Dover Publications, 2003. ISBN: 9780486432472 (cit. on p. 60).

[50] M. Kardar. *Statistical Physics of Fields*. Cambridge University Press, 2007. ISBN: 9780521873413 (cit. on pp. 63, 123).

[51] H. Goldstein, C. P. Poole, and J. L. Safko. *Classical Mechanics*. Addison Wesley, 2002. ISBN: 9780201657029 (cit. on p. 63).

[52] B. Audoly and Y. Pomeau. *Elasticity and Geometry: From hair curls to the non-linear response of shells*. OUP Oxford, 2010. ISBN: 9780191545023 (cit. on p. 64).

[53] M. Barrientos, A. Perez, and A. F. Ranada. "Weak chaos in the asymmetric heavy top". *European Journal of Physics* 16.3 (1995), p. 106 (cit. on p. 65).

[54] M. A. Davies and F. C. Moon. "3-D spatial chaos in the elastica and the spinning top: Kirchhoff analogy". *Chaos: An Interdisciplinary Journal of Nonlinear Science* 3.1 (1993), pp. 93–99 (cit. on p. 65).

[55] A. Altland and B. D. Simons. *Condensed Matter Field Theory*. 2nd ed. Cambridge University Press, 2010. ISBN: 9780521769754 (cit. on p. 69).

[56] J. Goldstone. "Field theories with Superconductor solutions". *Il Nuovo Cimento (1955-1965)* 19.1 (1961), pp. 154–164 (cit. on p. 69).

[57] J. Goldstone, A. Salam, and S. Weinberg. "Broken Symmetries". *Phys. Rev.* 127 (3 1962), pp. 965–970 (cit. on p. 69).

[58] H. B. Callen and T. A. Welton. "Irreversibility and Generalized Noise". *Phys. Rev.* 83 (1 1951), pp. 34–40 (cit. on p. 70).

[59] L. H. Kauffman. *Knots and Physics, Third Edition*. K & E series on knots and everything. World Scientific, 2001. ISBN: 9789812384836 (cit. on p. 74).

[60] J. F. Marko and E. D. Siggia. "Statistical mechanics of supercoiled DNA". *Phys. Rev. E* 52 (3 1995), pp. 2912–2938 (cit. on p. 74).

[61] J. Monod, J. Wyman, and J. P. Changeux. "On the Nature of Allosteric Transitions: A Plausible Model". *J. Mol. Biol.* 12 (1965), pp. 88–118 (cit. on p. 75).

[62] C.-J. Tsai, A. del Sol, and R. Nussinov. "Allostery: Absence of a Change in Shape Does Not Imply that Allostery Is Not at Play". *Journal of Molecular Biology* 378.1 (2008), pp. 1 –11 (cit. on p. 75).

[63] H. N. Motlagh, J. O. Wrabl, J. Li, and V. J. Hilser. "The ensemble nature of allostery". *Nature* 508.7496 (2014), pp. 331–339 (cit. on p. 75).

[64] N. Popovych, S. Sun, R. H. Ebright, and C. G. Kalodimos. "Dynamically driven protein allostery". *Nat. Struct. Mol. Biol.* 13.9 (2006), pp. 831–838 (cit. on p. 75).

[65] A. Cooper and D. T. F. Dryden. "Allostery without conformational change. A plausible model." *Eur. Biophys. J.* 11.2 (1984), pp. 103–109 (cit. on p. 75).

[66] R. J. Hawkins and T. C. B. McLeish. "Coarse-Grained Model Of Entropic Allostery". *Phys. Rev. Lett.* 93 (9 2004), p. 098104 (cit. on pp. 75, 76).

[67] R. J. Hawkins and T. C. B. McLeish. "Dynamic allostery of protein alpha helical coiled-coils". *Journal of The Royal Society Interface* 3.6 (2006), pp. 125–138 (cit. on p. 76).

[68] D. Ming, Y. Kong, M. A. Lambert, Z. Huang, and J. Ma. "How to Describe Protein Motion without Amino Acid Sequence and Atomic Coordinates". *Proceedings of the National Academy of Sciences of the United States of America* 99.13 (2002), pp. 8620–8625 (cit. on pp. 76, 77).

[69] T. C. B. McLeish, T. L. Rodgers, and M. R. Wilson. "Allostery without conformation change: modelling protein dynamics at multiple scales". *Physical Biology* 10.5 (2013), p. 056004 (cit. on p. 76).

[70] T. C. B. McLeish, M. J. Cann, and T. L. Rodgers. "Dynamic Transmission of Protein Allostery without Structural Change: Spatial Pathways or Global Modes?" *Biophysical Journal* 109.6 (2015), pp. 1240 –1250 (cit. on p. 76).

[71] R. Balian and C. Bloch. "Distribution of eigenfrequencies for the wave equation in a finite domain". *Annals of Physics* 60.2 (1970), pp. 401 –447 (cit. on p. 76).

[72] M. Kac. "Can One Hear the Shape of a Drum?" *The American Mathematical Monthly* 73.4 (1966), pp. 1–23 (cit. on p. 76).

[73] H. Kleinert. *Gauge Fields in Condensed Matter, Volume II*. Singapore: World Scientific, 1989. ISBN: 9971-50-210-0 (cit. on p. 78).

[74] R. P. Feynman, A. R. Hibbs, and D. F. Styer. *Quantum Mechanics and Path Integrals*. Dover Books on Physics. Dover Publications, 2010. ISBN: 9780486477220 (cit. on p. 80).

[75] A. Shapere and F. Wilczek. "Gauge kinematics of deformable bodies". *American Journal of Physics* 57.6 (1989), pp. 514–518 (cit. on p. 81).

[76] R. Rajaraman. *Solitons and Instantons: An Introduction to Solitons and Instantons in Quantum Field Theory*. North-Holland personal library. North-Holland Publishing Company, 1982. ISBN: 9780444862297 (cit. on p. 81).

[77] A. B. Migdal. "Superfluidity and the moments of inertia of nuclei". *Nuclear Physics* 13.5 (1959), pp. 655 –674 (cit. on p. 84).

[78] L. D. Landau and E. M. Lifshitz. *Quantum Mechanics: Non-relativistic Theory*. Butterworth-Heinemann. Butterworth-Heinemann, 1977. ISBN: 9780750635394 (cit. on p. 84).

[79] P. Grinfeld. "Hadamard's Formula Inside and Out". *J. Optim. Theory Appl.* 146.3 (2010), pp. 654–690 (cit. on pp. 84, 85).

[80] J. Hadamard. *Mémoire sur le problème d'analyse relatif à l'équilibre des plaques élastiques encastrées*. Mémoires présentés par divers savants à l'Académie des sciences de l'Institut de France: Éxtrait. Imprimerie nationale, 1908 (cit. on pp. 84, 85).

[81] P. R. Garabedian and M. Schiffer. "Convexity of domain functionals". *J. Anal. Math.* 2 (2 1952), pp. 281 –368 (cit. on pp. 84, 85).

[82] M. Schiffer. "Variation of domain functionals". *Bulletin of the American Mathematical Society* 60.4 (1954), pp. 303–328 (cit. on pp. 84, 85).

[83] L. Yan, R. Ravasio, C. Brito, and M. Wyart. "Architecture and coevolution of allosteric materials". *PNAS* 114.10 (2017), pp. 2526–2531 (cit. on p. 92).

[84] J. W. Rocks, N. Pashine, I. Bischofberger, C. P. Goodrich, A. J. Liu, and S. R. Nagel. "Designing allostery-inspired response in mechanical networks". *PNAS* 114.10 (2017), pp. 2520–2525 (cit. on p. 92).

[85] P. M. Reis, H. M. Jaeger, and M. van Hecke. "Designer Matter: A perspective". *Extreme Mechanics Letters* 5 (2015), pp. 25 –29 (cit. on p. 93).

[86] C. D. Santangelo. "Extreme Mechanics: Self-Folding Origami". *Annual Review of Condensed Matter Physics* 8.1 (2017), pp. 165–183 (cit. on pp. 93, 94).

[87] J. Shim, C. Perdigou, E. R. Chen, K. Bertoldi, and P. M. Reis. "Buckling-induced encapsulation of structured elastic shells under pressure". *Proceedings of the National Academy of Sciences* 109.16 (2012), pp. 5978–5983 (cit. on p. 93).

[88] R. Penrose. "A generalized inverse for matrices". *Mathematical Proceedings of the Cambridge Philosophical Society* 51.3 (1955), pp. 406–413 (cit. on p. 119).

[89] E. DiBenedetto. *Partial Differential Equations*. Second. Birkhäuser, 2010. ISBN: 978-0-8176-4551-9 (cit. on p. 120).